INFORMATION TO USERS

This manuscript has been reproduced from the microfilm master. UMI films the text directly from the original or copy submitted. Thus, some thesis and dissertation copies are in typewriter face, while others may be from any type of computer printer.

The quality of this reproduction is dependent upon the quality of the copy submitted. Broken or indistinct print, colored or poor quality illustrations and photographs, print bleedthrough, substandard margins, and improper alignment can adversely affect reproduction.

In the unlikely event that the author did not send UMI a complete manuscript and there are missing pages, these will be noted. Also, if unauthorized copyright material had to be removed, a note will indicate the deletion.

Oversize materials (e.g., maps, drawings, charts) are reproduced by sectioning the original, beginning at the upper left-hand corner and continuing from left to right in equal sections with small overlaps.

Photographs included in the original manuscript have been reproduced xerographically in this copy. Higher quality 6" x 9" black and white photographic prints are available for any photographs or illustrations appearing in this copy for an additional charge. Contact UMI directly to order.

ProQuest Information and Learning
300 North Zeeb Road, Ann Arbor, MI 48106-1346 USA
800-521-0600

Université d'Ottawa · University of Ottawa

ABSTRACT

The work described in this thesis is concerned with gaining insight into chemical processes which may be toxic in the biological model systems studied. The aim was to gain a detailed mechanistic understanding through the model systems which may aid in the understanding of how certain chemical processes may be implicated in terms of biological systems.

One of the studies undertaken involved determining if an applied magnetic field can affect the kinetics and population of free radicals in a DNA environment. Previous studies have shown that when radical-pairs are produced in a cage-like environment such as a micelle, that the rate of escape versus that of recombination is significantly altered when a magnetic field is applied. Our aim was to determine if DNA can act as a cage as well as the other half of the radical-pair through laser photolysis of a radical source which is associated with the DNA. Another aspect of the same study was to ascertain if the effects an applied field may have on the kinetics and population of radical results in enhanced radical-induced damage to DNA. In view of the ongoing controversy regarding the possible health effects of high magnetic fields this research could provide some mechanistic insight.

Another area of research was concerned with how a sequence of chemical reactions ultimately leading to the generation of peroxyl radicals is specific to the use of a laser as the source of radiation. Time-resolved work with various molecules and product studies resulted in the elucidation of a provisional mechanism for the laser-specific generation of this reactive oxygen species. In view of the ever-increasing use of lasers for various medical and cosmetic procedures, the possibility of laser-induced production of reactive species such as peroxyl radicals is an area worth looking into.

The final research area covered in this thesis involved the study of a physical sunscreening agent, specifically titanium dioxide, and its possible phototoxicity. In this case the model system was either an amino acid or a functioning enzyme in solution. Both time-resolved studies with amino acids and steady-state photolyses with enzymes were performed. After steady-state irradiation, the enzyme samples were assayed for activity to determine if the combination of titanium dioxide and UVA light affect the enzymatic activity in any way, indicating that some sort of photoinitiated damage had been done. The results clearly showed that while the extent of the deactivation of the two enzymes studied was quite different, both were clearly damaged significantly by the reactive oxygen species created upon UVA photolysis of TiO_2. UVA alone caused no impairment to the activity in the case of chymotrypsin and a small effect on horseradish peroxidase activity due to its absorption characteristics. As titanium dioxide is a common ingredient in commercially available sunscreens, knowledge regarding any possible phototoxic reactions is quite valuable.

ACKNOWLEDGEMENTS

I have had the extreme good fortune to have been a graduate student under the supervision of Tito Scaiano for the past several years. He is a model of excellence as a teacher, and his brilliance as a chemist is surpassed only by his kindness as a person. I am very grateful to him for taking a chance on me, and indebted to both he and Elda for their surrogate parenting over the years. I am deeply thankful to my parents who have provided moral and financial support throughout my seemingly endless career as a student. They allowed me the freedom to explore, but were, and still are, close by to lend a helping hand. I must also show appreciation to my husband who, through a mixture of humor and profound insight, kept me on the right path. Yes, Muffin, I'll start looking for a real job now. Sincere thanks must also be extended to Sensei C. Villeneuve and the many friends with whom I have studied martial arts over the years. Sensei has taught me, among many things, perserverence and patience. He has contributed significantly to my studies and to my life. I am indebted to Jeff Banks, Monica Barra, and Fran Cozens who helped me get started in my research as well as Lydia Martinez, Dean Weldon, and Chris Evans who gave generously of their knowledge and experience at various times. Much gratitude is extended to Dr. Jack McLean at Health Canada for his collaborative assistance. Thanks to Andre Simard and Gerry Charette, who kept the various instruments in the lab running smoothly so that research was never hampered by down-time. Finally, I am very grateful to Klara Konya and Mary King, with whom I have shared the ups and downs of balancing research and family. Knowing I was not alone in the struggle helped tremendously.

For those who believed: Mom, Dad, Junlong

and those who inspired: Jemi, Tia

TABLE OF CONTENTS

LIST OF FIGURES

LIST OF TABLES

LIST OF SCHEMES

LIST OF EQUATIONS

CHAPTER 1: INTRODUCTION

1.1 Toxicology

Toxicology is defined as the study of toxicants and is concerned with the nature of the toxicant, its interaction with biological systems, and with the safety evaluation or toxicity testing of potentially poisonous materials[1]. This definition requires that the word "toxicant" also be defined. A toxicant is a chemical substance which has a harmful or adverse effect on living organisms[1]. It is important to make clear that a chemical may be poisonous under one set of conditions, but in different circumstances it may be completely harmless, even essential for proper functioning of the organism.

There are two types of toxicity in terms of the length of time between exposure to a toxin and the manifestation of some sort of measurable deleterious effect; acute toxicity and chronic toxicity. Acute toxic effects occur rapidly as a result of exposure of an organism to a relatively large quantity of toxin, often as a single dose. Chronic toxic effects, on the other hand, result from frequent or infrequent exposure to low levels of toxin over a protracted time period, often years.

Toxic effects can be broadly categorized as affecting biological systems via three main pathways[2]:

1. enzyme systems

2. membranes

3. carcinogenic effects

1. Enzyme systems: Enzymes are vital for the proper functioning of all organisms. Any interference with the normal functioning of enzymatic processes, therefore, constitutes a toxic effect on the organism.

2. Membranes: Cells depend upon a continuous exchange of nutrients and metabolites between themselves and their surroundings for them to function properly. In order for this exchange to be efficient the integrity of the cell membrane must be maintained and nothing must interfere with the cellular transport mechanism. Anything which destroys the cell membrane or alters its transport processes is therefore toxic to the cell.

3. Carcinogenic effects: Carcinogenic or oncogenic materials induce the formation of tumors, which interfere with the proper functioning of organs and tissues within the organism, often resulting in its death. One of the major causes of cancer is probably damage to or mutations in DNA caused by chemical species. Ultimately such DNA damage leads to disruptions of the control mechanisms which are coded for in the genetic material. Any substance which causes DNA damage or mutations is therefore toxic.

It would be useful at this point to discuss in a bit more detail what exactly cancer is. Cancer is the common, catch-all name for approximately 200 specific diseases which share the common characteristic of abnormal cell growth. The underlying causes of cancer fall into four classes: genetic predisposition only, environmental factors only, environment + genetic predisposition, and unknown factors. The combination of environment plus heredity is estimated to account for ~ 60- 90% of all cancers, although the distribution of causality beween the two is not known[3]. The environment, in terms of this role as carcinogen, refers broadly to all interactions an organism has with its surroundings (e.g., air, food, water, living habits, etc.).

The work discussed in this thesis deals with possible toxic effects in all three areas discussed above (enzymes, membranes, genetic material) as studied in model systems which were designed to imitate biological systems to a greater or lesser degree. The source of potential toxicity in the cases studied, while the chemical precursor was different, is free radicals which are generated by light absorption. In some cases the light is part of the process which causes the toxicity, in others it is merely a way of generating the free radicals for study. In the third case a magnetic field is the source of the toxicity, as it plays a role in influencing the population and reactivity patterns of free radicals which may be present in the system.

1.2 Free Radicals

Free radicals are, as a broad definition, chemical species which are capable of independent existence that contain unpaired electrons[4]. The simplest example could be the solvated electron itself, which is an unpaired electron, and has a definite time of existence. The time of existence of course depends upon the conditions under which it is created in terms of solvent, presence of species with which it could react, etc.

The reason for the scientific interest in free radicals is that, as species which contain unpaired electrons, they are frequently very reactive. They are driven by the need to become stabilized as closed-shell species. In order to accomplish this, they can react quickly with organic molecules within their proximity. The results of this reactivity can be the creation of other species which may or may not be just as reactive as the original free radical, and may or may not be able to undergo further reactions.

For the purposes of this discussion, free-radicals will be divided into two groups, depending upon the type of atom on which the radical center is located. The first group are carbon-centered radicals, and the second are oxygen-centered radicals. Both types of

radicals are dealt with in this thesis, though the majority of work done involved radicals of the oxygen-centered variety.

Since the work dealt with here concerns mainly organic compounds, with the exception being the titanium dioxide discussed in chapter 5, this introductory discussion will focus on the organic radical species which were the subjects of interest for the results discussed later on in this thesis.

The carbon-centered radical species which was studied here is the ketyl radical, an example of which is shown below:

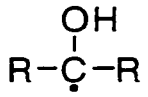

Figure 1.1 General structure of a ketyl radical.

A specific example of a ketyl radical is formed when the triplet excited state of benzophenone abstracts a hydrogen from a donor, as shown, below:

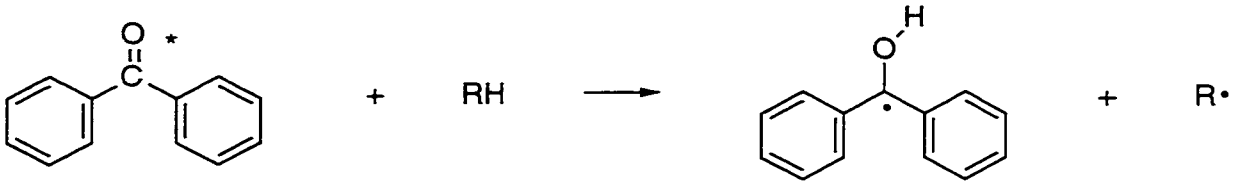

Scheme 1.1 Hydrogen abstraction by excited state benzophenone from a donor to produce a ketyl radical and an alkyl radical.

This particular ketyl radical (with substitutions) is one which was studied in research concerning the effects of applied magnetic fields upon radical populations and lifetimes. This work is discussed in chapter 3 of this thesis.

Of most concern in terms of health issues are radicals containing oxygen. In fact, according to the definition above, molecular oxygen itself would be classified as a free radical, since its electronic configuration is such that there are two unpaired electrons in the outer, antibonding π orbitals.

Probably the most studied radical species in terms of biological systems is the hydroxyl radical. This radical is highly reactive and known to damage biological molecules and tissues[4]. There are three main types of reactions which the hydroxyl radical participates in: hydrogen abstraction, addition, and electron transfer. If the species the hydroxyl radical reacts with is a non-radical species, then a different free radical is produced which may be more or less reactive than the original radical. Usually the radicals produced as a result of reaction of hydroxyl radicals with molecules are less reactive, as hydroxyl is extremely reactive, even in comparison with other radicals.

Hydroxyl radicals can react by hydrogen abstraction with almost any organic molecule, but in order to put its reactivity in context with the types of toxicity discussed earlier, let us assume that the substrate could be an amino acid within a particular enzyme. Hydroxyl radicals are known to react efficiently with amino acids by hydrogen abstraction[5,6]. If the radical were to abstract a hydrogen from the amino acid, then a radical center would be created within the protein. This radical would undoubtedly undergo further reactions which would likely disrupt the structure, and therefore the function, of the enzyme. According to the pathways of toxicity outlined earlier, then, the hydroxyl radical is a toxic species because it disrupts enzymatic processes. Hydrogen abstraction reactions by the hydroxyl radical are also efficient processes with phospholipids (important cell membrane constituents)[4] and with nucleotides and deoxyribose (parts of the DNA structure) [7-10]. Clearly, the hydroxyl radical is extremely toxic via all three pathways as a result of its high reactivity, and consequently low selectivity in terms of substrate.

The reactivity of one particular radical species, the hydroxyl radical, has been outlined above, but to a greater or lesser extent all free radicals may be toxic via at least one of the pathways discussed earlier. The topics to be discussed in the following pages deal with specific types of reaction mechanisms and precursors which may create free radicals or influence their reactivity *in vivo*.

1.2 Magnetic fields, radicals, and carcinogenesis

As mentioned with respect to the hydroxyl radical, attack by free radical species on the DNA molecules within cells[11,12] can lead to irreparable damage to the genetic material (i.e., mutations) which may ultimately manifest itself as the uncontrolled cell growth which characterizes all forms of cancer. It follows naturally from this that any factors which increase either the number of radicals or their lifetime within a cell might contribute to the toxicity of these species.

Within the context of this thesis the free radicals studied are not single species, but rather pairs of radicals, at least when they are generated. The radical pairs studied were created in an environment designed to be somewhat confining (a molecular "cage") so that the two halves of the pair cannot easily escape from one another. This design was intended to mimic the conditions within cells, as membranes such as the one surrounding the nucleus which contains the DNA are in effect cages which would confine any radicals to at least some degree.

If a pair of radicals are generated or "born" together within some sort of cage which keeps them in relatively close proximity of each other, then an applied external magnetic field can influence their reactivity, both toward each other and with the surrounding material. The source of this influence reflects contributions by two factors: the existence of the cage and the radical pair mechanism[13-23].

Radicals, as species containing unpaired electrons, have an overall spin. They are therefore susceptible to the influence of an applied magnetic field. A radical pair produced photochemically will "remember" what spin state the precursor excited-state species had, and be born from its parent with the same spin configuration as a consequence of Wigner's spin conservation rules[24]. A radical pair which is created in a singlet spin state can recombine readily to regenerate the precursor species, but one which is created as a triplet pair cannot recombine until one of the members undergoes a spin rephasing or a spin flip[25,26]. Triplet radical pairs have a non-zero spin angular momentum, unlike singlet radical pairs for which the value is zero. There are three ways (T_+, T_-, T_0) in which the electron spins may be oriented for a triplet radical pair, whereas there is only one spin configuration for a singlet radical pair. These orientations are pictured in figure 1.3 below:

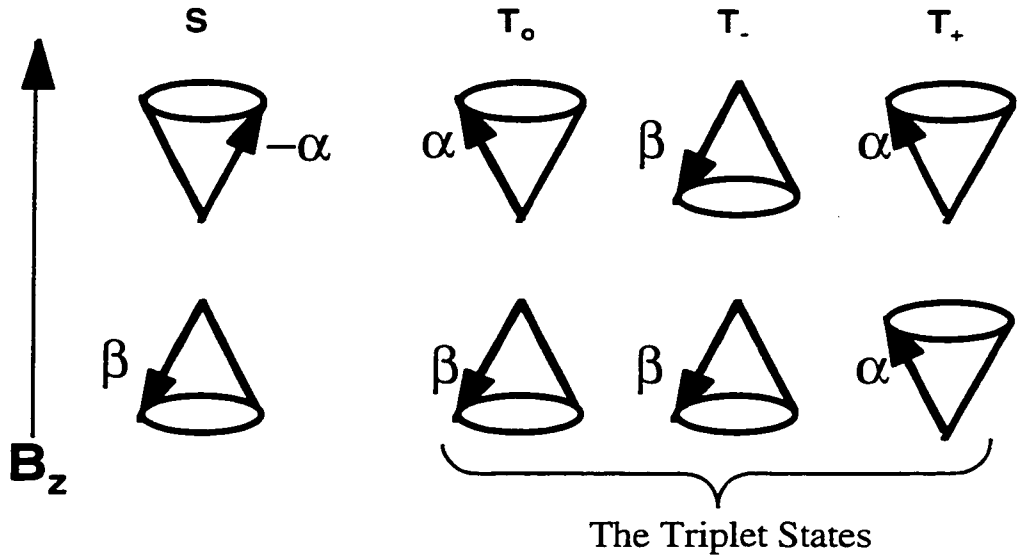

Figure 1.2 Vector representation of the singlet and triplet states of a radical pair.[25]

The z axis pictured above is the magnetic field axis, which is determined by the strongest magnetic interactions which the electron spins experience. As shown, the spin vectors which are precessing along the same direction of the z axis are termed α spins and those which are precessing in the opposite direction are β spins. Since there are two electron spins within a radical pair, the overall spin states are termed $\alpha\alpha$, $\beta\beta$, or $\alpha\beta$ for a triplet radical pair; whereas for a singlet radical pair only one configuration of spin states is available, the $-\alpha\beta$ configuration. These triplet spin configurations correspond to the commonly used designations T_+, T_-, and T_0 states, respectively. It is worthwhile to note that the spin vectors of the singlet state are not in phase, whereas those for the T_0 state are in phase with one another. For the spin configuration of the T_0 state to convert to the S state, then, a rephasing of the spin vectors must take place, whereas in the case of T_+ and T_-, more than a rephasing is required. One of the spin vectors must flip with respect to the z axis in order for interconversion between either T_+ or T_- and S to occur.

In the absence of an external magnetic field, the two ways in which intersystem crossing between the triplet sublevels and the singlet state occurs are through either spin-orbit coupling or hyperfine interactions[25,26].

Spin-orbit coupling involves the interaction between spin angular momentum and orbital angular momentum of the radicals. The magnetic field which is associated with these two momenta is what enables the intersystem crossing mechanism to be possible. There are two situations in which spin-orbit coupling is an important factor in intersystem crossing: when the electron density or atomic number associated with a particular atom is large (the heavy-atom effect), and when a strong interaction between two radical centers exists either through space or through bonds.

Hyperfine interactions also involve the internal magnetic forces of the radicals. In the absence of an applied magnetic field, the three triplet sublevels, T_+, T_-, and T_0 are

nearly degenerate in terms of energy. Hyperfine interactions can promote intersystem crossing from the S state to these sublevels or from the triplet sublevels to the singlet state. The hyperfine interaction involves the magnetic moment of an unpaired electron and the magnetic moment of a nearby nucleus. This interaction, which leads to the precession of angular momentum under a force or torque, can change the orientation of the electron spins between the parallel and antiparallel alignments (with respect to the z axis) and facilitate a spin flip.

An applied external magnetic field can influence the hyperfine interaction mode intersystem crossing, primarily at low field strengths of approximately 10-100 gauss; however, the primary influence studied at the higher fields utilized in the studies discussed in this thesis is the Zeeman splitting effect which is outlined below.

An applied magnetic field removes the energy degeneracy of the triplet sublevels T_+, T_-, and T_0 as shown below:

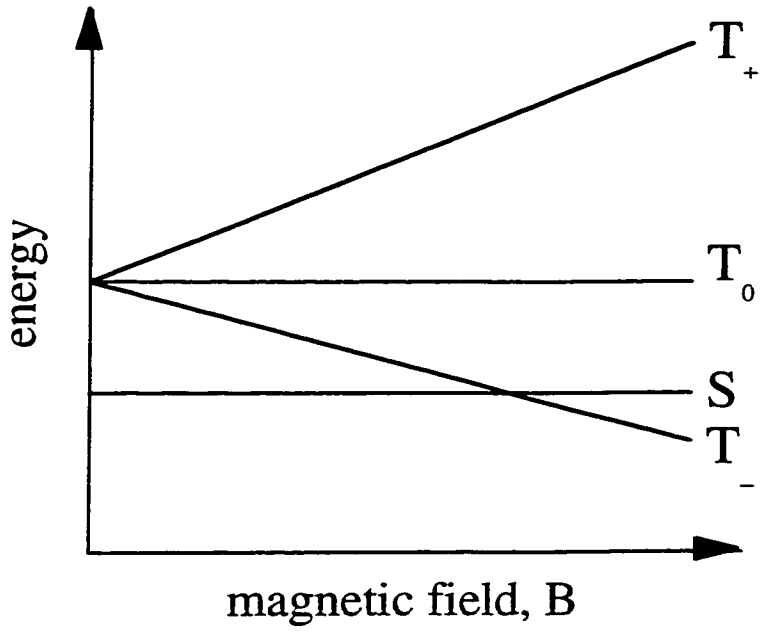

Figure 1.3 Representation of Zeeman slitting of triplet sublevels in the presence of an applied magnetic field[27].

As the strength of the magnetic field increases, so does the energetic separation between the T_+ and T_- sublevels from the T_0 level, which remains unaffected by the field. The consequence of this energy separation is that intersystem crossing from the T_+ and T_- sublevels is slowed down and eventually shut off, leaving only the T_0 sublevel as a pathway for conversion between the triplet state and the singlet state. It is important to note that this effect has nothing to do with the actual energy gap, as these energy splittings are insignificant compared to the thermal energy, kT. It is merely a reflection of the decrease in the probability of transition due to the absence of an energy matching between the T_+, T_-, and S states.

A triplet radical pair which is born together from an excited triplet state and which is confined in some way (within a micellar cage, for example) which is exposed to an applied magnetic field, then, cannot recombine to form products as readily as in the absence of a field, as the intersystem crossing which allows conversion to the singlet state which is necessary before recombination is slowed down dramatically by Zeeman splitting of the triplet sublevels. The proportion of radicals which diffuse away from their original partners and escape the cage is therefore greater in the presence of an applied field than in its absence. The radicals which escape from the cage are then free to react with whatever material is within their proximity. In the case of complete deactivation of the T_+ and T_- states to S by intersystem crossing, 2/3 of the radicals are free to escape the cage and only 1/3 can recombine[22]. These 2/3 are therefore available to undergo other reactions, reactions which could be damaging to the system under study. A diagram depicting the radical-pair mechanism is provided in chapter 3.

There is another factor which comes into play within caged radical pairs; however. Diffusion of the partners within the micelle also affects the intersystem crossing process. In solution, a triplet radical pair will separate from each other and not normally return to within each other's proximity. Within a cage, though, the pair may undergo several

separation/reencounter cycles before one of the radicals eventually escapes from the micelle. It is when the two radicals are relatively far apart from each other, yet within the cage, that spin evolution can occur, which may lead to a geminate recombination when the two halves of the pair "find" each other again.

In a biological system the radicals are not usually created in pairs as in the model systems studied here. The pairs can be formed by the random approach of two radicals to within proximity of each other that have been created via various processes (e.g., enzymatic pathways). Spin statistics predict that random encounters of radicals lead to the triplet spin state 75% of the time, while 25% of the time a singlet spin state is the result[24]. It would therefore be expected that an applied magnetic field has a significant influence over the proportion or random radical pairs that may combine with each other versus those which can diffuse away from each other and undergo other, possibly damaging, reactions with other biomolecules. The radical-pair mechanism, then, is not merely a rationale for explaining what happens when a triplet radical pair is created via a photochemical process from a precursor within a confining environment, but rather a plausible mechanism for the role magnetic fields may play in Carcinogenesis by increasing both the concentration of free radicals within a cell, as well as their lifetime. Since radical species are quite reactive with various molecules (amino acids, nucleic acids, membrane constituents) the overall effect of the magnetic field is to allow a greater amount of toxic species access to targets for an increased length of time. The field itself, then, is a toxin in that it is a contributor to the toxicity of other species.

1.3 Peroxyl radicals

The hydroxyl radical was discussed earlier to illustrate the toxicity of free radicals within biological systems. The hydroxyl radical is, in fact, one of the species participating in degradation reactions with the enzymes discussed later in this thesis, but it is also a

member, along with peroxyl radicals, of a class of species referred to as ROS, or reactive oxygen species. The ROS are a broadly-associated group of species which are forms of oxygen (such as superoxide anion), or contain oxygen as a reactive center (peroxyl radicals), which are very reactive with various substrates. The species which was of interest in terms of the laser-specific generation of ROS discussed in chapter 4 of this thesis is a peroxyl radical. Peroxy radicals have been determined to be one of the important intermediates in the process of lipid peroxidation, the process by which cellular membranes are degraded and also one of the toxicity pathways outlined earlier; thus, a preliminary discussion of membrane structure and the lipid peroxidation process, including the role played by peroxyl radicals will be undertaken here.

1.3.1 Membrane structure

Biological membranes are comprised primarily of lipids and proteins. The amount of protein depends largely on the number of functions the protein performs, but an average value is about 50% of the dry weight of the membrane. Some of these proteins are loosely attached to the membrane (extrinsic proteins) while others are tightly bound and even partially or completely embedded in the membrane (intrinsic proteins).

The lipid components of the biological membranes are generally amphiphilic in nature, with long hydrocarbon chains which associate with each other via hydrophobic and Van der Waals interactions. They also contain polar groups which are hydrophilic and therefore prefer to be associated with an aqueous environment. In animal cell membranes the main lipids are phospholipids.

If a lipid is placed in an aqueous environment, the hydrophobic groups will cluster together as far away from the water as they can get, while the polar, hydrophilic groups will orient themselves so as to have maximum contact with the water molecules and become

solvated. The best way for this to occur depends upon the relative amounts of water and lipid present within a given system. The first organized structures formed when phospholipids are added to water are micelles, but as the amount of phospholipid is increased, a lipid bilayer then forms with an aqueous interior and exterior. A single lipid bilayer may form (unilamellar) or several bilayers may form concentrically (multilamellar), if even more phospholipid is present.

It is generally agreed that the lipid bilayer is the basic structure of all cell and organelle membranes, along with the proteins which are present in different areas of the bilayer. Within each half of the lipid bilayer, protein and lipid molecules can diffuse very quickly. Exchange between the two halves of the bilayer, though, is a very rare occurrence. In order for the diffusion process to be quick, the membrane must be fluid. This is achieved through the presence of unsaturated and polyunsaturated fatty-acid side chains in the membrane lipids. Damage to these fatty acids tends to reduce membrane fluidity, which is known to be essential for the proper functioning of the membrane. The presence of the membrane and its integrity are therefore crucial to the proper function of the cell.

1.3.2 Lipid peroxidation

Lipid peroxidation has been broadly defined as the oxidative deterioration of unsaturated lipids[28]. This definition is not particularly informative, but it does imply that an oxidative process is involved in the degradation.

Initiation of a peroxidation sequence in a membrane or polyunsaturated fatty acid is due to the attack of any radical species that has sufficient reactivity to abstract a hydrogen atom from a methylene group of the fatty acid. Since a hydrogen atom has only one electron this leaves behind an unpaired electron on the carbon. The presence of a double

bond in the fatty acid weakens the C-H bonds on the carbon atom adjacent to the double bond and therefore allows the hydrogen abstraction process to proceed more easily than if the fatty acid were saturated. The resulting carbon-centered radical is stabilized by rearranging to produce a conjugated diene. This diene can then further react with oxygen to produce a peroxy radical. Peroxy radicals are quite reactive, and they will react further with the fatty acids by abstracting hydrogen. This is the propagation stage of the process, which may be repeated for a large number of cycles, thus causing further and further damage to the membrane constituents, with resulting formation of lipid hydroperoxides. An alternative reaction for the peroxyl radicals is to form cyclic peroxides[9].

The lipid hydroperoxides formed as a result of the propagation process of lipid peroxidation are relatively stable at normal physiological conditions, but if any transition metals are present in the system their decomposition is catalyzed. Cells do contain some transition metals in forms such as iron salt complexes and non-heme-iron proteins. These compounds can react with a lipid hydroperoxide, causing the O-O bond of the hydroperoxide to cleave, resulting in the formation of an alkoxy radical, as shown in figure 1.4 below:

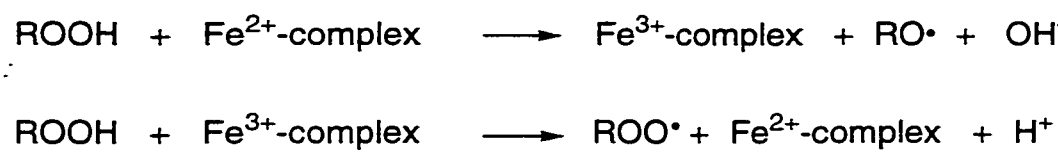

Figure 1.4 Reactions of iron complexes with lipid hydroperoxides[4].

The peroxy radicals produced in the case of reaction of the lipid hydroperoxide with the iron(III) complex are less reactive than the alkoxy radicals produced by hydroperoxide reaction with iron(II) complex, but in both cases the radical products will continue the lipid peroxidation chain-reaction process.

During the process of lipid peroxidation, the propagation series of reactions will usually proceed only to a certain extent before a membrane protein will be encountered by one of the radical species involved in the peroxidation process. This protein can then undergo radical attack and be damaged as well. The result of these radical attacks can be cross-link formation within the protein itself or between proteins.

Overall the general outcome of the lipid peroxidation process is a decrease in the membrane fluidity which is so crucial to its proper function. The membrane may then become more permeable to substances which are normally not able to cross it. In addition to this, the cross-linking within and among membrane-bound enzymes will definitely interfere with their function.

Lipid peroxidation, then, which is mediated by peroxyl radicals and catalyzed by iron salts, which are invariably present *in vivo*, is the dominant pathway by which peroxyl radicals can be toxic to cells. Any process which acts as a source of such radicals, then, such as the non-linear effect discussed in chapter 4 of this thesis, is definitely a pathway for toxicity.

1.4 Photocarcinogenesis, sunscreens, and titanium dioxide

Photocarcinogenesis is the evolution of cancer as a result of exposure to light. There is abundant evidence to support the conclusion that ultraviolet light exposure increases the incidence of two main types of skin cancers in humans: non-melanoma skin cancers (the most common and easily treated skin cancers) and malignant melanomas (more serious and deadly skin cancers).

Skin cancers do not affect all people equally. Different races are susceptible to varying degrees, and global location also affects the incidence of cancer. These two observations led to the eventual determination that there are two main risk factors for the development of skin cancer; genetic constitution and exposure to ultraviolet radiation[29].

Genetics determines how susceptible people are to photocarcinogenesis by affecting how much ultraviolet radiation is absorbed. Different genes give rise to different skin types with more or less melanin, the substance which gives skin its color. Melanin is a natural sun-protector. It absorbs the light, preventing it from penetrating through the outer layers of skin and damaging cells. Genes, of course, also determine susceptibility to all different types of cancers, but with respect to UV Carcinogenesis the role in skin type is the factor which is more prominent.

The other important factor in determining susceptibility to the development of skin cancer is exposure to ultraviolet radiation[30-32]. Studies have clearly shown that the higher the exposure of a population sample to UV, the higher the incidence of skin cancers within that population. Below is a diagram of the spectrum of light produced by the sun, as well as the actual spectrum of wavelengths which pass through the Earth's atmosphere to its surface. The portion of the spectrum visible to the human eye is from 400-700 nm and the UV spectrum is divided into three regions; UVC (200-280 nm), UVB (280-315 nm), and UVA (315-400 nm)[29]:

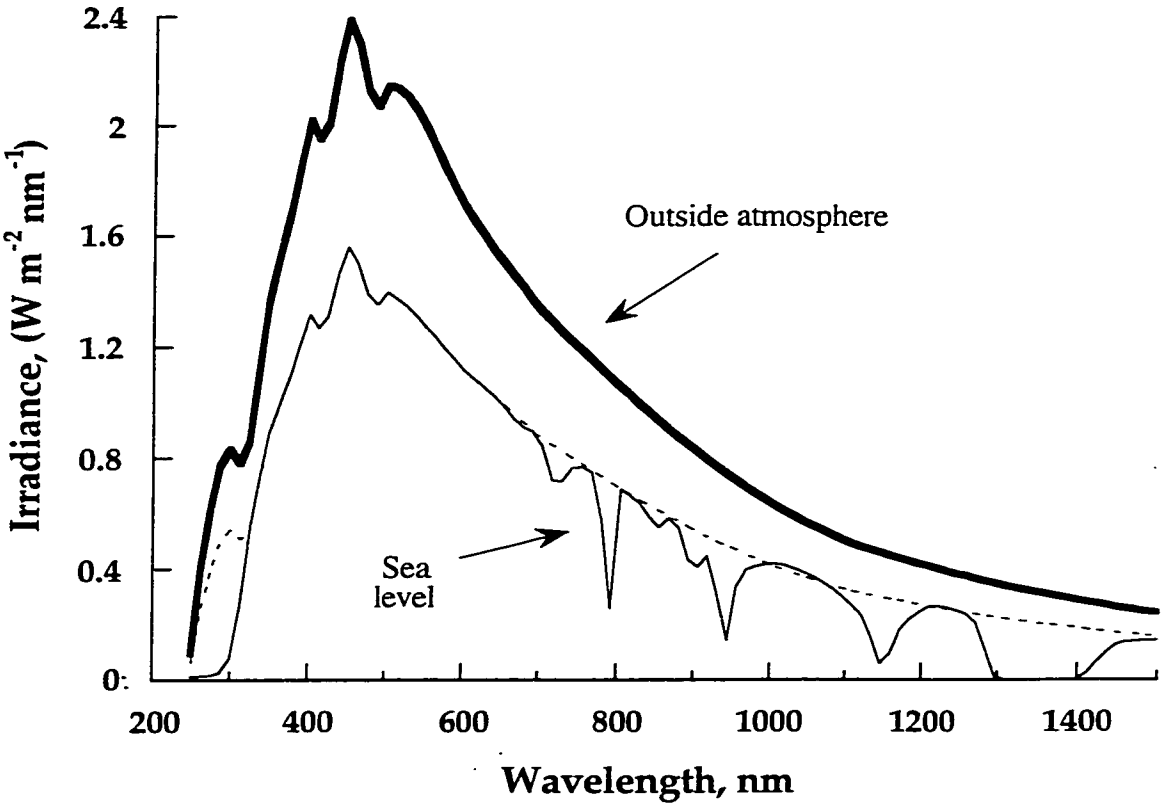

Figure 1.5 Spectrum of electromagnetic radiation produced by the sun as well as the spectrum of wavelengths which actually penetrate to the surface of the Earth (thin solid line)[33]. The dashed line indicates the spectrum of light which would penetrate to the Earth's surface in the absence of atmospheric constituents like ozone.

There are several specific wavelength bands at which the atmosphere attenuates the amount of light which reaches the Earth's surface. This attenuation is due to various atmospheric constituents such as water vapor. A very important role with respect to photocarcinogenesis is played by atmospheric ozone, which absorbs a large proportion of the solar light in the region around 260 nm, where the nucleic acids absorb strongly. Nucleic acid UV absorption has been strongly implicated in photocarcinogenesis[34], so the screening effect by ozone is a natural protective mechanism.

Much research has focused on the efficiency with which various wavelengths within the UV spectrum cause skin cancers, leading to what is known as an action spectrum for Carcinogenesis. Below is such an action spectrum as determined by one study[29]:

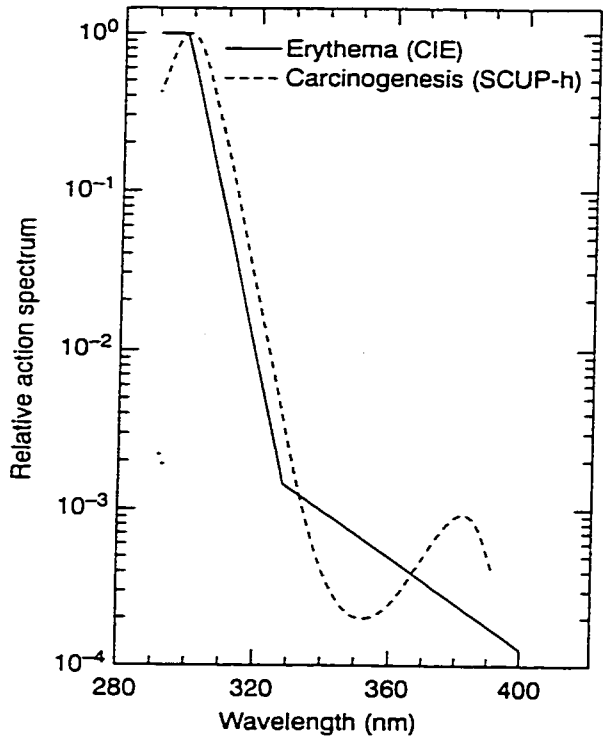

Figure 1.6 Action spectra for erythema (sunburn) and Carcinogenesis[29].

It can be seen in the above plot that the Carcinogenesis action spectrum corresponds very well to the action spectrum for erythema, or sunburn, generation. It would seem possible, then, that a similar initial event is involved in both processes. Further, an action spectrum can indicate the identity of the initial UV-absorbers that are responsible for the initiation of the photocarcinogenic process. The absorbing species could be some target biomolecule such as DNA, which undergoes a structural change as a result of UV absorption, thereby initiating the carcinogenic process. Alternatively, the absorbing species could be one which

does not act directly as a photocarcinogen, but which generates other carcinogenic species upon photoexcitation. An example of such a species would be a singlet oxygen sensitizer such as benzophenone or porphyrin.

Much effort has been made to unravel the pathway of photocarcinogenesis. A lot remains to be done at this point, but so far it has become evident that the pathway is long and complex, perhaps involving the interaction of several different specific UV-induced effects such as the creation of lesions on nucleic acids, effects on intracellular signal transduction, immune suppression, and oxidative stress[29].

Because the link between UV exposure and the development of skin cancers has been clearly established, public health officials have become actively involved in attempting to educate people about the dangers associated with UV light. Since genes and exposure are the two risk factors, and at this time we cannot alter our genetic makeup, the exposure factor is the only one over which we as individuals may exercise any control. The ways in which we can attempt to modulate our UV exposure are by avoiding the sun, using a physical barrier to keep skin from being exposed (hat, clothing), or applying some type of sunscreening lotion to any exposed skin prior to sun exposure.

Because avoiding the sun is not always possible or desirable, and in warm weather people prefer to wear relatively little clothing, sunscreens have become an extremely popular option for those who want to limit their UV exposure. Sunscreens are a branch of the enormously profitable cosmetic industry, with an extremely wide selection in terms of types (lotions, mists), UV-screening efficacy (known as SPF, or sun–protection factor), and price range.

Within the wide variety of sunscreening formulations available, there are two basic types of ingredients; chemical sunscreening compounds and physical sunscreening compounds. Chemical sunscreening compounds absorb UV radiation relatively efficiently, but once excited, they do not undergo any net reaction or energy transfer process and deactivate to the ground state by way of some process such as an isomerization which has

very little, if any, effect on the overall structure and absorption characteristics of the molecule. The same molecule can therefore undergo many cycles of absorption and deactivation. The skin underneath the sunscreen is therefore protected because the radiation is being absorbed preferentially by the chemical compound, and since the compound undergoes no net reaction, no secondary effects from its photoexcitation are induced. Chemical sunscreens are used primarily to protect users from the harmful effects of UVB. Cinnammate compounds such as the one shown in figure 1.6 are often used as chemical sunscreens.

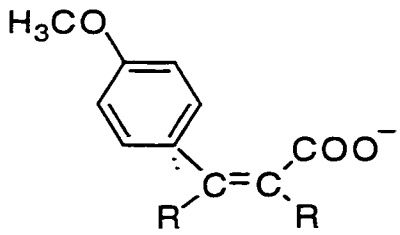

Figure 1.7 An example of a chemical suncreening compound.

Physical sunscreening compounds have become popular additives to sunscreen products in more recent years due to public demand for sunscreens which protect from photoaging, which occurs from exposure to UVA radiation. Most chemical sunscreens afford little protection in this region of the spectrum, so manufacturers turned to using small particles of highly refractive compounds such as zinc oxide and titanium dioxide. These particles scatter light in the UVA region and protect the skin by preventing the light from reaching its surface. The size of the physical sunscreen particles currently used in sunscreens is typically in the range of approximately 30 nm in diameter. The reason for this small size is to improve the esthetic qualities of the sunscreen. People want protection from the sun, but large particles would be visible on the surface of the skin, making it look

white. The drawback to small particles; however, is that the efficiency with which they scatter the light is significantly reduced.

Titanium dioxide is used as a whitening agent in many products such as paints due to its high refractive index. The refractive index depends upon the crystal structure, but has a value of about 2.6[35], which is relatively large as compared to zinc oxide which has a value of only 2.0[35].

It is interesting that as well as being very efficient UVA scattering agents, both zinc oxide and titanium dioxide are semiconducting materials. In the case of titanium dioxide, the band gap corresponds to the energy of light in the UVA region of the spectrum. Absorption of UVA light by titanium dioxide particles in an aqueous, oxygenated medium leads to the generation of several different reactive species such as hydroxyl radicals, superoxide anion, and hydrogen peroxide. These species are known to be toxic to various cellular constituents. Titanium dioxide, then, may not be acting merely as a UVA scattering agent within sunscreens, but may actually play a role as the primary initiator of toxic processes. The research described in chapter 5 of this thesis addresses the issue of the possible phototoxicity of titanium dioxide within sunscreens in relation to their effect on enzymatic activity. It is well-known that enzymes are susceptible to free radical attack due to the presence of numerous electron-rich sites. This property is exploited in the technique of photoaffinity labelling[36], by which the important catalytic residues of an enzyme's active site are identified. The technique involves the design and preparation of a compound which closely mimics the substrate of the enzyme, so that it will be bound by the active site. The difference however, is that there is a constituent such as a diazo group which upon photoexcitation generates a reactive carbene. This carbene may then bond covalently with the amino acid residues of the active site of the protein. Determining where cross-linking of the photoaffinity label with the protein occurs, as the specially designed compound is called, allows determination of which residues are important in catalysis. The free radicals

created via UV photolysis of TiO_2 , then, would be expected to react with various amino acid residues of the enzymes, perhaps affecting the catalytic activity.

The possible toxicity of different free radicals within the various biological model systems, then, is the theme of the research presented here. In the cases of chapters 4 and 5, the focus is on the possible generation of such species as a byproduct of the use of particular chemical compounds and exposure to UV light. In the case of chapter 3 it is the magnetic field which modulates the population dynamics of free radicals which may be naturally present in the system or generated from photolysis of certain pharmaceuticals.

1.4 References:

(1) Zakrzewski *Principles of Environmental Toxicology;* first ed.; American Chemical Society: Washington, 1991; Vol. 2, p 249.

(2) Landis, W. G.; Yu, M. H. *Introduction to Environmental toxicology;* second ed.; Lewis Publishers: Boca Raton, 1999, p 371.

(3) Pascoe, D. *Toxicology;* 1 ed.; Edward Arnold Ltd.: London, 1983; Vol. 149, p 58.

(4) Halliwell, B.; Gutteridge, J. C. *Free Radicals in Biology and Medicine;* first ed.; Clarendon Press: Oxford, 1985, p 331.

(5) Monig, J.; Chapman, R.; Asmus, K.D. *J. Phys. Chem.* **1985**, *89*, 3139.

(6) Hidaka, H.; Horikoshi, S.; Ajisaka, K.; Zhao, J.; Serpone, N. *J. Photochem. Photobiol. A: Chem* **1997**, *108*, 197.

(7) Dunford, R.; Salinaro, A.; Cai, L.; Serpone, N.; Horikoshi, S.; Hidaka, H.; Knowland, J. *FEBS Letters* **1997**, *418*, 87.

(8) Hidaka, H.; Horikoshi, S.; Serpone, N.; Knowland, J. *J. Photochem. Photobiology A: Chem.* **1997**, *111*, 205.

(9) Wamer, W.; Yin, J.; Wei, R. *Free Radical Biol. Med.* **1997**, *23*, 851.

(10) Horikoshi, S.; Serpone, N.; Yoshikawa, S.; Knowland, J.; Hidaka, H. *J. Photochem. Photobiol. A: Chem.* **1999**, *120*, 63.

(11) Koch, T.; Ropp, J. D.; Sligar, S. G.; Schuster, G. B. *Photochem. Photobiol.* **1993**, *58*, 554.

(12) Armitage, B.; Yu, C.; Devadoss, C.; Schuster, G. B. *J. Am. Chem. Soc.* **1994**, *116*, 9847.

(13) Kleinman, M. H.; Shevchenko, T.; Bohne, C. *Photochem. Photobiol.* **1998**, *68*, 710.

(14) Fujiwara, Y.; Yoda, K.; Tomonari, T.; Aoki, T.; Akimoto, Y.; Tanimoto, Y. *Bull. Chem. Soc. Jpn.* **1999**, *72*, 1705.

(15) Nakamura, Y.; Igarashi, M.; Sakaguchi, Y.; Hayashi, H. *Chem. Phys. Lett.* **1994**, *217*, 387.

(16) Evans, C.; Ingold, K. U.; Scaiano, J. C. *J. Phys. Chem.* **1988**, *92*, 1257.

(17) Evans, C. H.; Scaiano, J. C. *J. Am. Chem. Soc.* **1990**, *112*, 2694.

(18) Scaiano, J. C.; Abuin, E. B.; Stewart, L. C. *J. Am. Chem. Soc.* **1982**, *1041982*, 5673.

(19) Scaiano, J. C.; Lougnot, D. J. *Chem. Phys. Lett.* **1984**, *105*, 535.

(20) Scaiano, J. C.; Lougnot, D. J. *J. Phys. Chem.* **1984**, *88*, 3379.

(21) Cozens, F. L.; Scaiano, J. C. *J. Am. Chem. Soc.* **1993**, *115*, 5204.

(22) Scaiano, J. C.; Cozens, F. L.; McLean, J. *Photochem. Photobiol.* **1994**, *59*, 585.

(23) Lednev, V. V. *Bioelectromagnetics* **1991**, *12*, 71.

(24) Wayne, R. P. *Principles and Applications of Photochemistry;* second ed.; Oxford University Press: Oxford, 1988, p 268.

(25) Turro, N. J. *Pure Appl. Chem.* **1981**, *53*, 259.

(26) Molin, Y. *Spin Polarization and Magnetic Effects in Radical Reactions*; Elsevier: New York, 1984.

(27) Steiner, U. E.; Ulrich, T. *Chem. Rev.* **1989**, *89*, 51.

(28) Tappel, A. L. *Biochemical and clinical aspects of oxygen*; Academic Press: New York, 1979, p 385.

(29) Hawk, J. L. M. *Photodermatology;* first ed.; Arnold Publishers, Inc.: London, 1999, p 301.

(30) Blum, H. F. *Carcinogenesis by Ultraviolet Light*; Princeton University Press: Princeton, 1959.

(31) Kripke, M. L. *Journal of the National Cancer Institute* **1990**, *82*, 1392.

(32) Katsambos, A.; Nicolaidu, E. *British Medical Journal* **1996**, *312*, 1121.

(33) Coyle, J. D.; Hill, R. R.; Roberts, D. R. *Light, Chemical Change, and Life: A source book in photochemistry;* first ed.; Open University Press: Milton Keynes, 1982, p 406.

(34) Sutherland, J. C.; Griffin, K. P. *Radiat. Research* **1981**, *86*, 399.

(35) Mitchnick, M. A. *Cosm. and Toil.* **1992**, *107*, 111.

CHAPTER 2: GENERAL EXPERIMENTAL TECHNIQUES: LASER FLASH PHOTOLYSIS

2.1 Introduction

All of the research presented in this thesis involved the study of short-lived reactive intermediates at some point. In order to allow for such studies the laser flash photolysis system maintained in our laboratory was utilized. Following is a brief description of this system. Detailed descriptions of the various components are given in the theses of Alain Berenstain, Nadereh Mohtat, and Sonia Corrent[1-3].

2.2 Instrumentation

The laser flash photolysis system at the University of Ottawa employs several different light sources and detection systems. There are two nanosecond laser flash photolysis systems which may employ any of the following lasers as a source: EX530 Lumonics excimer (308 nm), EX510 Lumonics excimer (248 nm), a Molectron UV-24 nitrogen (337 nm), and two Surelite Nd:YAG lasers which may generate pulses at wavelengths of 1066, 532, 355, and 266 nm. The pulses of light emitted from all of these sources are of less than 10 ns duration, which allows for the study of very short-lived species.

2.2.1 Transmission detection

There are several types of detection systems available, depending upon the type of sample and the sort of experiment being performed. In this thesis the main detection system employed was that which measures a change in the optical density of the sample by way of a monitoring beam provided by a pulsed 150 W Xenon lamp. The Δ O.D. is measured as a function of time, which allows kinetic information about the transient being generated to be obtained. The system may be aligned such that the laser beam which generates the transient under study and the monitoring beam are either orthogonal to one another (90° excitation) or at a smaller angle (front-face excitation). Shutters which are computer-controlled allow exposure of the sample to either the laser or monitoring beam at the appropriate time of the experiment. After the laser pulse has generated the transient species of interest, the pulsed monitoring beam passes through the sample and through a monochromator which is computer controlled to select a particular wavelength. The photons of the monitoring beam after passage through the sample are detected by a photomultiplier tube and converted into an electrical signal. This signal is captured by a Tectronix 2440 oscilloscope which is connected to a Power MacIntosh computer equipped with LabVIEW 4.0 software. The software has been developed by people within the laboratory to create a protocol which allows the user to control the system and acquire data. Below is a schematic diagram of the laser flash setup with transmission detection:

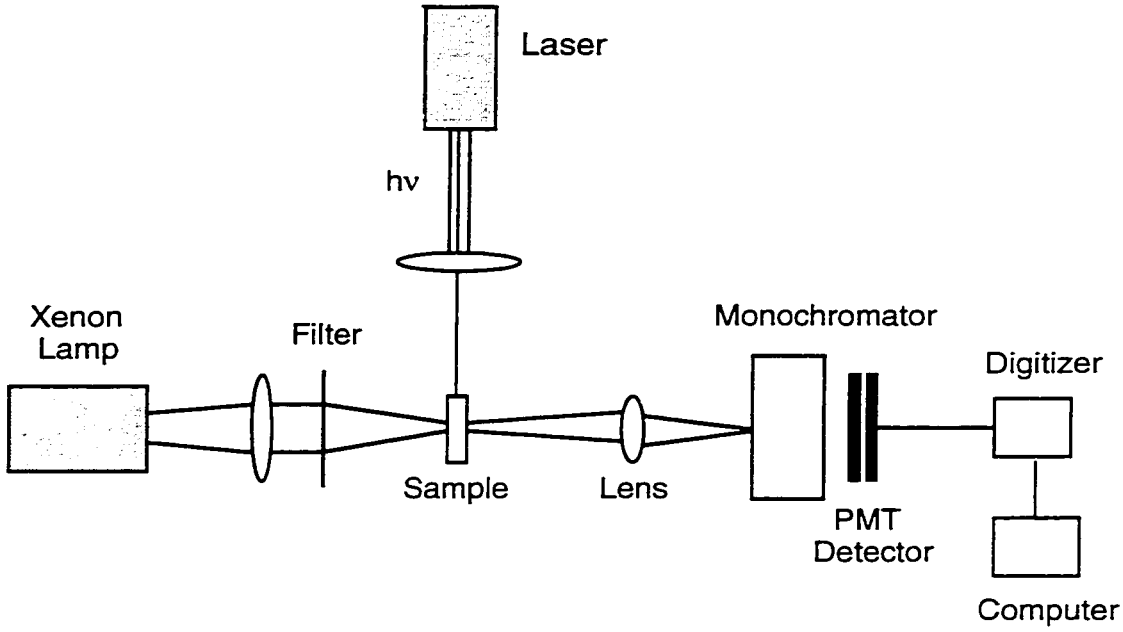

Figure 2.1 Schematic diagram of the nanosecond laser flash photolysis system with transmission detection.

As mentioned previously, the signal from the transient observed on the computer screen is not voltage, but ΔOD. The conversion from voltage to ΔOD was achieved within the LabVIEW software by way of the following expression:

$$\Delta OD = -\log\left(1 - \frac{Signal}{I_0}\right)$$

The acquisition of the absorption spectra of a transient is also possible with the above setup. Kinetics traces at various wavelengths are acquired and the ΔOD at preselected time windows is plotted versus wavelength.

2.2.2 Singlet oxygen detection

The nanosecond system described above is used for optically transparent samples for which an observable change in optical density is detectable upon generation of a transient. There are alternative detection systems available within this laboratory which utilize the same method of generating the transient of interest. One of these alternative detection systems is designed specifically to detect excited singlet oxygen.

Molecular oxygen is somewhat unique because the ground state has a triplet electronic configuration. The energy of this state is 22.5 kcal/mol. Since most excited triplet states have energies in excess of this value, energy transfer from the excited triplet state to oxygen is a common occurrence. The result of this type of energy transfer is the formation ofexcited singlet oxygen. The deactivation of oxygen in its lowest singlet excited state occurs mainly via a radiationless process, but there is a small component which decays through phosphorescence at 1269 nm. This emission can be detected in the laboratory by way of a germanium photodiode, which detects the luminescence from singlet oxygen in a time-resolved manner. This allows both the confirmation of the presence of singlet oxygen and the determination of the kinetics of its relaxation back to the ground state. Use of a standard solution for which the quantum yield of singlet oxygen generation is known , and which has the same absorbance at the laser wavelength as the sample under study allows quantum yield determinations.

The experiments leading to singlet oxygen detection involved concentrating the laser beam with a lens onto the sample to provide excitation. The luminescence was detected at 90^0 to the excitation beam with an EG&G Judson J16 8SP ROM5 germanium photodiode mounted on a modified BNC connector. A silicon filter was positioned between the sample and the detector to filter out any interfering light below 900 nm. Since the luminescence is very weak, the signal was amplified by a Stanford Research Systems low noise amplifier. The gain of the amplifier was typically set at 2-5 x 10^3. The signals were then captured by

a Tectronix 2440 digitizer and transferred to a Power MacIntosh computer for data storage and processing. Figure 2.2 shows a schematic for this type of detection system:

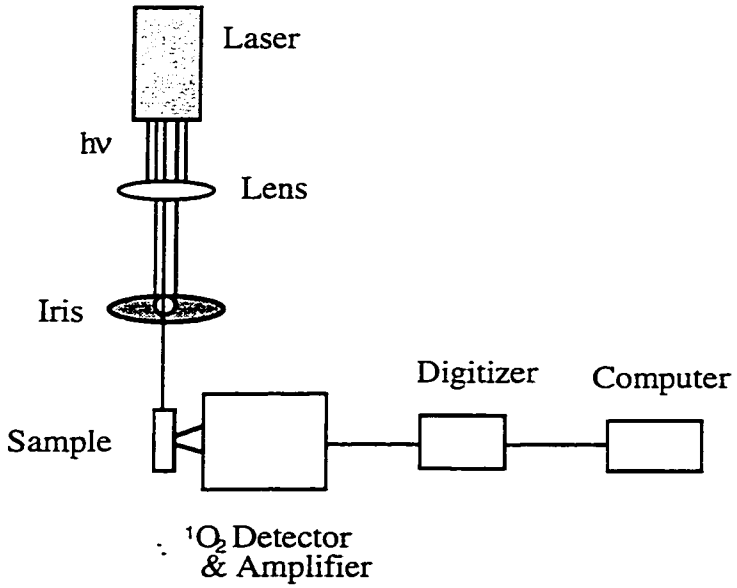

Figure 2.2 Schematic of singlet oxygen detection system.

2.2.3 Diffuse reflectance detection

Detection systems relying on changes in the light transmitted by a sample are useless for samples which are opaque light scatterers; thus, the diffuse reflected light from this type of sample is collected in a time-resolved manner and the same sort of information as that for transparent samples can be obtained. The diffuse reflected light has penetrated into the sample and then returned to the surface and away from it. Through the use of a 150 W pulsed Xenon lamp monitoring beam placed at an angle to the sample and the same light capturing hardware as discussed earlier for transmission detection (monochromator, PMT, digitizer, etc.) kinetic and spectral information about transients generated within

opaque media can be obtained. The difference in the treatment of the data is that instead of absorbances, the Kubelka-Munk function is used[4]:

$$F(R) = \frac{K}{S} = \frac{(1-R)^2}{2R}$$

K in the above equation = 2εC where c is the concentration. R and S are the reflectance and scattering coefficients, respectively. The fraction of the reflected light which is absorbed by the transient species, or the reflectance change Δr is equal to $\Delta J/J_0$ where J_0 is the reflectance intensity before excitation and ΔJ is the change in reflectance intensity after excitation.

Below is the setup for laser flash photolysis with diffuse reflectance detection:

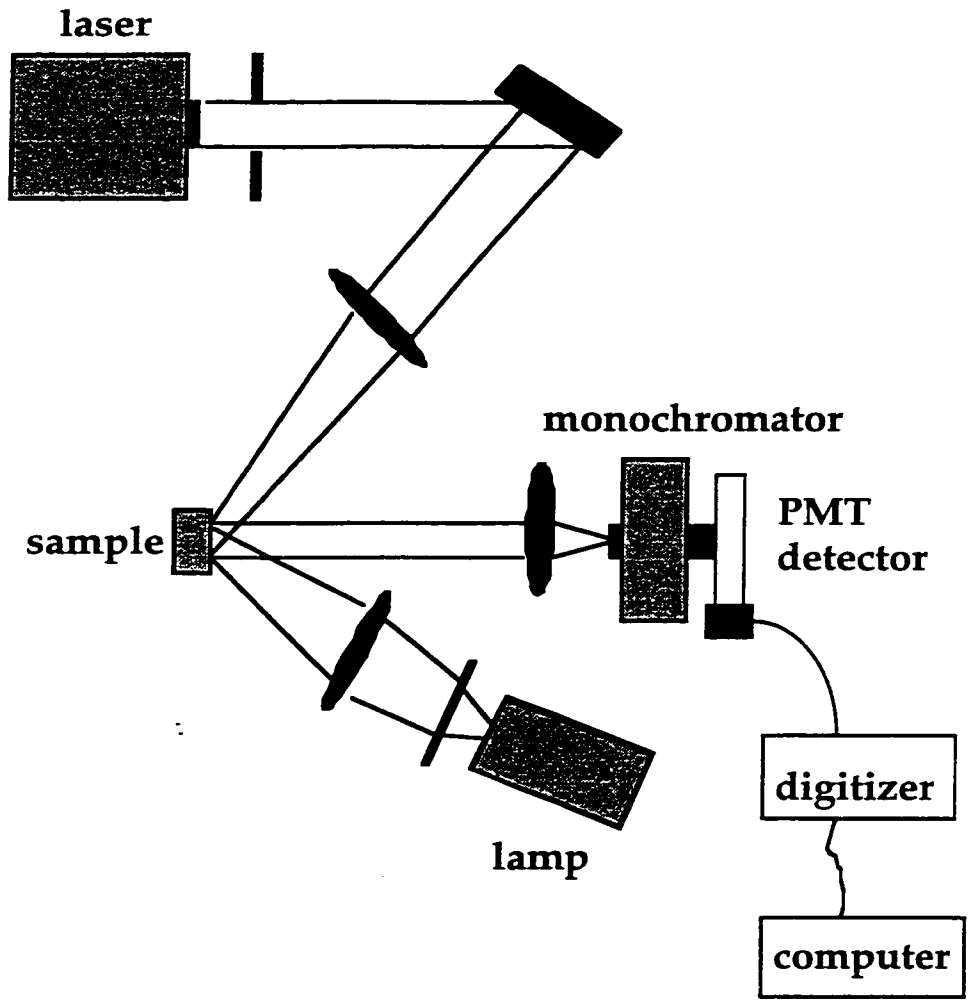

Figure 2.3 Schematic of setup for diffuse reflectance laser flash photolysis.

2.3 Applied DC field

For laser flash studies involving an applied external magnetic field a homemade magnet powered with either a Xantrex XKW 3000 watt DC power supply or a Hewlett-Packard 6282A power supply. The Xantrex power supply at 12 Amps allows magnetic fields of up to 6000 gauss to be produced and the HP power supply allows fields of 2400 gauss to be produced in the region of the sample. The magnet can be removed from the

region around the sample during zero-field experiments. The field strength of the magnet was calibrated with a gaussmeter by A. Thinsandote of the Radiation Protection Bureau of Health Canada and André Simard of the University of Ottawa.

2.4 Sample preparation for laser experiments

The preparation of samples for transmission laser flash photolysis and singlet oxygen laser flash photolysis involves ensuring that the samples have an absorbance value of approximately 0.2-0.5 at the laser wavelength to allow for adequate signal quality and avoid shock waves. The spectrophotometer used to determine the absorbance of laser samples was a Hewlett Packard HP-8451A diode array UV-VIS spectrophotometer.

2.5 References

(1) Berenstain, A. PhD Thesis, University of Ottawa, 1997.

(2) Mohtat, N. PhD Thesis, University of Ottawa, 1997.

(3) Corrent, S. PhD Thesis, University of Ottawa, 1999.

(4) Kubelka, P. *J. Opt. Soc. Am.* **1948**, *38*, 448.

CHAPTER 3: MAGNETIC FIELD EFFECTS ON RADICALS AND THE POSSIBLE INCREASE IN RADICAL-MEDIATED DAMAGE TO DNA

3.1 Introduction:

Thus far a clear-cut, conclusive link between exposure to magnetic fields and health risks has not been established. Contradictory results are more the norm than the exception. An illustration of this comes in the form of a headline in *Chemical and Engineering News*: "Health Effects of Electromagnetic Fields Remain Unresolved"[1].

More than one single mechanism by which magnetic fields could interfere with normal physiology has been proposed during the thirty or so years that the research has been ongoing in this field. Some researchers believe, for example, that the origins of magnetic field effects on health lie in disruption of intercellular communication[2]. Others believe that perhaps magnetic fields interfere with the function of the pineal gland, which produces melatonin[3,4]. Still others subscribe to the theory that the explanation lies in the effect magnetic fields have on the lifetime and population of free radicals produced by the body during normal physiological processes[5,6]. In fact any, all, or none of these mechanisms could be at the heart of any effect which might be established.

The mechanism which was studied in this work was the interaction of magnetic fields with free radicals, specifically radical pairs. It has been well established that external

magnetic fields influence the population and recombination kinetics of radical pairs[7-10] and a model for the possible role of magnetic field effects on free radicals has been proposed by researchers in this and other laboratories[6,11,12]. The experiments which will be described in this chapter were designed in the hope of extending the work done previously, and to determine the possible existence of a magnetic field effect, and to define the magnitude of this effect on a system containing free radicals and DNA. Base damage and DNA cleavage are well-known to occur via reaction of free radicals with this biomolecule[13,14]; thus, through these studies it was also hoped that any effect an applied magnetic field has on lifetimes and populations of free radicals could be correlated with an increase in free radical-mediated damage to the DNA structure. Two complementary approaches were taken. One type of study involved time-resolved laser flash study of free radicals created in solution with DNA. The decay pattern of the radicals was monitored in the presence and absence of an applied magnetic field to determine any difference in either the population or decay rate. The second approach involved steady-state photolysis of solutions containing free radical precursors and DNA in the presence and absence of an applied magnetic field. After photolysis the DNA was analyzed to determine the amount of strand breaks which were created. Comparisons of the amount of damage created in the presence and absence of the magnetic field were made in an attempt to establish if a cause-effect relationship could be established.

3.2 Results

3.2.1 Search for a suitable radical precursor

The first step necessary in the study of a free radical/DNA system involved finding a free radical precursor with properties which would make it desirable for use in these

studies. The ideal molecule to employ would be one which would associate itself readily with the DNA, so that once excited it would react with the DNA by way of hydrogen abstraction from the helix, creating a radical pair. The first molecules of interest were those which are not soluble in aqueous solution in the hope that they would bind to the DNA molecule, preferably by intercalation between the base pairs. In order for this to occur the molecule would have to be relatively flat. Another desirable trait was a photochemical tendency to intersystem cross efficiently to form the triplet state quickly and efficiently upon excitation. Another tendency desired was for the triplet state to be an efficient hydrogen abstractor. Carbonyl compounds generally exhibit these tendencies, so the "ideal" molecule would be a flat, hydrophobic carbonyl compound to act as the free radical precursor in these studies.

The first step in determining whether or not these molecules would prove suitable for these purposes was assessing their solubility in DNA solutions. In order to be adequate for study enough probe molecule had to enter into solution to give an absorption of > 0.1 above 280 nm. This characteristic was necessary in order to allow for photolysis of probe selectively without any interference by direct DNA absorption. The wavelength of irradiation must therefore be approximately 280 nm or above where DNA has essentially no absorption. Absorption spectra of DNA alone and DNA plus the potential probe molecules were simply compared to determine whether or not sufficient probe concentration incorporates into the DNA structure.

Several compounds were tested for their suitability to act as a free radical probe molecule; phenanthrenequinone (**1**), benzophenone-4'-pyridinium bromide (**2**), benzophenone (**3**), anthraquinone (**4**), 2,3,4,5,6-pentafluorobenzophenone (**5**), duroquionone (**6**), and xanthone (**7**). The chemical structures of these compounds are shown below:

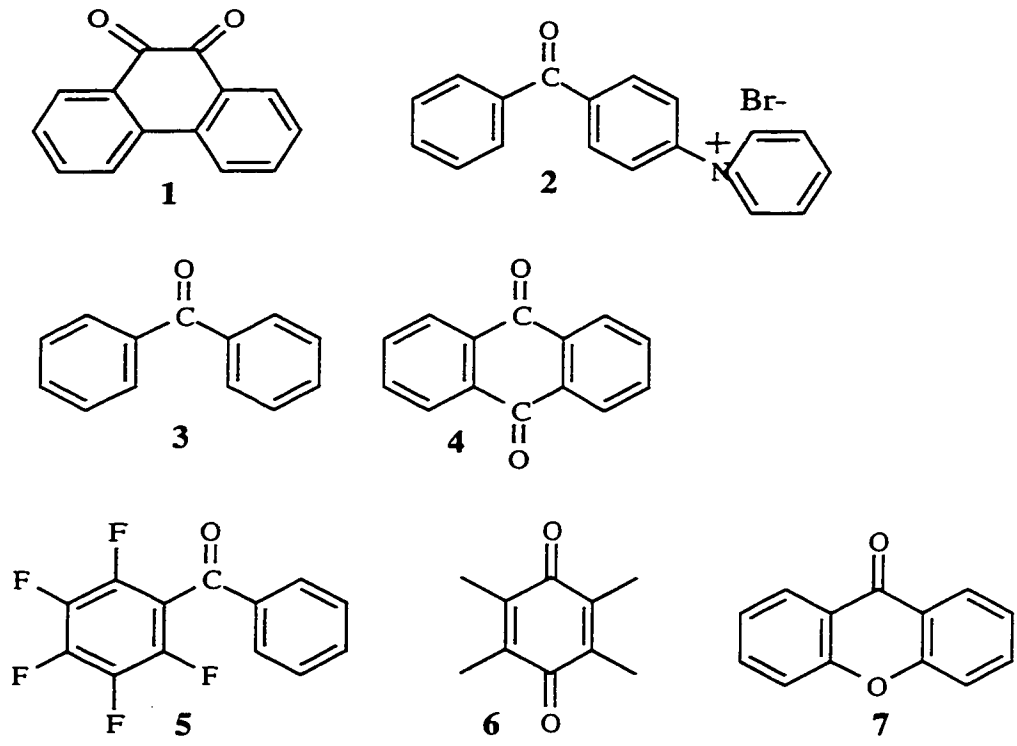

The first step in determining whether these molecules would prove suitable for these purposes was assessing their solubility in DNA solutions. In order to be adequate for study enough probe molecule had to enter into solution to give an absorption of > 0.1 above 280 nm. This characteristic was necessary in order to allow for photolysis of probe selectively without any direct absorption from the DNA interfering. The wavelength of irradiation therefore has to be around or above 280 nm where DNA has essentially no absorption. Absorption spectra of DNA alone and DNA plus the potential probe molecules were simply compared to determine whether or not sufficient probe concentration incorporates into the DNA structure.

3.2.2 The ethidium bromide technique

The next step after the solubility tests were complete was to irradiate the probe molecules in the presence of DNA and determine whether these free radical precursors cause lesions to the DNA helix. The assay for damage used was the ethidium bromide fluorescence technique pioneered by LePecq and Paoletti [15-17]. This technique involves treating the DNA with the intercalative dye ethidium bromide (**8**):

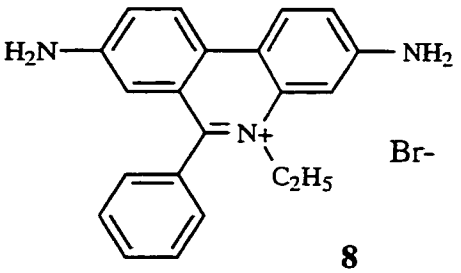

8

When this dye intercalates between the base pairs of DNA, it becomes highly fluorescent in the visible region, with the peak fluorescence centered around 610 nm upon excitation at 510 nm. If the DNA has strand breaks, then the dye does not intercalate where the strand breaks are, and the fluorescence intensity is decreased in comparison to the same concentration of undamaged DNA. The technique is quite sensitive, with a minimum number of strand breaks being easily detected.

It was decided to test this technique with the equipment in this lab and determine if it would be suitable for the free radical/magnetic field systems. DNA was therefore irradiated in solution with 254 nm light, which is well known to cause significant damage, and analyzed afterward with the ethidium bromide fluorescence technique to determine how well different levels of damage could be detected. It should be noted at this point that several different types of DNA from various sources were tested in this fashion to determine if a particular type of DNA is more sensitive to the technique employed for detecting damage. It was determined that calf thymus DNA was suitable for our purposes and it was therefore used most of the time. Other types of DNA were sometimes employed,

such as phage DNA and plasmid DNA, but the bulk of the experiments utilized calf thymus DNA which was purchased for these experiments.

Below are a series of fluorescence spectra acquired after DNA had been photolysed for various times with 254 nm light:

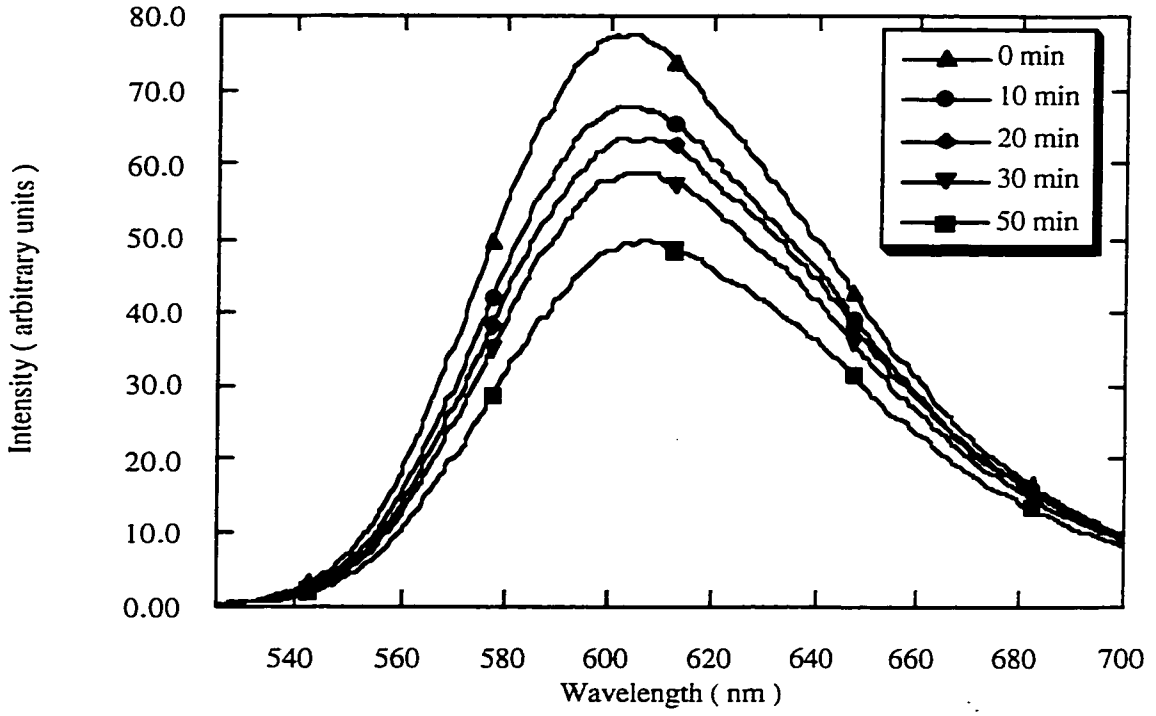

Figure 3.1 Fluorescence curves for **8** ([2.0 x 10^{-12} M] added after irradiation) obtained after 254 nm irradiation of DNA for various times. $\lambda^{exc} = 510$ nm.

It can readily be seen that the fluorescence steadily decreases with time, indicating that the amount of damage to the DNA is steadily increasing upon irradiation. Another way of looking at the same data is to view the fluorescence intensity vs. time at a given wavelength:

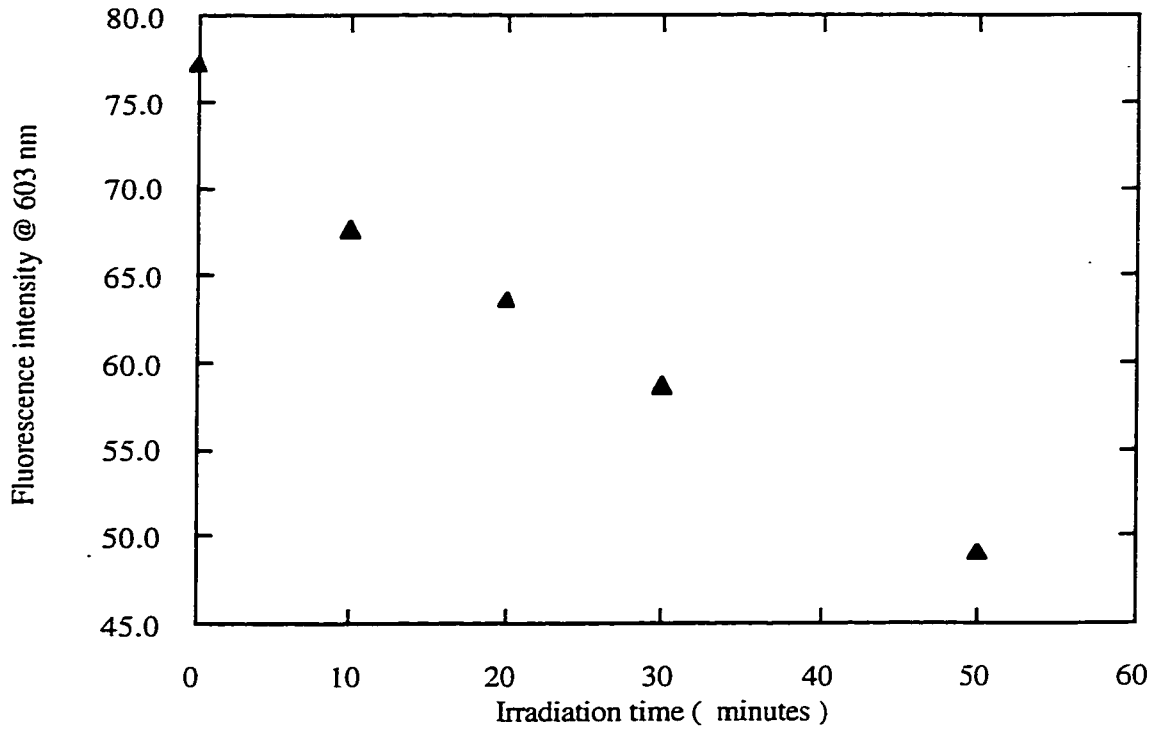

Figure 3.2 Plot of fluorescence intensity vs irradiation time for DNA photolysed at 254 nm. $\lambda^{exc} = 510$ nm

It can be seen that from Figure 3.2 that the fluorescence decreases steadily with irradiation dose. The decrease was expected on the basis of the papers describing the assay, so at this point we were quite confident that the assay would suit our needs as a tool to assess DNA damage.

3.2.3 Photolysis and assay of DNA/probe molecule solutions

To determine whether the probe molecules studied did in fact cause damage to DNA upon photoexcitation, solutions were prepared of probe molecule plus DNA and they were photolysed with UV light > 280 nm. After the photolysis was complete, the DNA samples were treated with the ethidium bromide dye and the fluorescence spectra were acquired to determine how much, if any, damage had occurred. In order for more accurate comparisons to be made, the spectra were integrated over the peak emission wavelengths and the areas were recorded, instead of simply comparing the peak intensities. Below are the results obtained from the fluorescence assay when the maximum amount of **1** was dissolved with phage DNA and irradiated at 300 nm:

Sample	Time Photolysed (min)	Integration Window	Area	Contains 1
1	30	590-620 nm	5131	Y
2	30	590-620 nm	5504	Y
3	30	590-620 nm	5643	N
4	30	590-620 nm	5616	N
5	0	590-620 nm	5305	N

Table 3.1 Area values of fluorescence spectra of ethidium bromide for samples of DNA irradiated in the presence and absence of **1**.

These values are not very different from one another, and the dark sample has a lower intensity of fluorescence than those which were photolysed, which is contrary to what should be observed. The most likely source of scatter in the data is the lack of a sufficient number of samples. The irradiations were performed in quartz fluorescence cuvettes with round tops which could easily be capped for the purposes of nitrogen purging. The sheer expense of these cells limited the number which were available for use in any one experiment. Another experiment which utilized **4** as the probe molecule showed a similar scatter:

Sample	Time photolysed (min)	Integration window	Area	Contains 4
1	0	590-620 nm	1438	N
2	0	590-620 nm	1326	Y
3	60	590-620 nm	1246	N
4	60	590-620 nm	1227	Y
5	60	590-620 nm	1252	N
6	60	590-620 nm	1331	Y

Table 3.2 Area of fluorescence curves for various samples irradiated at $\lambda > 280$ nm for one hour in the presence and absence of **4**.

Once again the results are very scattered, with no clear indication that the samples which contained **4** were damaged any more than the ones which did not. Perhaps **4** does not react efficiently with the DNA due to poor binding affinity or whatever reaction it indergoes with the DNA does not cause strand breaks, which is what the ethidium bromide assay detects. Nevertheless, these experiments were continued in the hope of finding a probe which efficiently damages DNA. The next experiment utilized **6** as the free radical precursor:

Sample	Time photolysed (min)	Integration window	Area	Contains 6
1	0	590-620 nm	1178	N
2	0	590-620 nm	1125	Y
3	0	590-620 nm	1051	Y
4	60	590-620 nm	1165	N
5	60	590-620 nm	1078	N
6	60	590-620 nm	1011	Y
7	60	590-620 nm	1063	Y

Table 3.3 Area under fluorescence curves for DNA samples irradiated at $\lambda > 280$ nm in the presence and absence of **6**.

The results this time were not as scattered, with the fluorescence area being consistently less for the photolysed samples as compared to the dark ones. The average

fluorescence loss, however, was 5 % for both the samples which contained **6** and those which only contained DNA. This result was puzzling, but it was later determined that the cutoff filter used in this experiment had some light transmission below 280 nm which was probably allowing some direct DNA photolysis. The damage detected was therefore caused predominantly by direct photolysis of the DNA and not due to the probe molecule, either in this case or in the ones shown previously. The solution to this difficulty would be either using different filters or using a different probe with such a high absorption above 260 nm that any minor direct absorption by the DNA would not occur due to screening by the probe molecule. The problem with the probes utilized to this point was their lack of solubility in the DNA solution. The maximum amount that would go into solution had been used in these experiments, but the absorptions above 280 nm were not very great. It was at this time that ionic species such as **2** began to be considered as possible probe molecules. The positive charge of molecules such as these would make them more water-soluble as well as causing them to be electrostatically attracted to the overall negative charge of the DNA molecule. This would increase the likelihood of the probe binding to DNA and causing damage to the helix upon photolysis. Preliminary experiments led to the conclusion that **2** would likely prove to be the best probe molecule for our needs so it was used for a series of irradiation experiments. Modest amounts of **2**, which is readily soluble, absorb sufficiently that direct absorption of light by the DNA by stray light below 280 nm would not be a problem.

Below are the results obtained after the fluorescence assay was completed for samples which had been photolysed at $\lambda > 280$ nm in the presence and absence of **2** (0.3 mg/ml):

Sample	Time photolysed (min)	Integration window	Area	Contains 2
1	0	590-620 nm	2320	N
2	0	590-620 nm	1627	Y
3	60	590-620 nm	1396	N
4	60	590-620 nm	417	Y
5	60	590-620 nm	1539	N
6	60	590-620 nm	631	Y

Table 3.4 Area of fluorescence curves obtained from ethidium bromide assay of DNA samples photolysed in the presence and absence of **2**.

It can be clearly be seen, in this case, that there is significant difference between those samples which contained **2** and those which did not. Although there was only one sample each of the unirradiated samples, the difference between the two was very large, indicating that perhaps the probe molecule was interfering with the binding of the ethidium bromide. This was encouraging because good binding of the probe was a criteria necessary for the success of the experiments. The other encouraging result was the 68% decrease in fluorescence observed for the samples containing **2** as compared to the 10% decrease in fluorescence for the samples of DNA alone. Although some damage to the DNA occurred by direct photolysis despite the screening by **2**, much more damage had been done in the presence of **2**, indicating that **2** is an efficient DNA cleavage agent. Repeated experiments of the same type gave slightly lower values for fluorescence loss in

the presence of probe (~ 50%), but similar values for fluorescence loss in the absence of **2** (~15%). At this point it was concluded that **2** had all the necessary characteristics to make it an appropriate probe for use in magnetic field studies and such experiments were begun.

3.2.4 Photolysis of 2 in presence and absence of an applied magnetic field

For the experiments involving the magnetic field it was decided to employ phage DNA, specifically PBr 322, as the nucleic acid component of the samples. This decision was undertaken because other experiments had shown that this DNA was the most sensitive to the ethidium bromide assay which we were using. Due to the covalent closed circular nature of this DNA, any strand nicks cause large changes in the conformation, with a single strand break causing relaxation from the supercoiled form and double strand breaks causing conversion to the linear form. For the other experiments with **2**, calf thymus DNA was sufficient, since the differences in fluorescence were quite large, but any magnetic field effect observed was expected to be much smaller in magnitude, so a more sensitive substrate would offer the best chance for resolving such an effect. Below are the results of a typical experiment involving the photolysis of PBr 322 DNA containing ~0.3 mg/ml **2** in the presence and absence of an applied magnetic field:

Sample	Time photolysed (min)	Magnetic field strength (gauss)	Integration window	Area
1	0	0	590-620 nm	568
2	0	0	590-620 nm	583
3	40	460	590-620 nm	376
4	40	460	590-620 nm	383
5	40	460	590-620 nm	355
6	40	0	590-620 nm	385
7	40	0	590-620 nm	368
8	40	0	590-620 nm	472

Table 3.5 Fluorescence area values obtained by ethidium bromide assay for DNA + **2** photolysed in the presence and absence of an applied magnetic field.

The data above looks encouraging if the averages are simply calculated for all samples and these numbers are compared (408 for zero field vs. 371 for 460 G field). The problem is that one value for the area of one sample not exposed to the field is quite far above the other two values and increases the average and standard deviation. If this increase in standard deviation is taken into account, then the average fluorescence intensity from the MF-exposed samples is the same as the unexposed ones, as shown in Figure 3.3, below:

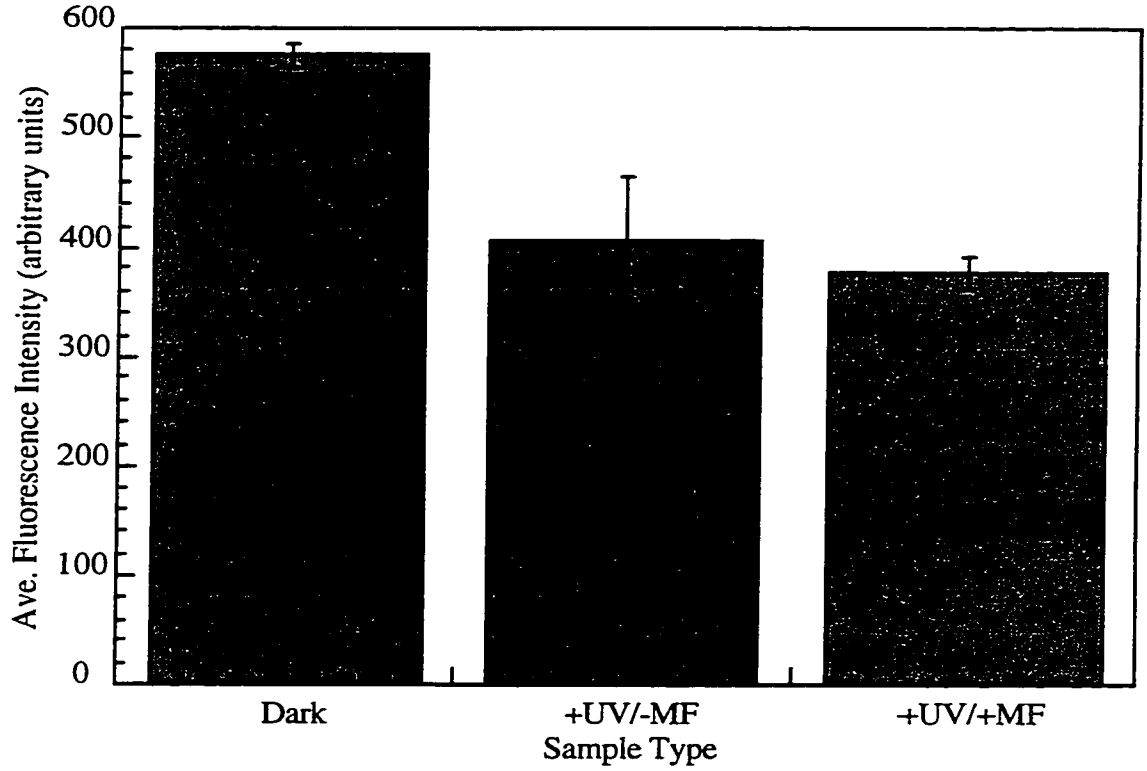

Figure 3.3 Average fluorescence area values obtained for DNA + **2** photolysed in the presence and absence of an applied field. Standard deviations are shown as error bars.

This result could be interpreted in two ways; either the magnetic field does not interfere significantly with the lifetime and population of the radicals created by the photolysis of **2**, or the effect is small enough in magnitude that it can be hidden by the normal variability of the assay technique. The effect of applied fields to systems of this type is well-characterized [7], so the latter is more likely than the former.

It is possible that the radicals are not held together very effectively by the DNA molecule. The rate of escape of one of the partners of the pair would therefore be very

efficient so that any magnetic field effect on lifetime and population would be very slight. The difference in damage done to the DNA with and without an applied field is therefore very small, too small to be detected unequivocally by the ethidium bromide technique.

3.2.5 Photolysis of 3 in micellar/DNA solution

Since no statistically significant increase in damage could be detected with the system containing the pyridyl-substituted benzophenone, **2**, and DNA, it was decided to modify the approach somewhat and utilize micelles as the cage in which to keep the radical pair together, rather than the DNA molecule itself, which appears not to be a very effective cage in these systems. With micelles the radical pair mechanism is well established with respect to magnetic fields[9,18-20] and the fraction of escape of one of the partners is increased markedly by the application of a magnetic field in the case of benzophenone (**3**)[10]. It was decided then, to place **3** in micellar solution which also contained DNA. Compound **3** would be confined into the micelles due to its poor water solubility and upon excitation by UV light the triplet state would be generated very quickly and efficiently[10]. This excited triplet state could then abstract a hydrogen atom from the hydrocarbon chains of the micelle, creating a triplet radical pair which would be susceptible to the effects of an applied magnetic field. See scheme 3.1 below:

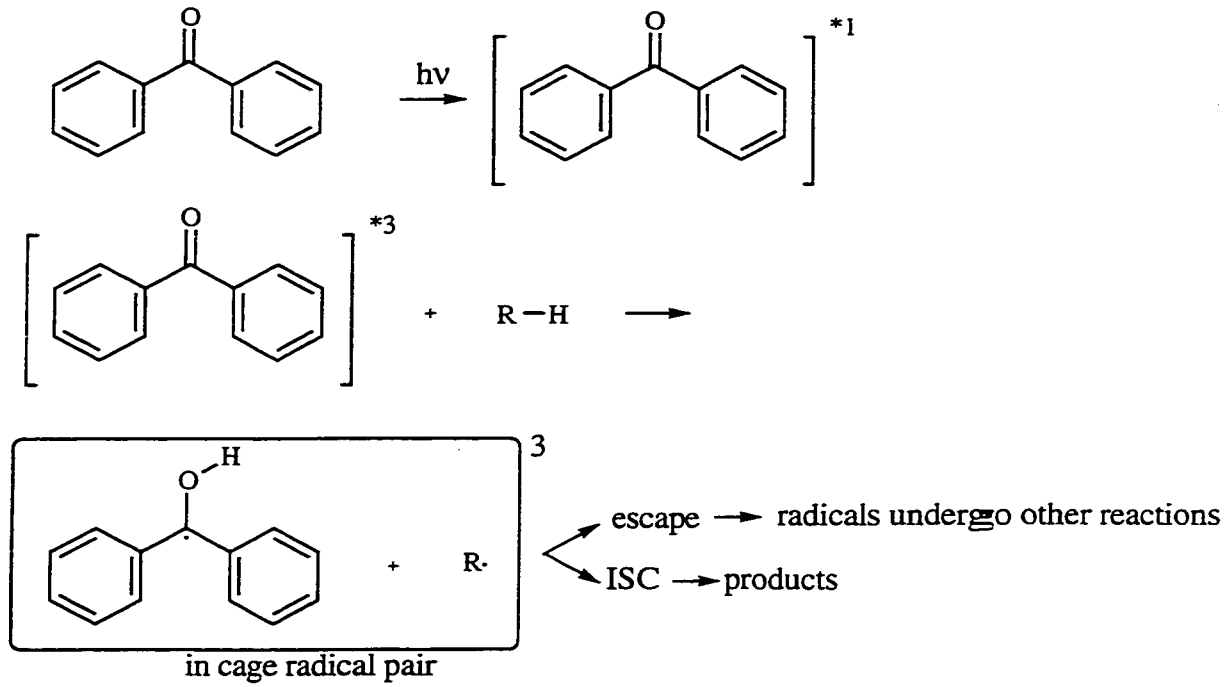

Scheme 3.1 Photoexcitation of **3** in micellar environment to create ketyl / hydrocarbon triplet radical pair in a micellar cage.

Once the triplet radical pair is created, one of the partners can escape from the micelle and undergo other reactions, in this case likely reacting with the DNA which is in the aqueous phase. An applied magnetic field slows down intersystem crossing significantly by way of Zeeman splitting of the triplet sublevels, T_+, T_-, and T_0. Crossing from T_+ and T_- would then be shut off by the splitting, so only 1/3 of the radicals can recombine to form products in competition with the escape. The other 2/3 of radicals may escape the micelle and undergo other processes. The more radicals which escape the micelle, the more which are available to react with the DNA, causing damage to it. This was the rationale which motivated these experiments.

Prior to undertaking these experiments, it was necessary to determine if the presence of the micelles would interfere with the ethidium bromide assay in any way. It is well-known that ethidium bromide associates with surfactants such as SDS and that this

association causes a fluorescence enhancement of the dye[21]. This enhancement would interfere with the DNA assay. It was therefore necessary to determine the relationship between ethidium bromide fluorescence and SDS concentration in this system in order to determine if dilution of the micellar solutions would eliminate the problem and how much dilution would be required. Below is a curve constructed after ethidium bromide fluorescence at various SDS concentrations was determined in the absence of DNA:

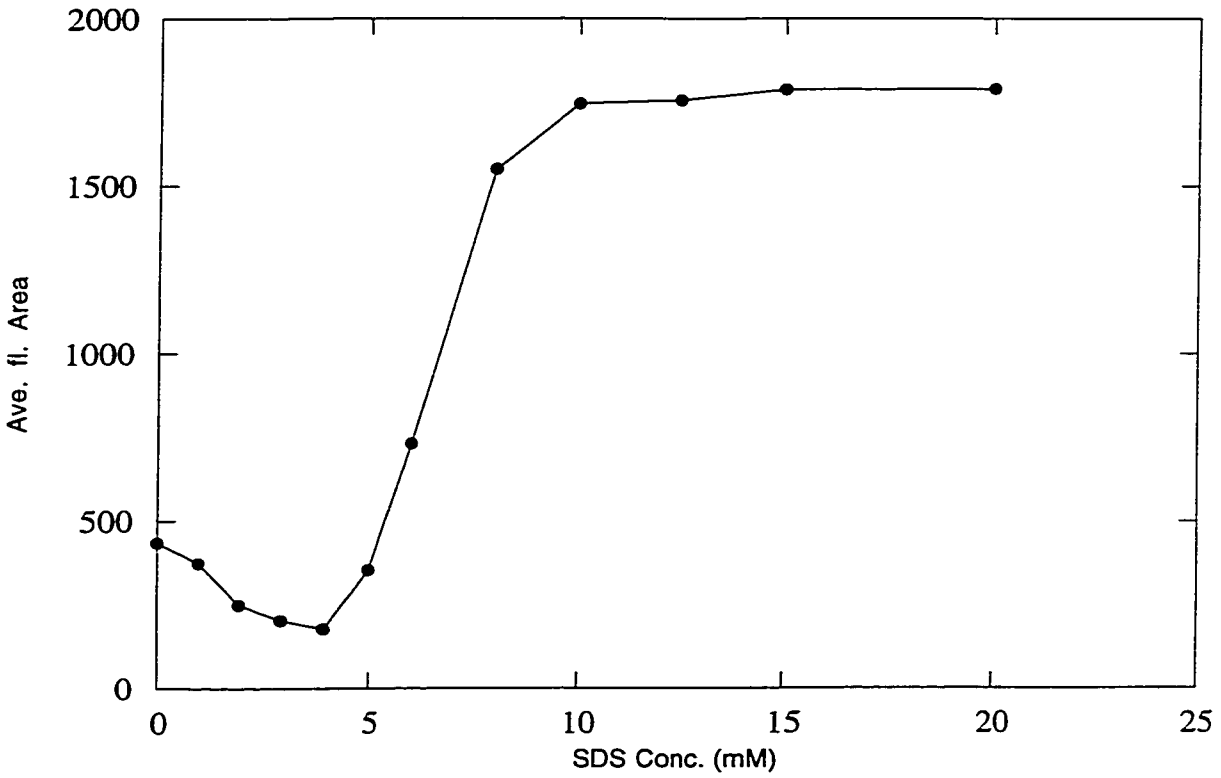

Figure 3.4 Plot of area under the fluorescence curve for ethidium bromide (7.2×10^{-6} M) as a function of SDS concentration in the absence of DNA. λ^{exc} = 510 nm; integration area = 525-700 nm.

From this data it is clear that the fluorescence of ethidium bromide becomes very efficient once the SDS reaches the CMC, or critical micelle concentration. This value is approximately 8 mM for SDS. It was therefore necessary to dilute the solutions after photolysis and destroy the micelles prior to performing the assay to assess the damage to the DNA.

Once these conditions were well established the actual photolysis/analysis of the system containing **3**, SDS, and DNA could be undertaken. Below is a typical set of data acquired after an experiment involving PBr 322 DNA:

Sample	Time photolysed (min)	Magnetic field strength (gauss)	Integration window	Area
1	0	0	590-620 nm	1628
2	0	0	590-620 nm	1628
3	20	460	590-620 nm	1499
4	20	460	590-620 nm	1329
5	20	0	590-620 nm	1411
6	20	0	590-620 nm	1454
7	20	0	590-620 nm	1293
8	20	460	590-620 nm	1388

Table 3.6 Table of fluorescence area values obtained for **3** + SDS + DNA photolysed at $\lambda > 280$ nm.

Interpretation of the data can be facilitated if the average values are shown as in figure 3.5 below:

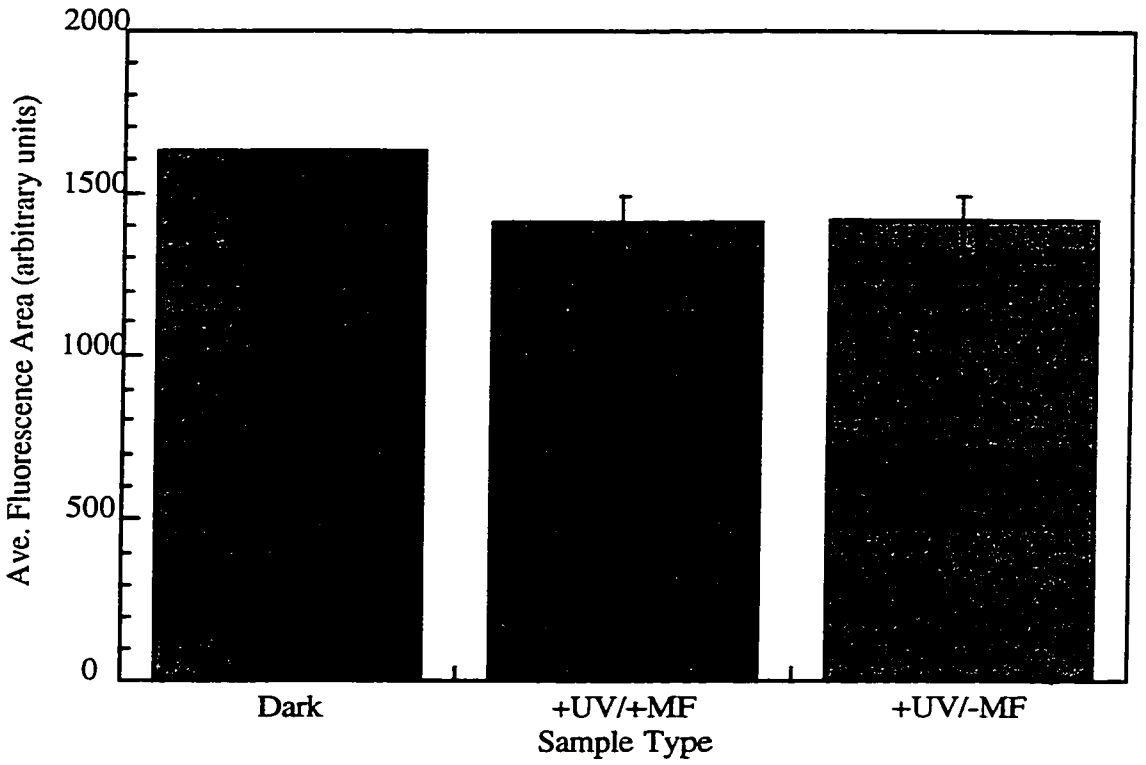

Figure 3.5 Plot of average fluorescence area for samples containing **3** + SDS + DNA photolysed at $\lambda > 280$ nm. Error bars show standard deviation.

The average fluorescence values for the data shown above are 1406 and 1411 in the presence and absence of an applied field, respectively. Essentially there is no difference in the damage done to the DNA, even though according to time-resolved experiments involving **3** in micellar environments and magnetic fields a clear increase in the radical escape from the micelles was shown[18]. It is entirely possible that the difference in damage is small because all of the radicals which escape the micelle would not necessarily react

with the DNA, and even if many of them did, the damage to the DNA which resulted might not lead to strand breaks, for which our assay technique is specific. Also, the dilutions the samples had to undergo would only exaggerate the scatter between them and very possibly mask any small effect.

3.2.6 Association constants

In order to determine if the probe molecules being utilized in the irradiation experiments were actually binding to DNA and to learn how effectively some of the them were binding, attempts were made to determine the association constants between several probe molecules and DNA. An association constant a measure of just how much, if any, of the probe molecules are binding to the DNA. Ethidium bromide fluorescence was exploited in these determinations as well. A set amount of ethidium bromide was added to DNA solution, then varying concentrations of probe molecule were added incrementally. The fluorescence spectra of ethidium bromide was measured at each concentration of probe molecule and a systematic decrease in fluorescence as greater concentrations of probe entered the system was anticipated. This would indicate that the DNA-associated ethidium bromide was being replaced by the probe molecule and a Scatchard plot would yield a value of the actual association constant. Attempts were made to determine values for compounds **2**, **4**, and **6**.

Unfortunately, in the cases of **4** and **6**, no clear downward trend in fluorescence intensity could be observed, even at fairly high probe concentrations. It was assumed then that there is no particular association, other than weak hydrophobic interactions, between the DNA and these molecules. This might explain why the irradiation experiments yielded ambiguous results. If these molecules are not really associated with the DNA upon excitation, then the likelihood that they will react with the DNA to a significant degree is

much reduced. Even if the probe is not associated with the DNA upon reaction, it must be in close proximity to it in order for the hydrogen abstraction process to create a probe-DNA radical pair. By measuring the intensity of fluorescence of a dye, in this case **8**, at various concentrations of **5** it is possible to determine how well **5** binds to DNA. If **5** displaces **8** from its binding to DNA, a result indicated from the assays shown previously, a value of the association constant can be taken from a plot of fluorescence intensities and **5** concentrations. Such a plot is known as a Scatchard plot[22]. One of the forms of a Scatchard plot consists of I/I_0 vs. $I/I_0/C$ where I_0 is the initial intensity of fluoresence of **8** in the absence of **5**, I is the intensity of fluoresence of **8** in the presence of a particular concentration of **5**, and C is the concentration of **5**. This particular form of Scatchard plot has a negative intercept, and the slope yields a value for the association constant of **8** with DNA.

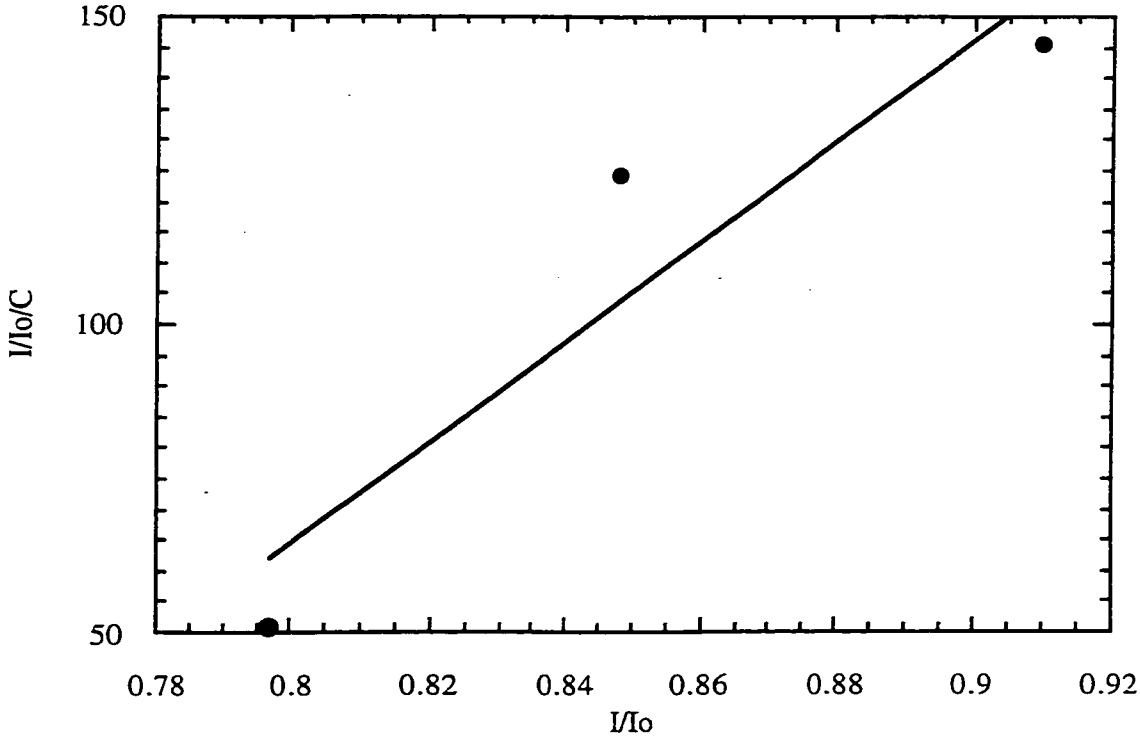

Figure 3.6 Scatchard plot for **2** as measured by decrease in fluorescence of **8** as concentration of **2** increases.

The slope of this plot is 818 ± 110 L/ mol, which is not a relatively very large number. It does, however, support the conclusion previously drawn from the steady-state irradiation experiments that **2** is the best of the probe molecules utilized, at least to this point, in reacting with the DNA upon photoexcitation. Obviously this has a lot to do with the fact that **2** does associate to at least some degree with the DNA molecule which allows for facile H-atom abstraction once the excited state of **2** has been created.

At this time it was decided that time-resolved experiments involving free radical precursors in DNA environments would be undertaken to gain some insight into the actual processes taking place after the generation of the radical pair. Perhaps in this manner some further explanation could be found as to why an increase in DNA damage was not clearly established via the experiments done previously.

3.2.7 Laser flash photolysis experiments

The laser flash experiments were performed utilizing the substituted benzophenone compounds **2** and **5**. Solutions were prepared similar to those used in the steady state experiments with the probe being dissolved in the DNA solution as much as possible in the case of **5**, and a sufficient amount to give an absorbance of ~0.3 in the case of **2**. The laser wavelength used for these experiments was 308 nm, which eliminates direct absorption by the DNA but is in the range where the probe molecules absorb fairly strongly. The photochemical characteristics of the two compounds were expected to be somewhat similar given that they both have benzophenone as the main chromophore with a pyridine substitution in the case of **2** and several fluorine atoms in the case of **5**. An efficient intersystem crossing from the excited singlet state to the triplet state and hydrogen abstraction by the triplet state from the any suitable donor (in this case the DNA) are

behaviors which are exhibited by benzophenone [23]. Fluorinated benzophenones generally exhibit very fast rates of hydrogen-abstraction so **5** was chosen for this reason[24]. Compound **2** is a charged benzophenone-like species with a certain affinity for DNA, so it was hoped that laser flash photolysis experiments involving these two derivatives would reveal similar photochemical tendencies. The benzophenone-like ketyl radical and the DNA radical which would result from the H-atom abstraction would be born with a triplet spin configuration, since the precursor benzophenone was in the triplet state. This radical pair should be susceptible to the application of an external magnetic field. Unlike the steady state experiments, the laser flash photolysis studies allow the direct monitoring of the behavior of the radicals and therefore the determination of any effect on lifetime and population without the need of any probe such as ethidium bromide.

For these experiments the DNA which was utilized was calf thymus DNA, as the amounts necessary were much greater than in the steady state experiments and the cost of other types of DNA is very high. Solutions were prepared containing ~ 50 μg/ml DNA and enough probe molecule to give sufficient light absorption (~0.3-0.4) at the laser wavelength.

3.2.7.1 LFP experiments with 5

Solutions containing **5** and DNA were photolysed at 308 nm and the ketyl radical of **5** was monitored at 540 nm. Only this half of the radical pair generated by the hydrogen atom abstraction could be monitored, but any effect caused by the application of a magnetic field would apply to both radical partners of the pair. The applied field was 1500 Gauss. Traces were acquired in a field-on / field-off, field-off / field-on sequence to be sure that any effect observed was due entirely to the applied field and not simply due to the order of

data acquisition. Several pairs of data were then analyzed by plotting and comparing the normalized decay traces. Below is a set of normalized decay traces:

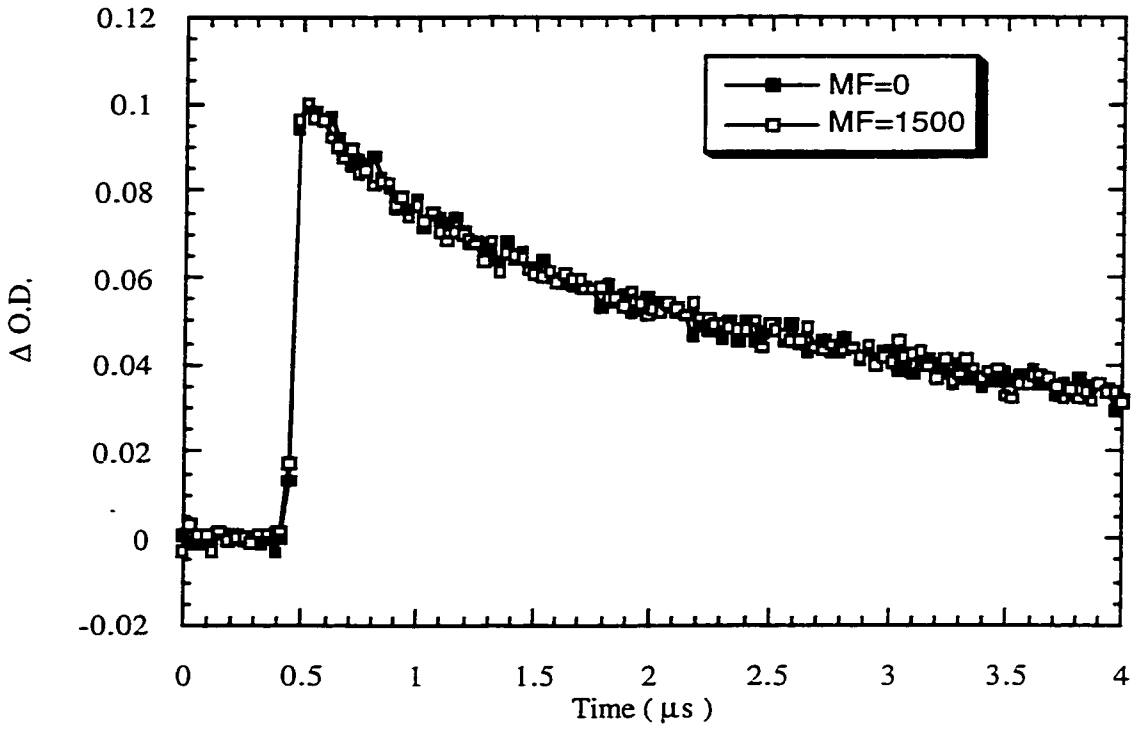

Figure 3.7 Normalized decay traces for the ketyl radical of **5** in the presence and absence of a 1500 Gauss applied magnetic field.

It can clearly be seen that there is no detectable difference in the decay of the ketyl radical in the presence and absence of the field. This result is contrary to what was expected, as benzophenone ketyl radicals are clearly influenced by applied fields in micelles and in protein environments[10,25]. Why then would such an effect be absent in the case of DNA? In order to ascertain whether the effect is very small and not visible by the comparison of only one set of traces, a sum of 10 pairs of data sets was constructed and plotted. The result is shown below:

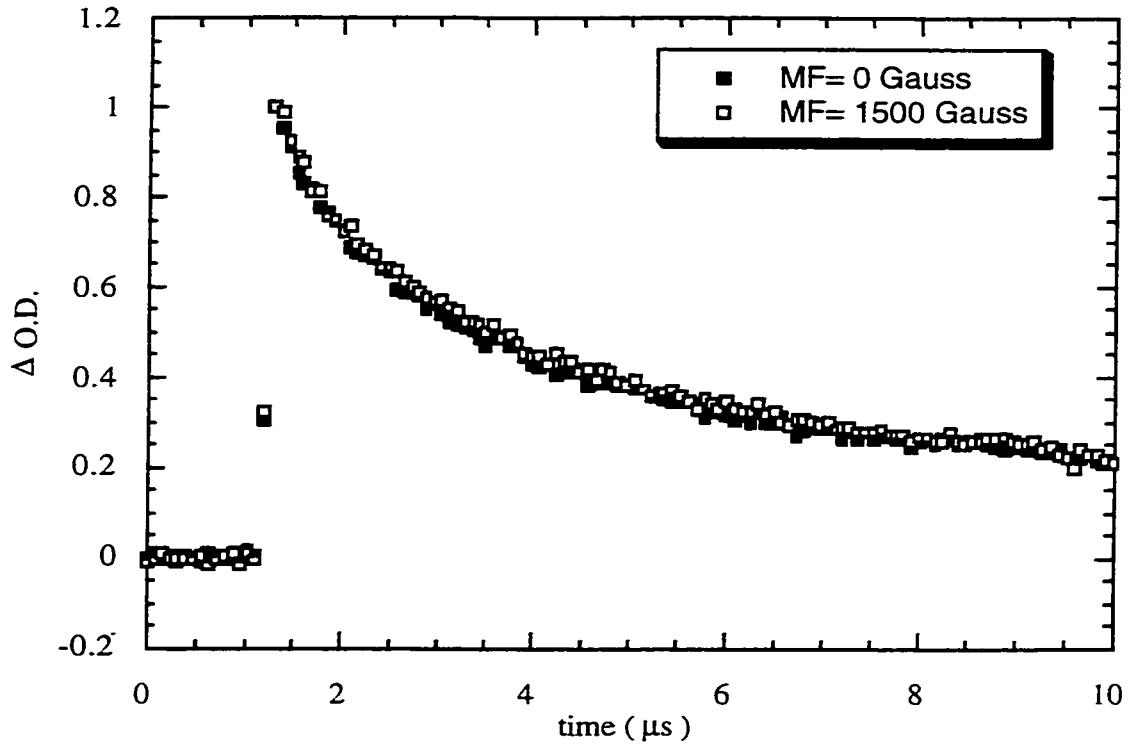

Figure 3.8 Normalized sum of ten decay traces of the ketyl radical of **5** in the presence and absence of an applied field.

Once again there is no apparent difference in the decay rate whether the field is applied or not, with the two traces largely overlapping each other on the entire timescale of the decay. It seemed at this point that even though hydrogen abstraction from the DNA is in fact occurring in this system, as evident by the presence of the ketyl radical, the resulting radical pair is unaffected by a 1500 G magnetic field. This is indeed an unexpected result for a triplet radical pair.

Careful study of the raw decay curves revealed that the top ODs (the first optical density value acquired after the laser pulse) of the traces acquired when the field was applied were systematically higher than the top ODs of the traces acquired in the absence of the field. This could indicate that the magnetic field is affecting the system, but on a very

short timescale. The normalization process is therefore hiding the effect by bringing the two top ODs in line with each other.

Below is a set of individual traces which have not been normalized:

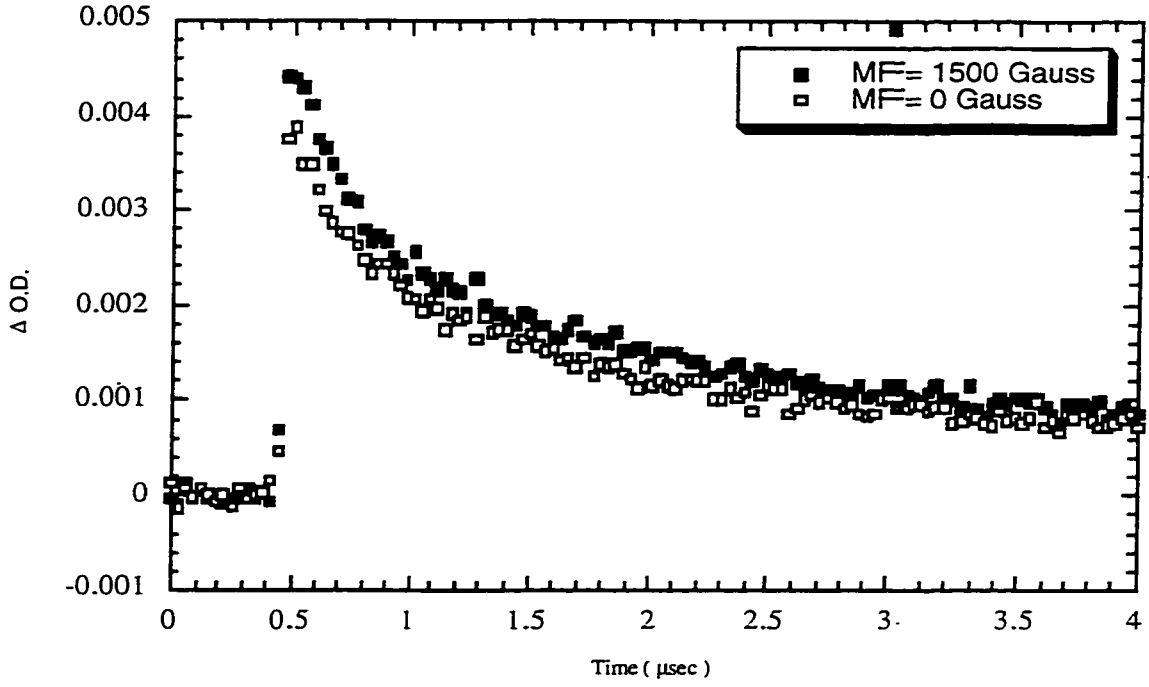

Figure 3.9 Unnormalized decay traces of ketyl radical of **5** acquired in the presence and absence of an applied field.

From these two traces it can be clearly seen that there is in fact a difference, but not on the timescale of the decay. The difference is largely in the yield of ketyl radicals before monitoring begins. The magnetic field then, is affecting the system on a very short timescale. This is likely due to poor confinement of the radical pair. The radicals are not held together long enough for the magnetic field to affect the recombination and escape processes very much or for very long. Essentially the escape process is so efficient that the

spin evolution required to allow recombination cannot compete with escape and therefore no magnetic field can be observed on the timescale of the decay of the radical.

Once it was determined that the normalization process was in fact hiding the effect, several sets of raw data were added together in the same manner as the normalized traces to get an idea of the magnitude of the change in ketyl radical yield. Below are the combined traces from ten sets of data:

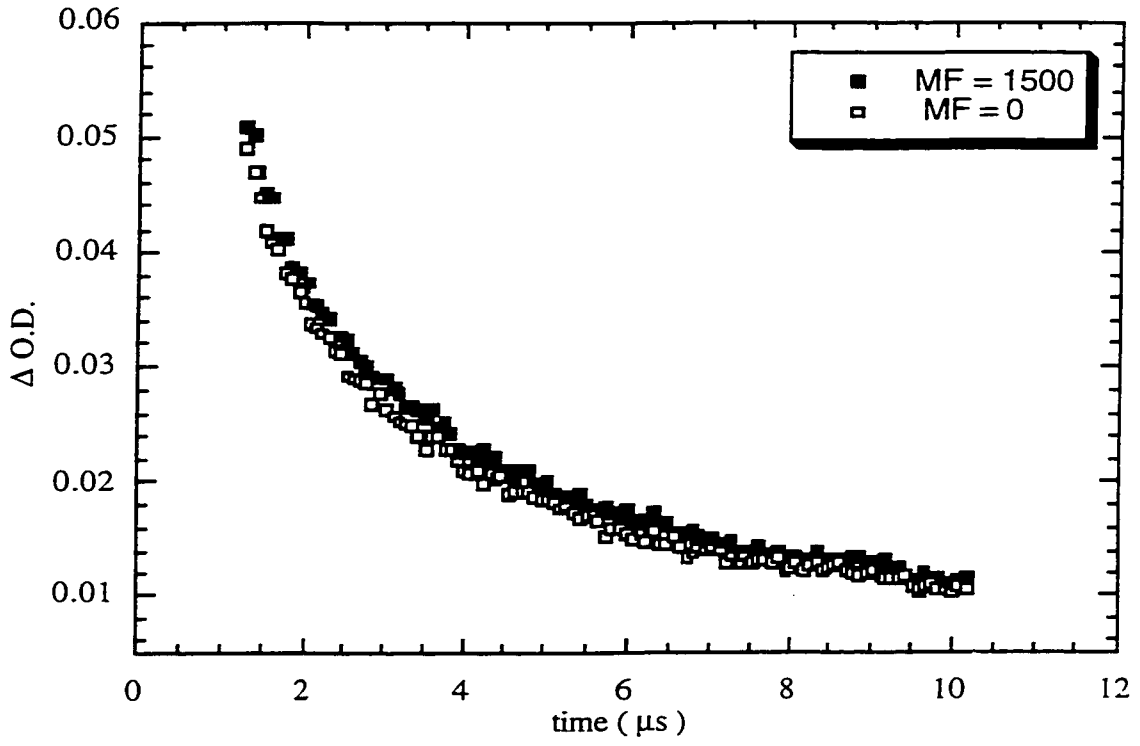

Figure 3.10 Sum plot of ten data traces for decay of ketyl radical of **5** in the presence and absence of an applied field.

The above plot shows that in the presence of the applied field the decay trace is shifted slightly above the trace in the absence of such a field. The difference between the two has appeared before the monitoring begins and continues until the end of the decay process.

Another way of looking at the same data is to plot the ratio of the difference between the two traces divided by the trace acquired without the applied field, as shown in equation 3.1:

$$R = \frac{\Delta OD_{+MF} - \Delta OD_{-MF}}{\Delta OD_{-MF}}$$

Equation 3.1 Equation for the calculation of the ratio between kinetics traces acquired in the presence and absence of an applied field.

where Δ O.D.$_{+MF}$ refers to the linetics trace acquired in the presence of an applied field and Δ O.D.$_{-MF}$ refers to the trace acquired in the absence of a field. R, then, is the difference between the kinetics trace divided by the trace acquired without an applied field. If the applied field increases the population of radical and their lifetime, the R will be a positive number expressed as a precentage of the trace acquired without a field. This equation also allows the determination of the timescale of any effect, as the entire kinetics traces are utilized in the calculation of R. Below is a ratio plot obtained for **5**:

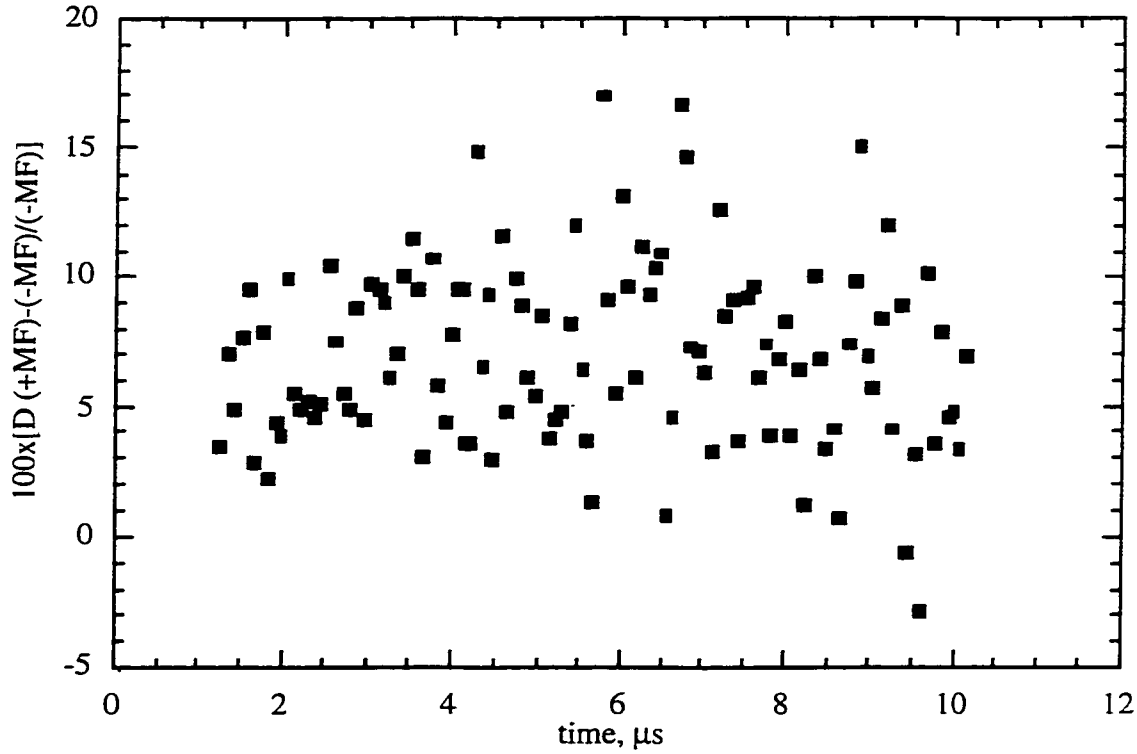

Figure 3.11 Plot of ratio of decay traces for ketyl radical of **5** in presence and absence of applied field.

The above plot of the difference between the traces acquired with and without the applied field divided by the trace acquired without the field. It is therefore the percentage difference between the traces relative to that acquired without a field. Though there is a lot of scatter in the points, it is clear that they fall above the zero line, indicating a clear difference between the traces acquired in the presence and absence of an applied field. The average value for this difference is ~ 6.4 % if the points are averaged, and no trend with time can be seen. This percentage is lower than what is observed in micellar and protein environments [10,23], but nevertheless it is significant and reproducible.

It should be noted that attempts to monitor the triplet state of **5** were made, but at 600 nm, where the triplet has a characteristic absorption, another absorption due to the signal from the radical-anion of **5** is overlapping. Deconvolution of the two was not possible. The only conclusions which could be drawn are that the triplet lifetime is short, and that some electron transfer is occurring as well as the hydrogen abstraction processes.

3.2.7.2 Laser flash experiments with 2

In an attempt to improve the association between the DNA and the probe molecule, a positively charged benzophenone-like molecule, **2**, was used in the steady state photolysis experiments with some success. It was then expected that laser flash experiments with **2** would show an increased effect of the magnetic field on the decay characteristics of the radical pair as monitored through the ketyl radical of **2**.

Below are a typical set of individual decay traces for the ketyl radical of **2** as monitored at 560 nm:

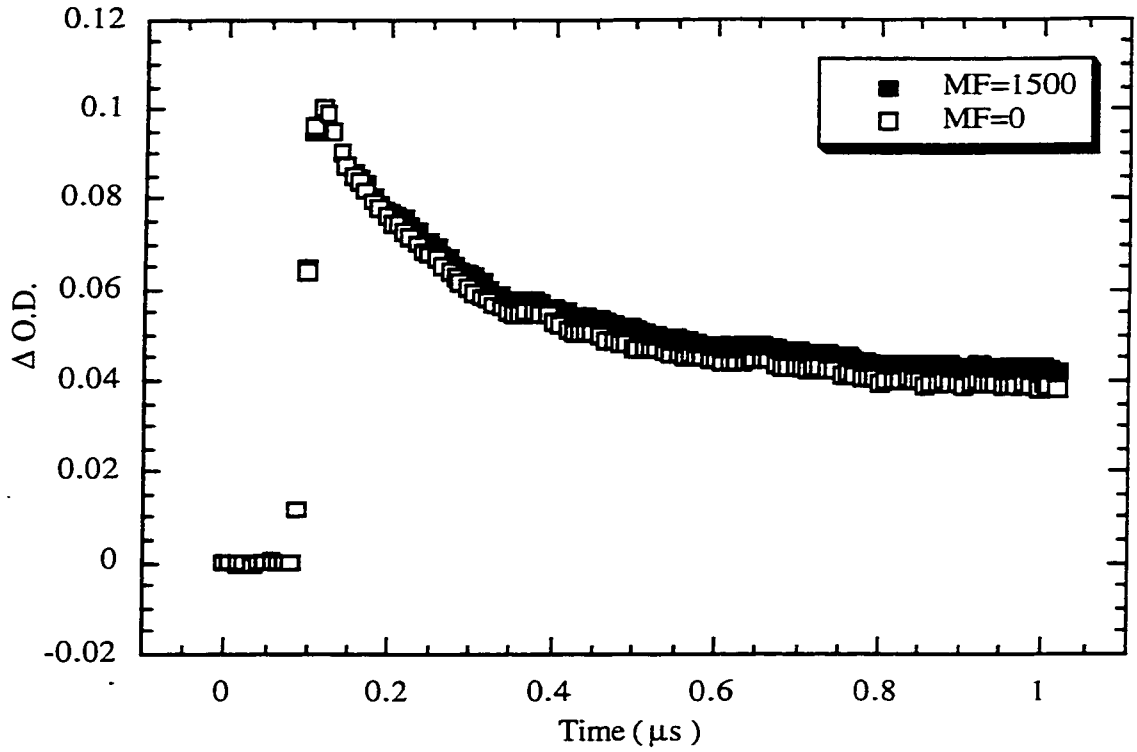

Figure 3.12 Decay traces for ketyl radical of **2** as acquired in the presence and absence of an applied magnetic field.

In this case the two traces have been normalized, and for these results the normalization process does not hide the effect of the magnetic field. Analysis of the raw data indicated that the magnetic field does not affect the beginning of the decay, but over the course of the decay the effect becomes evident as can be seen by the divergence of the two curves over time.

If several sets of data are combined, then a plot such as that shown below is the result :

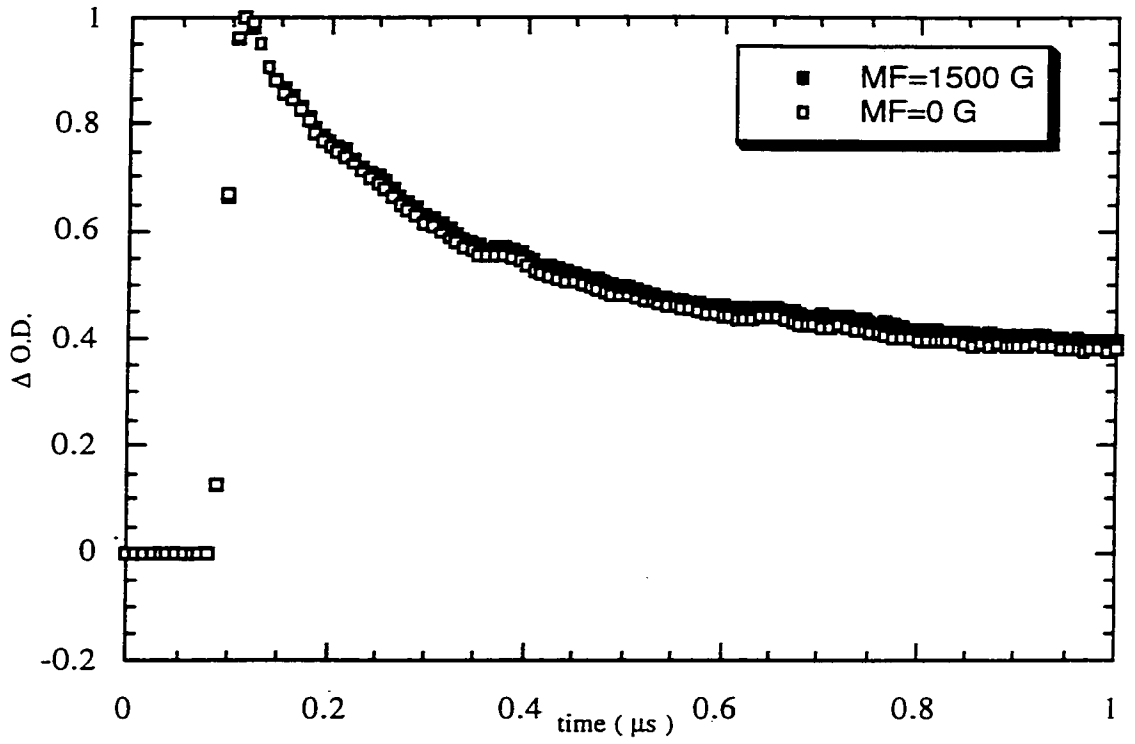

Figure 3.13 Combined decay traces for the ketyl radical of **2** as monitored in the presence and absence of an applied field.

If the difference between the two traces is divided by the trace in the absence of a field as shown previously for **5**, the following ratio plot is obtained:

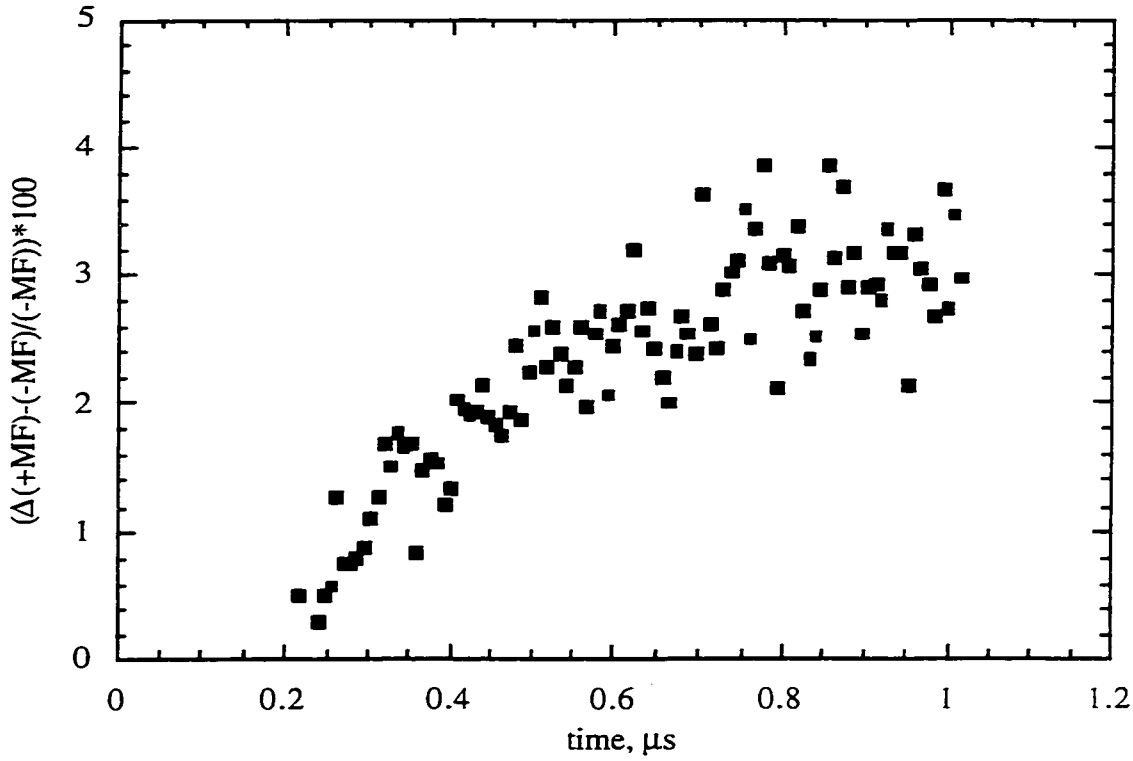

Figure 3.14 Difference between the decay rate of ketyl radical of **2** in presence and absence of an applied field of 1500 G.

The magnitude of the effect in this case is approximately the same as that for **6**, but in this case the effect evolves over the course of the decay of the radical rather than manifesting itself prior to the start of monitoring. It is worth noting that some overlap between the absorption of the ketyl radical of **2** and the triplet state of **2** could be masking some of the effect, but though not great in scope, the change in the decay kinetics of the ketyl radical is real and reproducible in this system.

3.3 Discussion

It is clear from the laser flash photolysis experiments that the radical pairs generated when the probe molecules are excited are affected by an applied DC magnetic field. The lifetime of the radicals is increased and the residual radical population remaining after a period of time is greater when the field is present. This effect occurs because of Zeeman splitting of the triplet sublevels by the applied magnetic field, which slows or shuts off intersystem crossing to the singlet state, as discussed in the introduction section of this thesis. This result is in line with what is expected on the basis of the radical pair mechanism, which was also discussed earlier. A triplet radical pair of which neither can undergo spin evolution cannot recombine to form products within the "cage", which in the time-resolved studies outlined here was DNA itself. The rate at which one of the partners escapes from the cage to undergo other processes was shown to be increased. The effects are not nearly as pronounced, though, as those found in studies using micelles, vesicles, and proteins as the cage holding the radicals together. Obviously DNA does not sequester the radical pair as effectively as these other organized systems. Poor confinement of the radicals allows for the more mobile half of the pair, in this case the ketyl radical of the probe, to easily escape from the proximity of its radical partner. The spin evolution, then, which leads to recombination and which is the factor affected by the magnetic field, becomes relatively unimportant to the overall decay processes. In other systems the competition between these two processes is more even and greater magnetic fields are therefore observed. An interesting difference between these studies with DNA and previous work with micelles and proteins is the timescale on which the magnetic field effect is observed. In the case of **5**, the effect was hidden by the normalization process because it occurs before monitoring of the ketyl radical begins and shows up merely as a consistent increase in the top O.D., which reflects the yield of radicals. The difference, then, between the kinetics of the radicals in the absence and presence of an applied field manifests itself within less than 50 ns. This is much shorter than the effects seen on the microsecond time

scale in the other cage systems studied. While it was not possible to study the triplet state of **5** directly due to interference by the absorption of the radical anion of **5**, the observation of the radical anion itself yielded some information. The radical anion signal evolves rapidly, as there was no evidence for a time-resolved growth. This indicates that the triplet lifetime of **5** is short, though no actual value can be determined. The observation of a signal due to the radical anion of **5** also indicates that some electron transfer reactions between the DNA and **5** is occurring in addition to hydrogen abstraction by the triplet state of **5** to yield the ketyl radical.

In the case of **2**, it appears that electrostatic forces serve to increase the confinement of the radical pair. The effect of the magnetic field upon the kinetics of the decay, while still very small, can still be observed when the traces acquired in the presence and absence of an applied field are normalized, unlike the case of **5**. The effect, while still occurring on a very short timescale, evolves over the course of the laser experiment, as indicated by the ratio plot shown in figure 3.14. This result is similar to what has been observed for radical pairs in proteins and micellar environments. The confinement of the radicals is still relatively poor when **2** is the radical precursor, as illustrated by the short timescale of the effect, but the electrostatic forces which come into play in the case of **2** have a significant effect on the kinetics of escape of the ketyl radicals from DNA. A signal due to the radical anion of **2** was also observed, which again indicates at least some electron transfer is occurring between DNA and the probe molecule.

It is worthwhile to note that since the ketyl radicals of both **2** and **5** were observed via the laser-flash experiements, both of these molecules are abstracting hydrogen from the DNA, probably from the sugars which are on the outside of the backbone. According to studies by Giese et al.[26] this could lead to strand breaks (and oxidized guanine) by cleavage of one of the sugar-phosphate bonds. Subsequent electron transfer from guanine to the sugar radical cation produced as a result of the hydrogen abstraction process would lead to

possible mutations. The observation of ketyl radical then, is an indication that these probes are inflicting damage to the DNA.

In terms of the steady state experiments, the time-resolved results do give some insight. The effects the applied field exerts on the radicals is small as quantified by the laser flash photolysis experiments, so it is not terribly surprising that the amount of DNA strand breaks is not increased to an extent which is readily detectable via the ethidium bromide technique. The magnitude of the change in decay rate and residual signal was found to be about 6% in the cases of **2** and **5**. The reproducibility of the ethidium bromide technique is less than this, with ±10% variation among samples, so that no unequivocal effect can be detected. Also, since the ethidium bromide assay is specific for strand breakage, other lesions which may be caused by reactions of radicals with DNA would not be detected. The handling required, particularly in the case of the experiments with micelles, impairs the reproducibility among samples. The ambiguous yet compelling results obtained via the steady-state irradiations are therefore consistent with the very small field-induced differences in radical population and lifetime measured in the time-resolved experiments.

The magnetic fields applied during these experiments are far in excess of what would be encountered by people in their daily lives, or even by those who are exposed to magnetic fields in their workplace. This fact aside, though, the results obtained suggest the possibility that an applied field does affect the lifetime and population of radicals in a DNA environment. The effect is quite small, but it is measurable.

It should be mentioned at this point that though it may seem that the choice of probe molecules was motivated merely by experimental concerns (i.e., need for compounds which possess certain photochemical and absorption characteristics). Benzophenone-like molecules, however, are in fact part of a class of drugs used as anti-inflammatories (e.g., ketoprofen and fenofibrate). These drugs are known to be phototoxic to some degree[27-33], and this phototoxicity is related to UV light absorption by the benzophenone chromophore.

It may be more biologically relevant, then, to use these compounds as probes for magnetic field effects than it would appear on the surface.

Though no dramatic effects in radical behavior were observed in either the steady-state or time-resolved work outlined here, insight into the radical-pair mechanism was obtained for a system in which DNA acts as both the cage and one of the halves of the radical pair. The answer to the question of whether or not magnetic fields affect human health is still not known, but additional information regarding the possible molecular basis for health effects has been obtained.

3.4 Experimental details

Probe molecules **1**, **2** and **5** were of very high purity and used as received. Compounds **1** and **5** were purchased from Aldrich, and compound **2** was a generous gift from Professor Daniel J. Lougnot. Compounds **3**, **6**, and **7** were recrystallized from ethanol and compound **4** was recrystallized from chloroform.

Laser flash photolysis experiments with compounds **2** and **5** were performed using calf thymus DNA as purchased from Aldrich at a concentration of ~ 200 μg/ml. In the case of **2** the concentration of probe was also ~200 μg/ml, but in the case of **5** the concentration is not accurately known due to the method of preparation. Several mg of **5** were stirred overnight with the DNA solution and the excess probe was removed by centrifugation.
All solutions were prepared in millipore filtered water as early experiments had indicated that the Tris buffer used for the DNA acted as a quencher of the excited states created by photolysis of the probe molecules.

Steady state experiments were performed using calf thymus DNA at a typical concentration range of 50-150 μg/ml. The concentration of probe molecule was the maximum that would dissolve except for the cases of **2** and **7**, where the concentration was typically ~100 μg/ml. Steady state photolysis was carried out in phosphate buffer solutions which did not quench the excited states. Sodium dodecyl sulfate and **8** were purchased as extra high purity products from Fluka and used as received. The concentration of ethidium bromide used for the assay was 1.8 x 10^{-5} M and SDS was 12 mM during photolysis, diluted to 4 mM before assay.

All samples were purged with nitrogen prior to laser flash photolysis or steady state photolysis. Solutions containing surfactant were purged above the solution first, then inside for a short time to avoid excessive foaming.

Steady state irradiations were performed using a Hg/Xe lamp with a 280 nm cutoff filter. A homemade electromagnet capable of generating magnetic fields of up to 500 G was used to supply the applied field. Samples were contained in 10x10 mm quartz Hellma cuvettes. Fluorescence spectra were acquired using a Perkin Elmer LS-50 spectrofluorometer and data was transferred to disk and plotted, if necessary, using Kaleidagraph software.

Laser flash photolysis experiments were performed on the setup described in detail elsewhere in this thesis with samples contained in 7x7 mm quartz cells.

3.5 References:

(1) Hileman, B. In *C. & E. News*; 1993; pp 15.

(2) Belyaev, I. Y.; Alipov, Y. D.; Matronchik, A. Y. *Bioelectromagnetics* **1998**, *19*, 300.

(3) Reiter, R. J. *Biomed. Pharmacol.* **1993**, *47*, 439.

(4) Reiter, R. J. *Biometeorology* **1994**, *1*, 135.

(5) Grissom, C. B. *Chem. Rev.* **1995**, *95*, 3.

(6) Scaiano, J. C.; Cozens, F. L.; McLean, J. *Photochem. Photobiol.* **1994**, *59*, 585.

(7) Scaiano, J. C.; Lougnot, D. J. *J. Phys. Chem.* **1984**, *88*, 3379.

(8) Scaiano, J. C.; Cozens, F. L. *J. Am. Chem. Soc.* **1993**, *115*, 5204.

(9) Scaiano, J. C.; Lougnot, D. J. *Chem. Phys. Lett.* **1984**, *105*, 535.

(10) Scaiano, J. C.; Abuin, E. B.; Stewart, L. C. *J. Am. Chem. Soc.* **1982**, *1041982*, 5673.

(11) Lednev, V. V. *Bioelectromagnetics* **1991**, *12*, 71.

(12) Scaiano, J. C. *The Spectrum* **1995**, *8*, 3.

(13) Armitage, B.; Yu, C.; Devadoss, C.; Schuster, G. B. *J. Am. Chem. Soc.* **1994**, *116*, 9847.

(14) Breslin, D. T.; Schuster, G. B. *J. Am. Chem. Soc.* **1996**, *118*, 2311.

(15) Paoletti, C.; LePecq, J. B.; Lehman, I. R. *J. Mol. Biol.* **1971**, *55*, 75.

(16) Morgan, A. R.; Lee, J. S.; Pulleyblank, D. E.; Murray, N. L.; Evans, D. H. *Nucleic Acids Res.* **1979**, *7*, 547.

(17) Birnboim, R. C.; Jevcak, J. J. *Cancer Res.* **1981**, *41*, 1889.

(18) Cozens, F. L.; Scaiano, J. C. *J. Am. Chem. Soc.* **1993**, *115*, 5204.

(19) Evans, C.; Ingold, K. U.; Scaiano, J. C. *J. Phys. Chem.* **1988**, *92*, 1257.

(20) Scaiano, J. C.; Mohtat, N.; Cozens, F. L.; J., M.; Thansadote, A. *Bioelectromagnetics* **1994**, *15*, 549.

(21) Atherton, S. J.; Dymond, C. M. G. *J. Phys. Chem.* **1989**, *93*, 6809.

(22) Klotz, I. M.; Hunston, D. L. *Biochemistry* **1971**, *10*, 3065.

(23) Turro, N. J. *Tetrahedron* **1982**, *38*, 809.

(24) Boate, D. R.; Johnston, L. J.; Scaiano, J. C. *Can. J. Chem.* **1989**, *67*, 927.

(25) Mohtat, N.; Cozens, F. L.; Hancock-Chen, T.; Scaiano, J. C.; McLean, J.; Kim, J. *Photochem. Photobiol.* **1998**, *67*, 111.

(26) Meggers, E.; Kusch, D.; Spichty, M.; Wille, U.; Geise, B. *Angew. Chem., Int. Ed.* **1998**, *37*, 460.

(27) Maguery, M. C.; Chouini-Lalanne, N.; Ader, J. C.; Paillous, N. *Photochemistry and Photobiology* **1998**, *68*, 679.

(28) Boscá, F.; Miranda, M. A.; Carganico, G.; Mauleón, D. *Photochem. Photobiol.* **1994**, *60*, 96.

(29) Bosca, F.; Miranda, M. A. *J. Photochem. Photobiol., B: Biology* **1998**, *43*, 1.

(30) Martínez, L. J.; Scaiano, S. C. *J. Am. Chem. Soc.* **1997**, *119*, 11066.

(31) Miranda, M. A.; Boscá, F.; Vargas, F.; Canudas, N. *Photochemistry and Photobiology* **1994**, *59*, 171.

(32) Monti, S.; Sortino, S.; Deguidi, G.; Marconi, G. *J. Chem. Soc.,Faraday Trans.* **1997**, *93*, 2269.

(33) Vargas, F.; Canudas, N.; Miranda, M. A.; Boscá, F. *Photochemistry and Photobiology* **1993**, *58*, 471.

CHAPTER 4: NONLINEAR CASCADE EFFECTS

4.1 Introduction

Lasers have moved way beyond the science-fiction movie screen where their most frequent use was in blasting creatures from outer space. Lasers are now common tools which have become widely utilized in applications as diverse as microlithography and presentation pointers. Perhaps the most explosive growth in laser use has been in the medical field[1-5] where new procedures are continually being defined which exploit laser technology. Photodynamic therapy and cornea surgery are two medical applications which have probably seen the greatest growth in popularity in recent years, but other areas such as neurosurgery, angioplasty, and skin surgery are being developed more and more. It is very possible that the laser may become as common as the scalpel in medical procedures in years to come.

Lasers are being exploited in medicine because the nature of the laser beam allows for excellent accuracy in delivery to the site where it is needed, and the power can be precisely controlled so that the depth of the tissue cut or ablated is well-defined. These are definite advantages when working with cornea and other vitally important tissues where scarring is not just aesthetically unpleasant, but interferes significantly with function. Damage to areas other than the specific site where the beam is aimed, so called "collateral

damage" also tends to be very limited when lasers are used, which has advantages over traditional surgical techniques.

This chapter deals with the generation of radical species via laser flash photolysis. The unique feature of the results presented here is that a given reaction sequence will only occur when a high-power, pulsed light source, such as a laser, is used to initiate the reaction. The implication is that the common use of lasers in medical procedures may have unexpected chemical consequences which are specific to the characteristics of the laser beam. The research dealt with here involves a model system which is not biological in nature, but the general characteristics may be extrapolated to biological systems.

If a laser is used for some sort of medical procedure and there is some species present (whether by accident or by design) which absorbs at the wavelength emitted by the laser, then this species will likely be excited. What follows will depend upon the photochemical characteristics of the excited molecule, but reactions with oxygen are certainly possible given that oxygen is present to some extent in tissues. Such reactions may create reactive oxygen species (ROS) which are known to be very damaging to biological material. The results presented here involve the creation of ROS via a novel pathway only accessible in the case of laser excitation.

4.2 Results

This chapter deals with the laser-specific generation of phenylperoxyl radicals via a cascade of reactions in oxygen-rich media. Various precursors were utilized during the course of these studies and the same general mechanism was found to be applicable in all cases. The specific results obtained with different molecules will be outlined in the following pages.

4.2.1 Initial studies with photoinitiator compounds

The first indications that some sort of novel series of reactions was being initiated by laser photolysis came when some preliminary studies with two commercial photoinitiators were undertaken. The two molecules studied are known commercially by the trade names Irgacure #184 (**1**) and Darocure #1173 (**2**). Below are their structures:

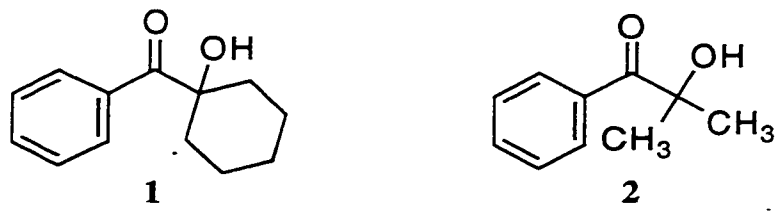

1 **2**

Figure 4.1 Chemical structures of photoinitiator compounds **1** and **2**.

It can be easily seen that one half of the above molecules are identical. As this half contains the conjugated double bonds and the carbonyl, it will most likely be the chromophore which is observed upon laser flash photolysis. Compounds containing carbonyl groups such as those shown above may undergo bond cleavage at the site next to the carbonyl group. This type of cleavage is known as Norrish Type I behavior. This type of reaction is known to be fast and efficient for compounds of this type.[6] Below is the sequence of Norrish cleavage in the case of **1**:

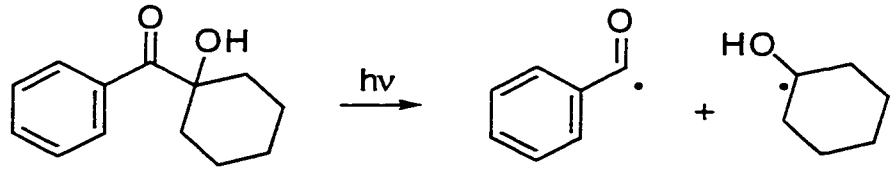

Scheme 4.1 Illustration of Norrish type I cleavage of compound **1**.

In this case, the products of the cleavage process are a benzoyl radical and a ketyl radical. Compound **2** would undergo the same process, also generating a benzoyl radical, but with a different ketyl radical as the other product.

Since the main chromophore is the benzoyl radical, it would be expected that this would be the dominant feature of a transient absorption spectrum acquired in the absence of any sort of process which would remove the benzoyl radical from the system. Below is a transient absorption spectrum acquired after 308 nm laser photolysis of compound **1** in the absence of oxygen:

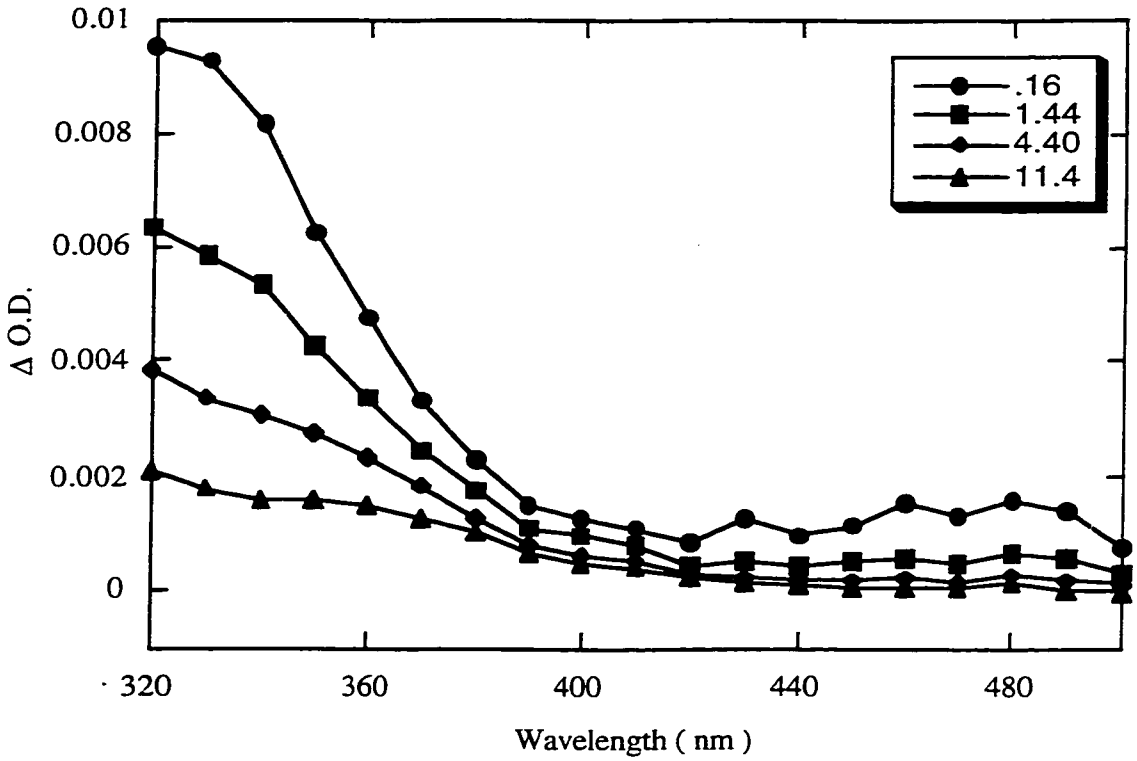

Figure 4.2 Transient absorption spectrum of **1** obtained in nitrogen-saturated acetonitrile. Legend refers to the center of the time window analysed, in μs.

This spectrum is quite uncomplicated, with only one main absorption band. Another spectrum acquired upon 308 nm photolysis of compound **2** yielded the following transient spectrum:

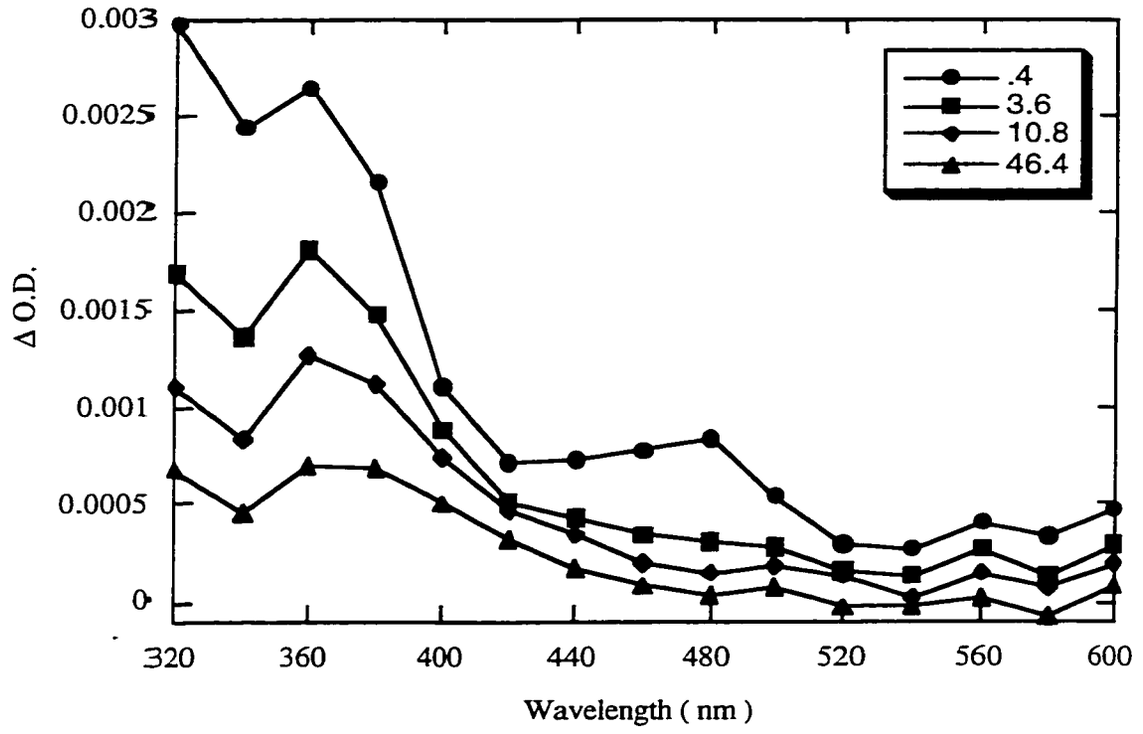

Figure 4.3 Transient absorption spectrum of **2** in nitrogen-saturated acetonitrile. Legend refers to center of time window, in μs.

It can be easily seen that these two spectra are very similar, with the UV absorption band being the only significant feature. The conclusion can easily be drawn, then, that the benzoyl radical is responsible for this absorption band.

It is well-known that benzoyl radicals react with molecular oxygen with a rate constant of 1.8 x 10^9 M^{-1} s^{-1} [7], according to scheme **2**:

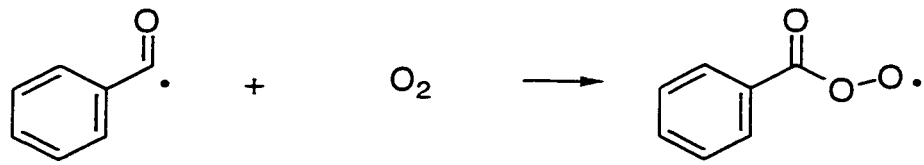

Scheme 4.2 Reaction of benzoyl radical with oxygen to produce benzoyl peroxyl radical.

In the presence of oxygen, therefore, a spectrum corresponding to the benzoyl peroxyl radical is expected to be observed. Below is a spectrum of **1** acquired under conditions of oxygen saturation:

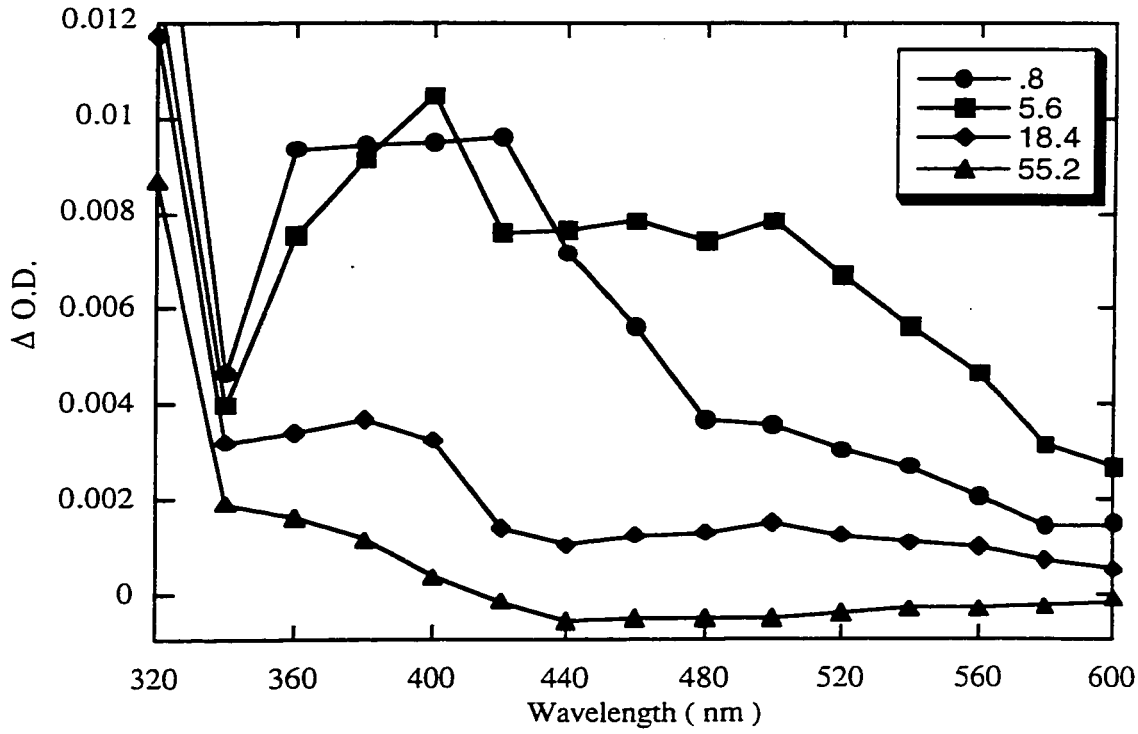

Figure 4.4 Transient absorption spectrum obtained in oxygen-saturated acetonitrile upon lfp of **1**. Centers of time windows are in μs.

There is a growth of signal in the visible region, centered at approximately 480 nm, in this spectrum which was not present in the absence of oxygen. The rate of growth of this signal; however, is not consistent with the formation of the benzoyl peroxyl radical, which under these conditions should occur on a much faster time scale (τ ~ 50 ns). The kinetics of this growth are illustrated in figure 4.5:

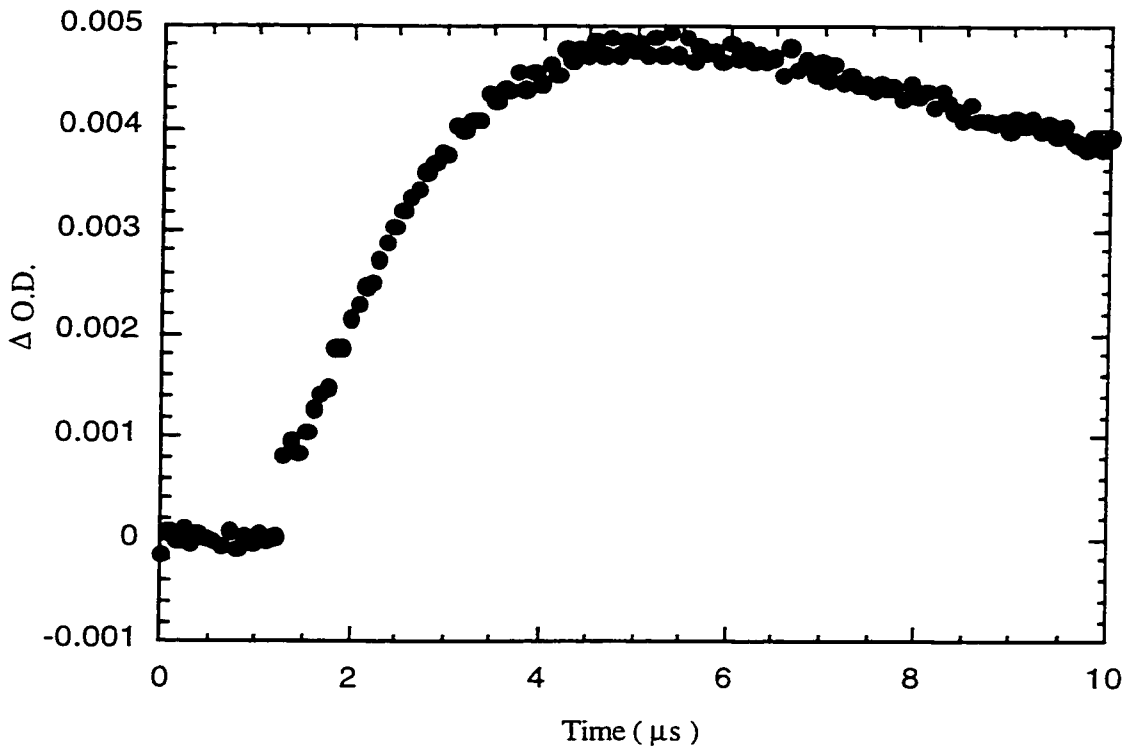

Figure 4.5 Kinetics trace at 480 nm acquired for **1** under oxygen-saturation conditions.

This trace indicates that it takes approximately 5 μs for the signal at 480 nm to reach its maximum intensity. This is not consistent with the formation of benzoyl peroxyl, as that reaction would be much faster.

To determine whether the same type of signal is observed with a similar compound, a transient absorption spectrum under oxygen was also obtained for **2**:

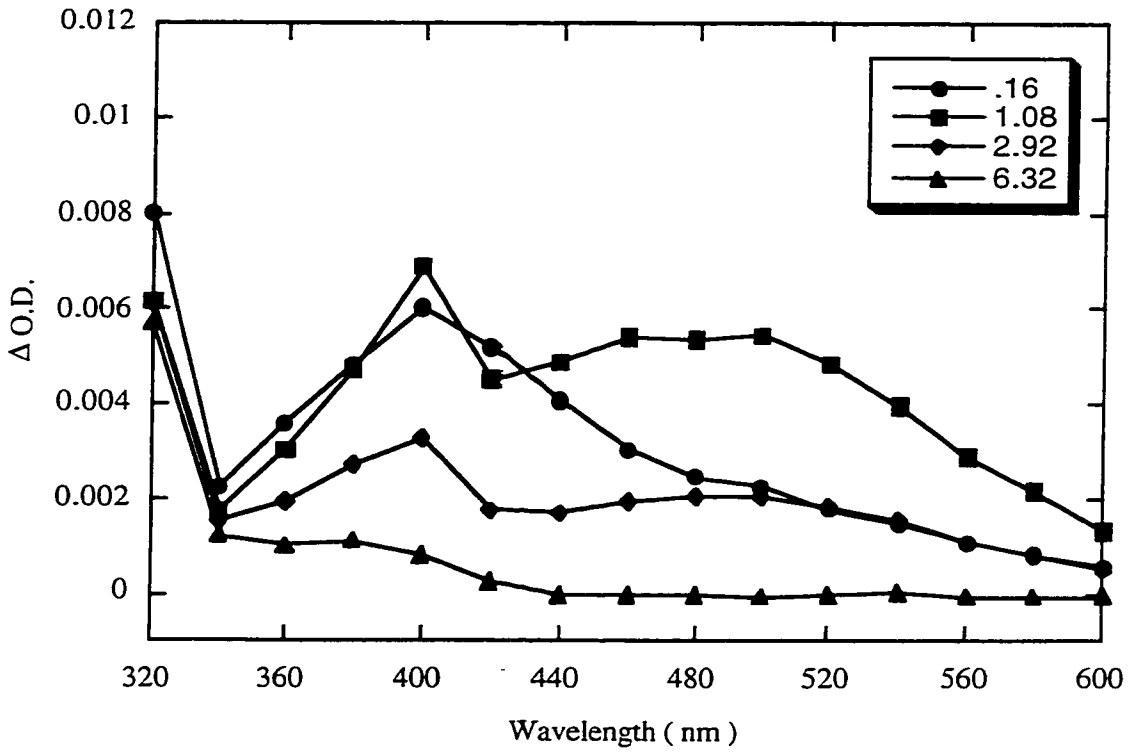

Figure 4.6 Transient absorption spectrum obtained in oxygen-saturated acetonitrile upon lfp of **2**. Time windows are in μs.

This spectrum is virtually identical to the one obtained for **1**; thus, it would appear that the benzoyl radical is involved in the process which leads to this signal. Since the rate of appearance of this signal is not consistent with the absorption being due to the benzoyl peroxyl radical, then the signal must be due to some other transient being formed.

There is evidence that benzoyl peroxyl radicals can react with one another to form a short-lived intermediate, benzoyl tetroxide[8-10], as shown below:

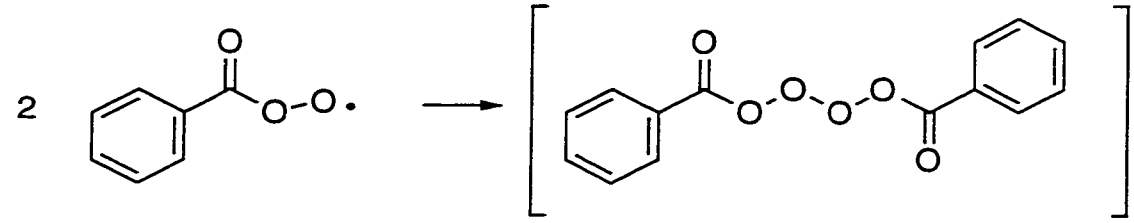

Scheme 4.3 Formation of benzoyl tetroxide by self-reaction of two benzoyl peroxyl radicals.

The tetroxide would quickly dissociate via two pathways[8,10,11]:

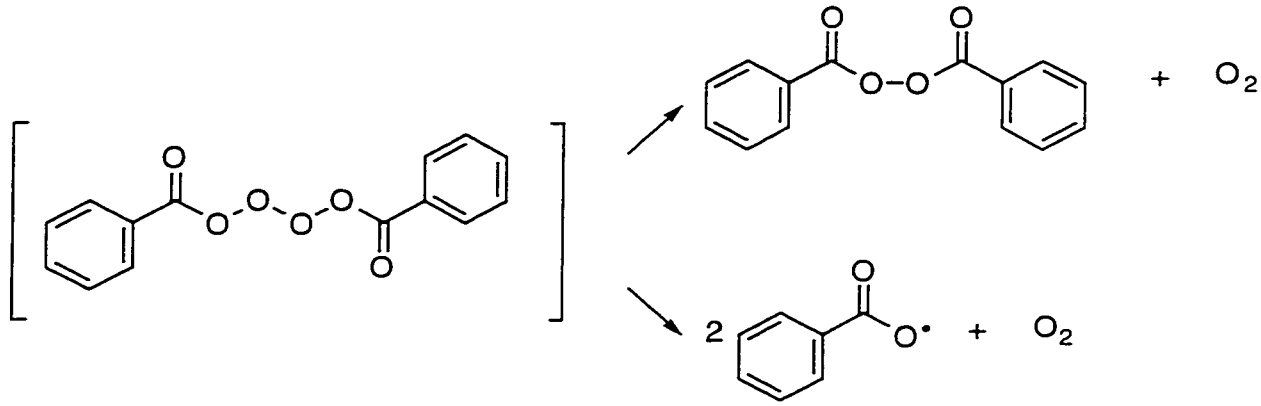

Scheme 4.4 Proposed dissociation of benzoyl tetroxide intermediate.

There has been much interest in determining whether or not the tetroxide is formed as a true intermediate. Indirect evidence of its existence has been found[9-11], but so far no direct proof has been brought forward to confirm that the tetroxide is formed by the self reaction of peroxyl radicals. The speculation in the literature about a possible tetroxide intermediate raised the possibility that the unexplained absorption band at 480 nm formed upon photolysis of **1** and **2** under oxygen might in fact be this elusive transient.

In order for the formation of ground state benzoyl peroxide (as shown in the top process in scheme 3.4), which has a singlet spin configuration, the oxygen formed must have the same singlet spin configuration as dictated by Wigner's Spin Conservation Rules[12]. Since the ground state of molecular oxygen is a triplet, this spin configuration would correspond to the lowest singlet excited state of the oxygen molecule. The bottom process of scheme 3.4 illustrates the formation of molecular oxygen and benzoyl radicals. These species may have a variety of spin configurations, also as dicated by the same set of rules for spin conservation, but since the radical-pair may have either an overall singlet or triplet spin configuration, the oxygen formed via this process may be in the ground state. Other work has shown that singlet oxygen is in fact produced upon reaction of peroxyl radicals [13-16], but generally the yields are quite low. Since this laboratory is equipped with the necessary detection system to measure the infrared emission from excited singlet oxygen, it was decided to attempt to observe an emission from singlet oxygen upon laser photolysis of **2**. Observation of singlet oxygen emission corresponding to the decomposition of the unknown signal at 480 nm would lend support to the assignment of this absorption to the tetroxide.

4.2.2 Laser flash photolysis with singlet oxygen detection of 2

The most common photochemical method of generating excited singlet oxygen is through triplet-triplet energy transfer to oxygen from an excited triplet state of some molecule. Molecular oxygen is somewhat unusual in that its ground state spin configuration is a triplet. An excited singlet state of some molecule, the sensitizer, then, can intersystem cross to the triplet state. After this, it can transfer its energy to oxygen, bringing the sensitizer back to its ground state and generating excited oxygen in the singlet state. This process is illustrated below:

$$\text{Sens} + h\nu \longrightarrow {}^1\text{Sens} \xrightarrow{\text{ISC}} {}^3\text{Sens}$$

$${}^3\text{Sens} + {}^3O_2 \longrightarrow \text{Sens} + {}^1O_2$$

Scheme 4.5 Representation of photochemical process leading to the generation of excited singlet oxygen.

Excited singlet oxygen deactivates to the ground triplet state primarily by non-radiative means, the rate of deactivation depending upon the solvent. A small portion (~1%) of the excited oxygen, though, decays via the emission of light in the infrared region of the spectrum, at ~1269 nm, but with the exact wavelength dependent upon the solvent[17-19]. The light emitted by this deactivation pathway can be observed with the proper equipment. Through the use of a standard solution, then, the efficiency of singlet oxygen generation can be determined for a given reaction.

A more detailed discussion of the singlet oxygen detection system was given in Chapter #2, so it is sufficient to note here that a standard solution of benzophenone, for which the quantum yield of singlet oxygen generation is known to be 0.36 in acetonitrile[20], with the same optical density as **2** at 308 nm (the laser wavelength) was used in these experiments. Below is the chemical structure of benzophenone (**3**):

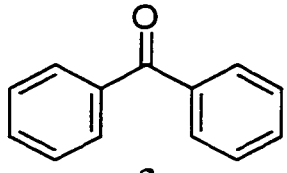

3

Below is a typical decay trace for the emission of singlet oxygen sensitized by the standard, **3**:

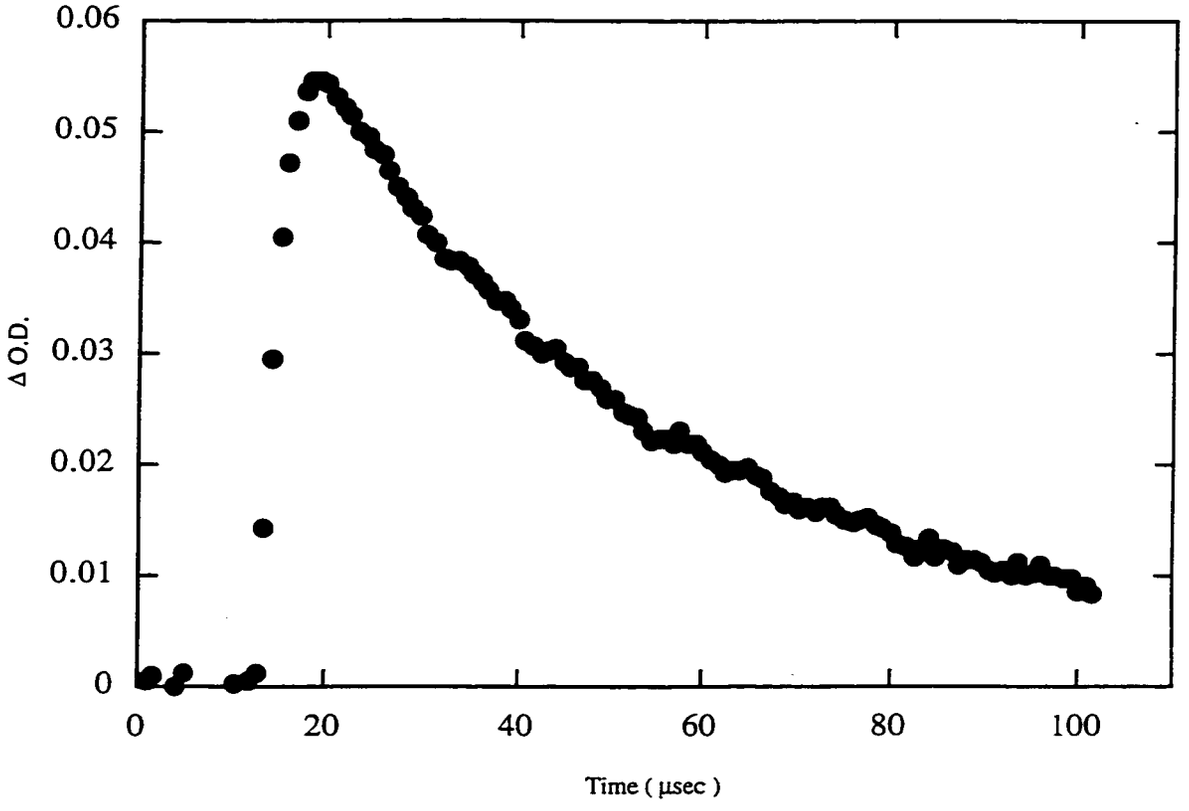

Figure 4.7 Decay of emission in near-IR from excited singlet oxygen sensitized by **3** in oxygen-saturated acetonitrile.

This signal conforms in magnitude and lifetime to what would be expected for **3** in this solvent, so the next step was to determine if an emission from singlet oxygen could be detected upon laser flash photolysis of **2** under the same experimental conditions. Below

are traces acquired with **2** as sensitizer under nitrogen-saturated and oxygen-saturated conditions:

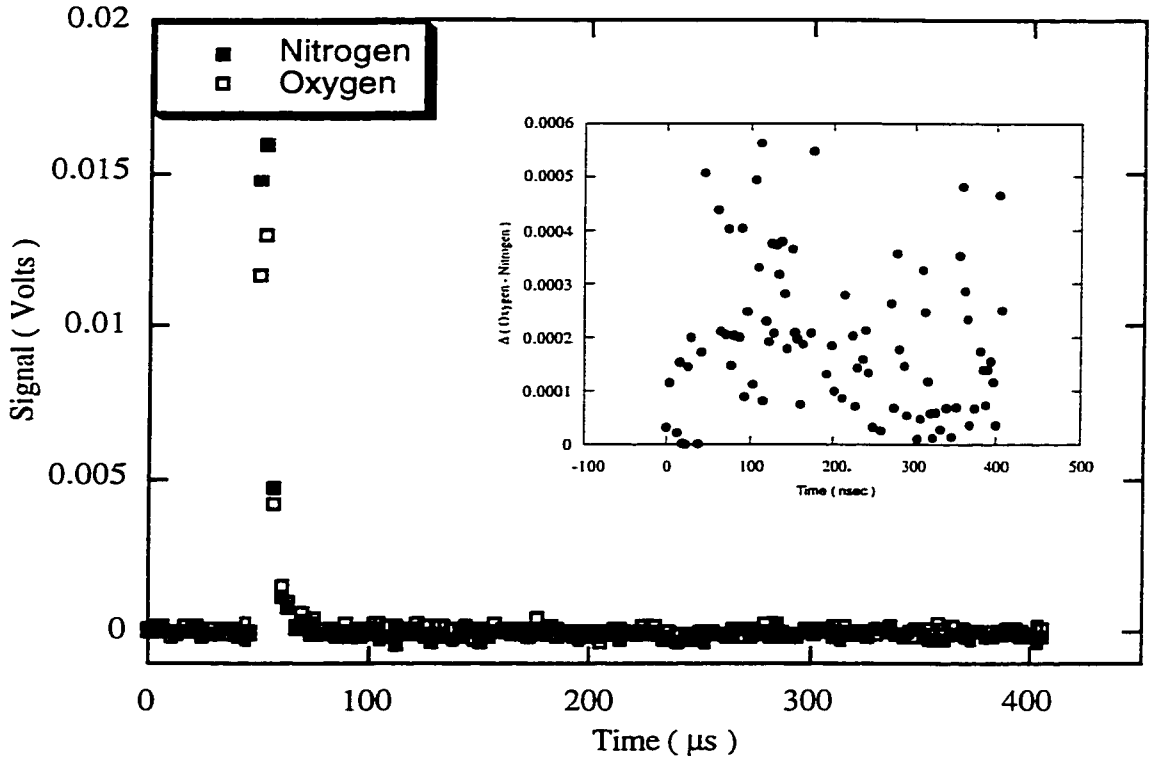

Figure 4.8 Data acquired upon lfp of **2** in oxygen-saturated and nitrogen-saturated acetonitrile, monitored in the near-infrared region. **Inset:** Difference between the two traces.

There is no clear difference between the traces acquired under oxygen and nitrogen. In fact, they appear to be identical, which indicates that no singlet oxygen is being generated upon photolysis of **2**. This observation does not support the hypothesis of the formation of a tetroxide species. In order to be more certain as to whether or not some very small emission was present, the traces acquired in the absence and presence of oxygen were

subtracted from one another, as shown in the inset above. It can be seen that the points lie above the zero line, particularly at the beginning, and then trail back toward zero with time. An estimate of the singlet oxygen yield based on this data would be at most about 4%. Other studies of the termination of peroxyl radicals have found yields of singlet oxygen which are similar in magnitude to this[15,16,21], so although the results of the singlet oxygen experiment are not conclusive, the possibility that a tetroxide intermediate is formed cannot be eliminated.

It became clear at this point that an alternate assignment for the 480 nm signal may be required. A closer examination of the data and further thought about the chemistry which was occurring led to the formulation of an alternate hypothesis which would still fit with all the facts, but which is based on better-understood, more well-established chemistry. Further experiments were then undertaken to prove that this alternate mechanism is feasible.

4.2.3 Involvement of phenyl peroxyl radicals

As mentioned above, closer examination of the system led to the possibility of a mechanism, which though it might involve the tetroxide, does not lead to its assignment as the transient detected in previous laser flash experiments. Below is a provisional mechanism:

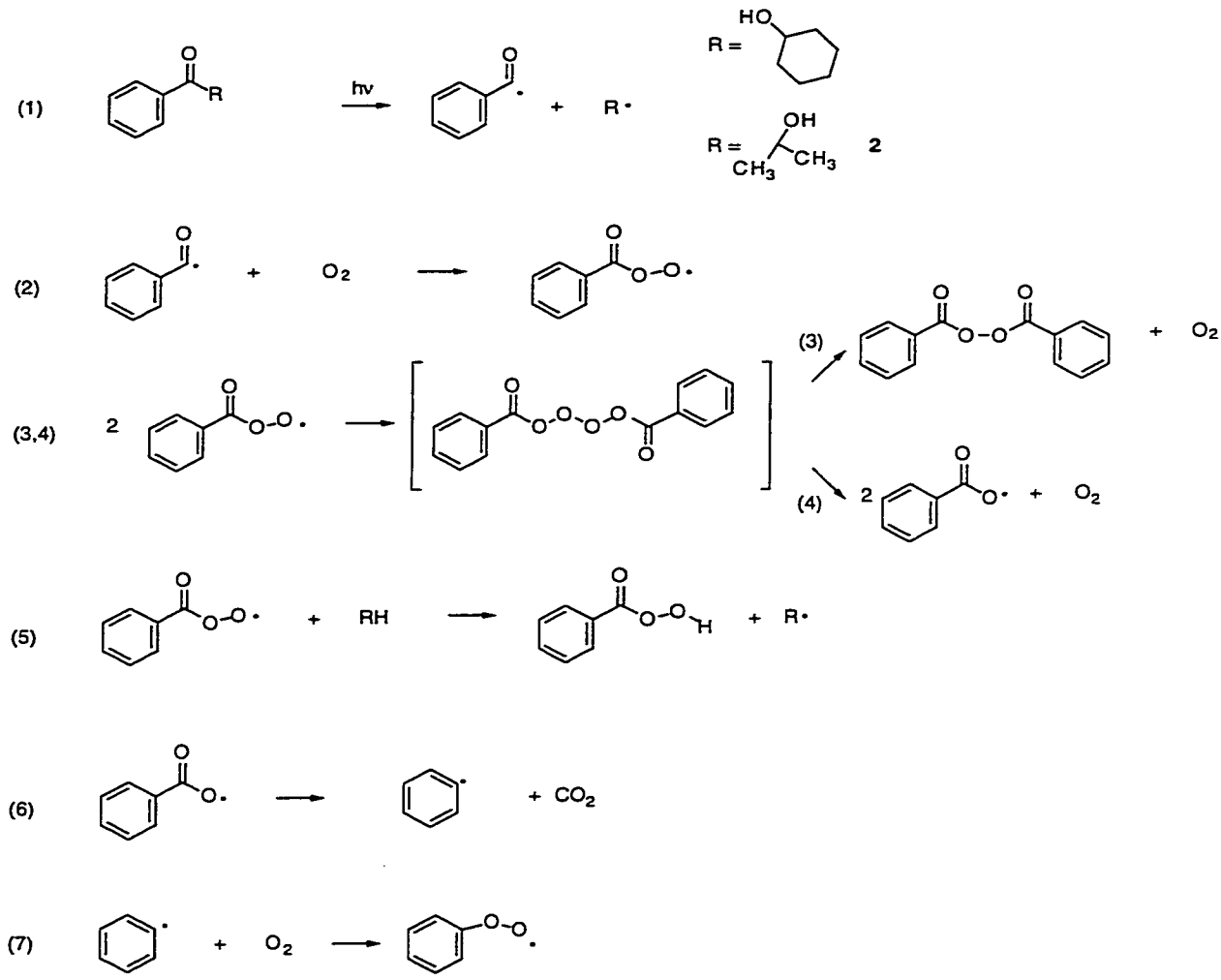

Scheme 4.6 Provisional mechanism for reaction of radicals generated by laser photolysis of **1** and **2** in the presence of oxygen.

The first step in this process, the cleavage of the bond next to the carbonyl, is known to be a fast process, as mentioned previously[22] so this radical cannot be responsible for the transient absorption at 480 nm, which is formed on a relatively long timescale. Step (2) above occurs with a rate constant of 1.8×10^9 M^{-1} s^{-1}, so under oxygen saturation (0.01 M) this process too would be too fast ($\tau \sim 50$ ns) to be attributable to the 480 nm signal, which has a half-life of about 1 ms. Under normal conditions benzoyloxyl radicals

decay by hydrogen abstraction reactions such as shown in step (5) to generate peracids. However, under high-intensity laser irradiation conditions radical-radical reactions are more likely to occur, which would allow for the sequences shown in (3) and (4). This tendency is particularly true in a solvent such as acetonitrile, which has very low reactivity toward generally electrophilic radicals. Whether or not the tetroxide intermediate is involved in these two reactions is not clear, but it is certainly a possibility.

The next step was to determine if the signal at 480 nm is in fact due to the phenyl peroxyl radical and to attempt to gather evidence in favor of the mechanism shown above. These experiments involved utilizing other precursor molecules and studying the transient absorption spectra and kinetics, as well as product characterization.

Although it was postulated that the hydroxyalkyl radicals resulting from the bond cleavage of **1** and **2** were in no way related to the signal observed at 480 nm, it was decided that it was necessary to prove this conclusively in order to lend support to the proposed mechanism. In order to do this, a different precursor to the same hydroxyalkyl, or ketyl, radical produced from **2** was studied by laser flash photolysis. Acetone (**4**) in the presence of a hydrogen donor solvent like isopropanol (**5**) undergoes the following photoreaction:

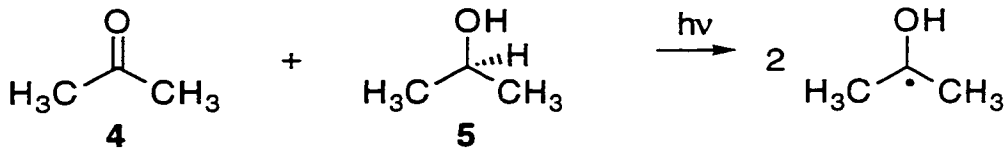

Scheme 4.7 Photoreduction of **4** by **5** to produce two identical ketyl radicals.

Upon laser flash photolysis of **4** with **5** as solvent at 308 nm under air, a transient absorption spectrum was acquired which is shown in figure 4.9 below. The spectrum was

acquired under air (20% oxygen) rather than pure oxygen to avoid excessive quenching of the acetone triplet state which abstracts hydrogen from **5**.

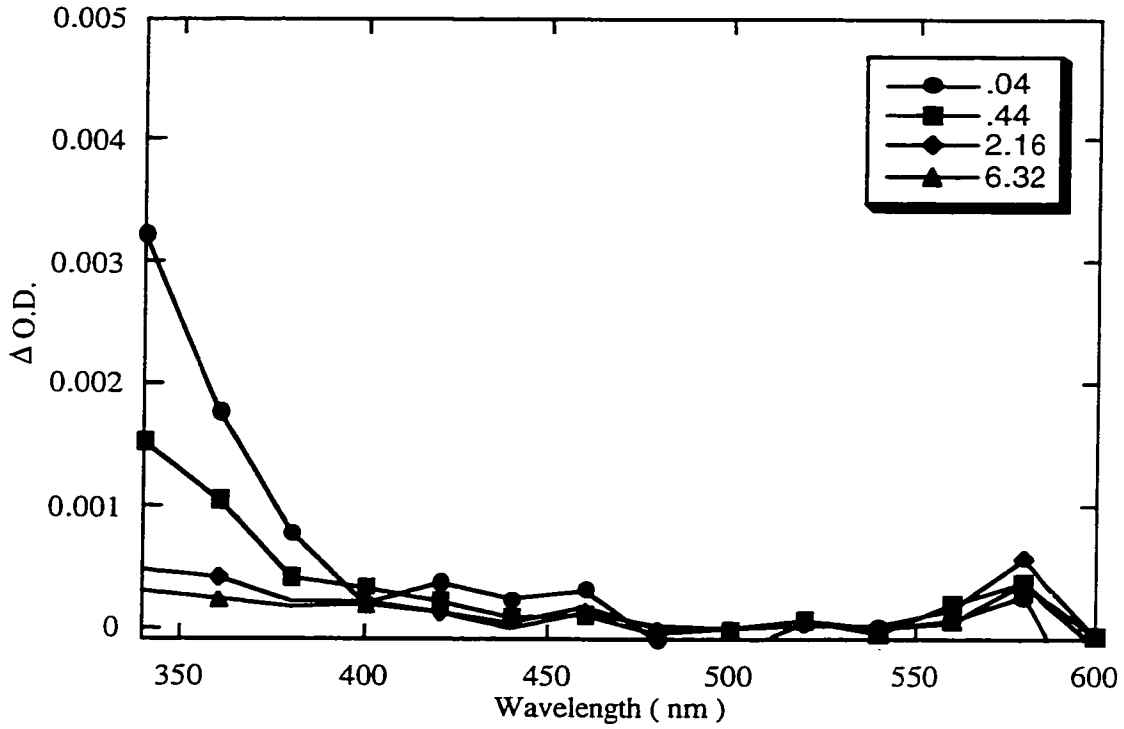

Figure 4.9 Transient absorption spectrum of **4** in **5** solvent under air upon photolysis at 308 nm. Times shown in legend are centers of time windows, in μs.

It can be seen from the above spectrum that no signal at 480 nm is produced from this photoreaction, which proves that in fact the ketyl radical produced from **2** is not the origin of the growth signal at 480 nm.

Looking again at the benzoyl radical as the likely source of the signal growth led to attempts to determine if in fact these radicals ultimately lead to phenyl peroxyl radicals, the species appearing slowly in the other transient absorption studies. Transient spectra of phenyl peroxyl radicals which appeared in the literature at around this time [23,24] showed

absorption maxima which correspond very well to 480 nm, allowing for minor differences due to the different solvents utilized. It was expected, then, that these experiments would very likely confirm the generation of phenyl peroxyl radical from benzoyl radicals.

The first experiment of this type involved laser flash photolysis of 2,2-dimethylpropiophenone ketone (**6**), shown below:

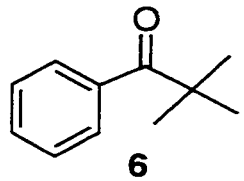

6

This compound undergoes Norrish Type I cleavage at the bond α to the carbonyl upon photoexcitation with a rate constant of 8.5×10^6 s^{-1}[25]. This leads to the generation of benzoyl radicals, which through the proposed mechanism would lead ultimately to the phenyl peroxyl radical. This would be detected as a growth in signal at 480 nm. Below is a transient absorption spectrum obtained upon 308 nm laser photolysis of **6**:

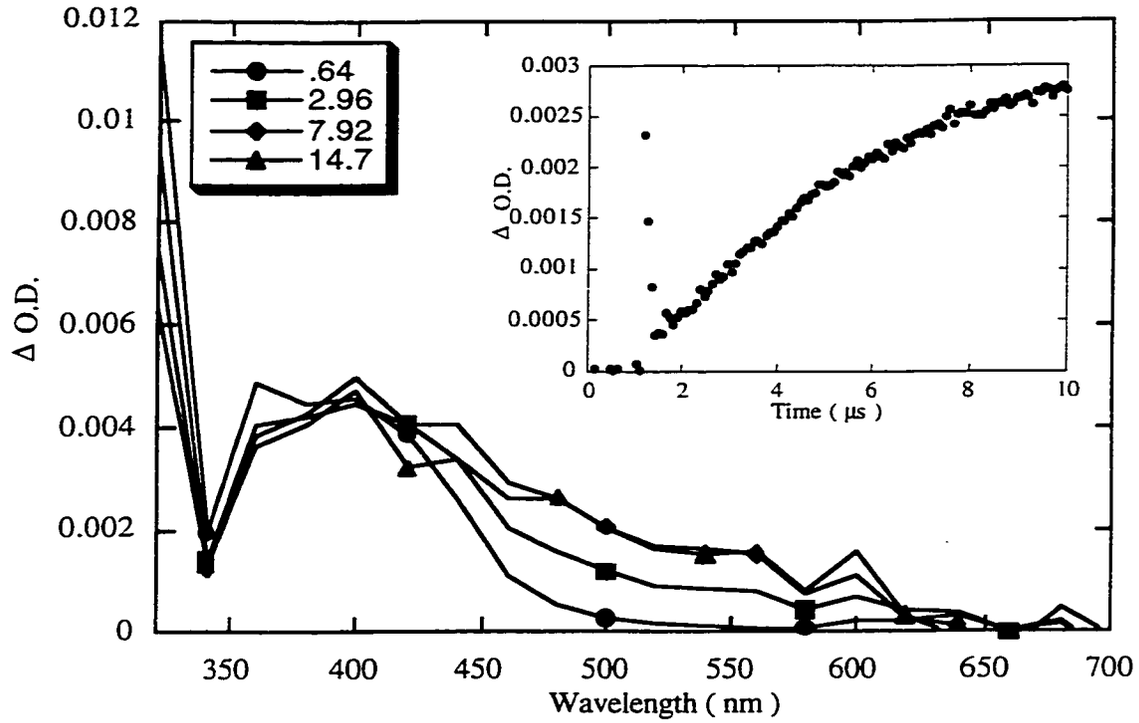

Figure 4.10 Transient absorption spectrum obtained by lfp of **6** in acetonitrile solvent under air after excitation at 308 nm. Legend indicates centers of time windows analysed, in μs. **Inset:** Kinetic trace acquired at 480 nm under the same conditions.

This spectrum is not as clean as the ones obtained for **1** and **2**, but there is clearly a growth in signal, as shown by the inserted kinetic trace, with a maximum at approximately 480 nm. This growth in signal occurs on the same timescale as detected for the photoinitiators. This result points to the involvement of the benzoyl radical as the source for this growth by way of the formation of phenylperoxyl radicals.

In an effort to prove conclusively that the orirgin of the 480 nm signal is the benzoyl portion of the photoinitiator molecules, another experiment was undertaken; the laser flash photolysis at 355 nm of benzaldehyde (**7**) in a solvent composed of a 1:2 vol/vol

ratio of acetonitrile and t-butyl peroxide (**8**). The following is what would be expected to occur:

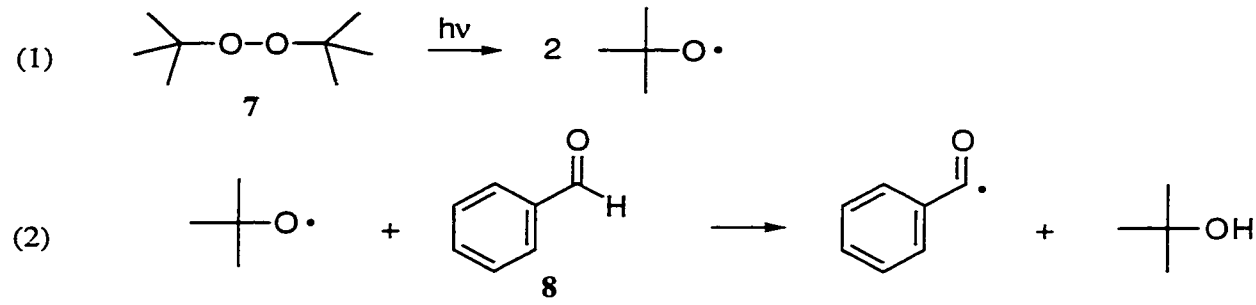

Scheme 4.8 Alternate pathway for generation of benzoyl radicals by 355 nm photolysis of **7** with **8** as solvent.

The t-butoxy radicals created in step (1) above abstract hydrogen from benzaldehyde with a rate constant of 6.8 x 10^7 M^{-1} s^{-1} [26]. This experiment can also be done under an oxygen atmosphere, as is necessary to generate phenyl peroxyl radicals, because the t-butoxyl radicals are not quenched by oxygen. This provides a pathway by which benzoyl radicals, which ultimately result in phenyl peroxyl radicals, can be created. Below is a transient absorption spectrum obtained by 355 nm laser photolysis of **7** under nitrogen-saturated conditions:

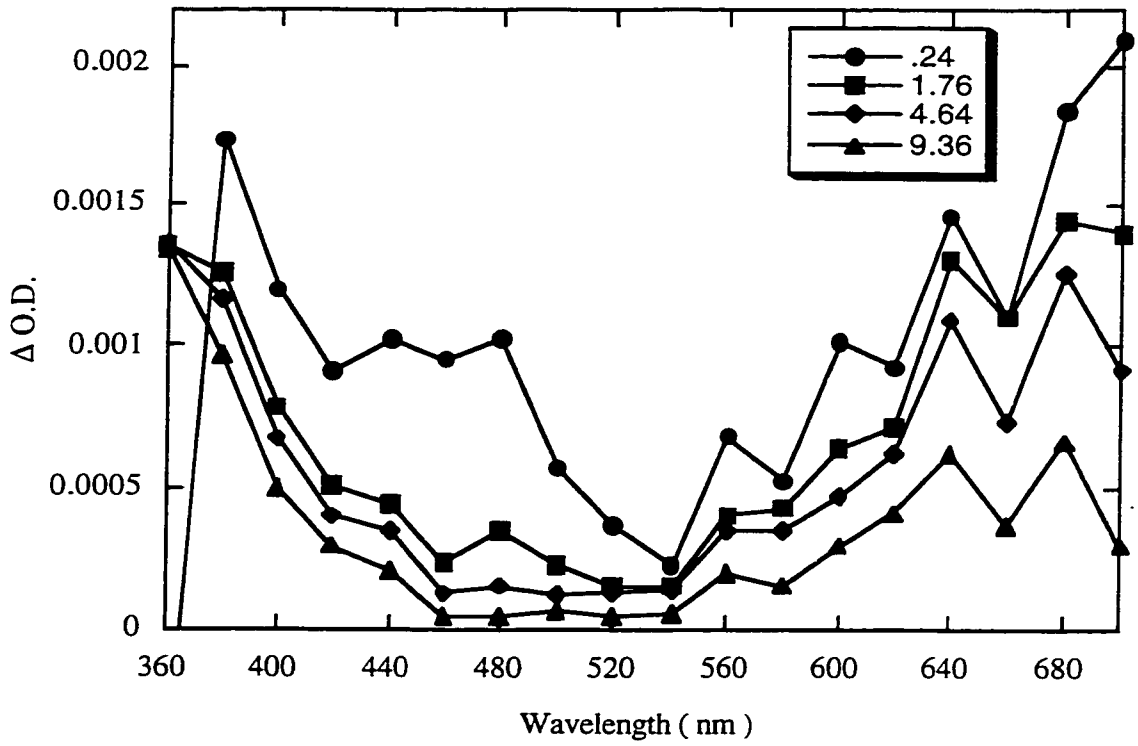

Figure 4.11 Transient absorption spectrum of **7** in **8** solvent under nitrogen upon 308 nm excitation. Legend indicates centers of time windows, in ms.

No signal growth can be observed in this spectrum, which is expected in the absence of oxygen. Another spectrum acquired under oxygen-saturated conditions is shown in figure 4.12. Note that the vertical scale in figure 4.11 is approximately five times smaller than below.

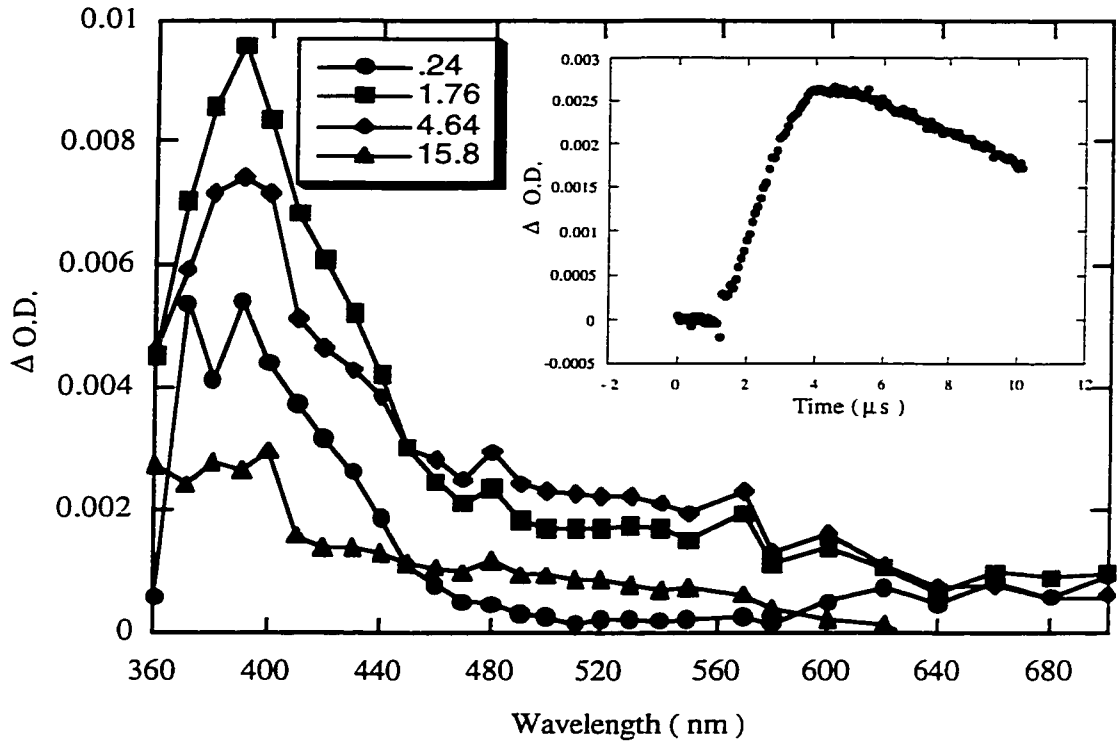

Figure 4.12 Transient absorption spectrum of **7** in **8** acquired under oxygen-saturated conditions upon 308 nm excitation. **Inset:** Kinetic growth as monitored at 480 nm.

This spectrum, in contrast to the one acquired under nitrogen, shows the characteristic growth and subsequent decay of an absorption band centered at approximately 480 nm, which is what is expected. It seemed clear at this point, then, that the benzoyl radical created from all the precursors studied was undergoing the reaction sequence described previously, ultimately leading to the formation of phenylperoxyl radicals.

A similar experiment was done using benzoyl peroxide (**9**) as the radical precursor. In this case, the reaction sequence would be joined at a later step (step (6) in scheme 3.6) as shown below, but the phenylperoxyl radicals would still be produced:

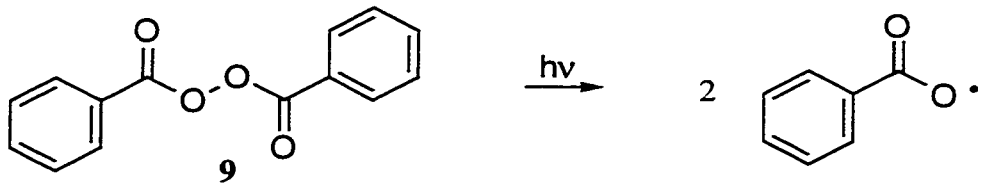

9

Scheme 4.9 Generation of benzoyloxyl radicals upon laser photolysis (308 nm) of **9**.

This experiment would then further support the chain sequence proposed. Below is a transient absorption spectrum acquired upon laser flash photolysis (λ excitation = 308 nm) of **9** in oxygen-saturated acetonitrile:

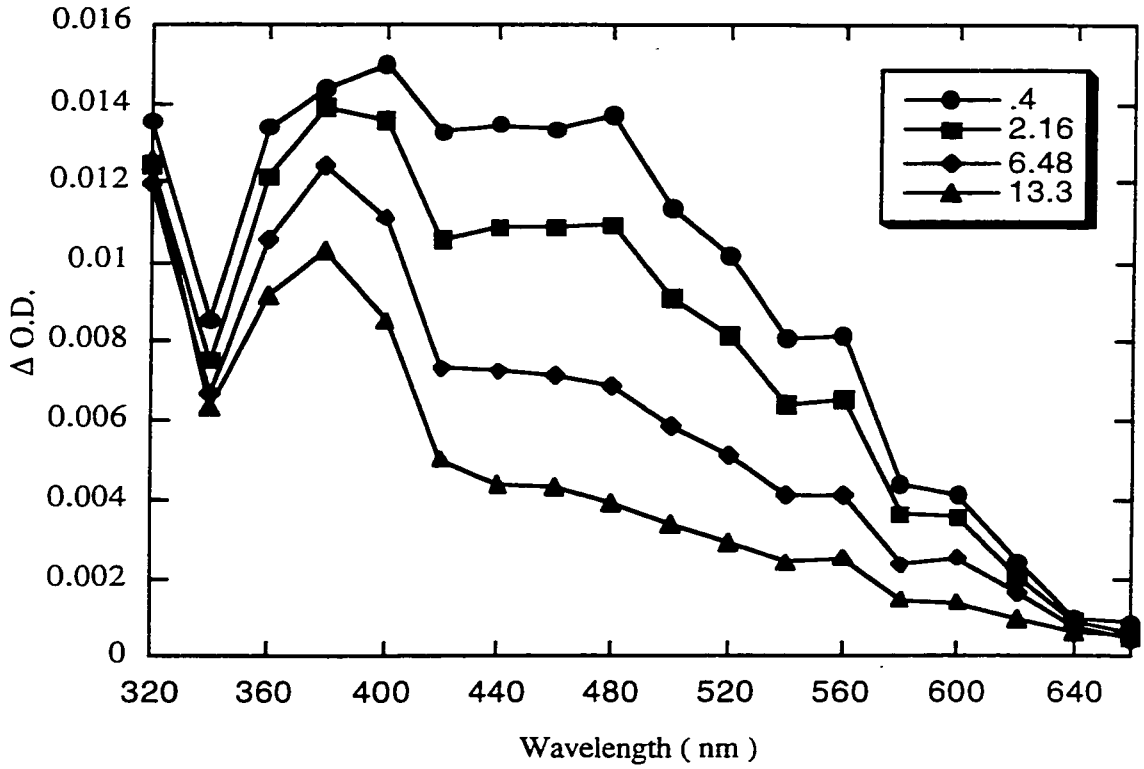

Figure 4.13 Transient absorption spectrum of **9** in oxygen-saturated acetonitrile. Legend indicates centers of time windows, in μs.

In this case the same absorption band as observed previously is present. The difference lies in the timescale of its appearance, as illustrated by the kinetic trace shown in fig 4.13, below:

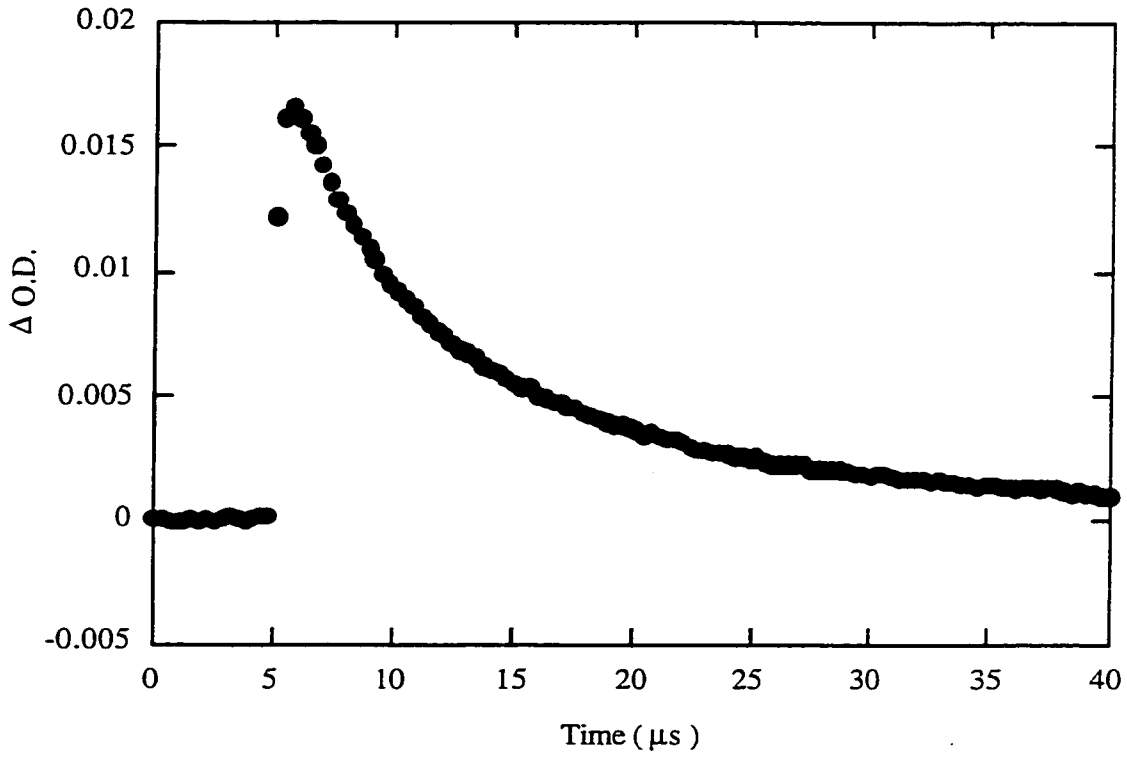

Figure **4.14** Kinetic trace at 480 nm for **9** acquired under same conditions as spectrum shown in 4.13.

This trace was acquired on the same timescale as those obtained for the other various precursors, so since the sequence of reactions is joined at a later step, it would be expected that the phenyl peroxyl radicals would appear on a shorter timescale. This is exactly what is observed.

4.2.3 Power and oxygen dependence of 480 nm signal

Further data was gathered regarding the proposed reaction scheme by way of the effect of laser power on the growth kinetics of the 480 nm signal. Calibrated neutral density filters were used to attenuate the laser beam and kinetics traces were acquired at various power levels to determine how the rate of growth of the signal was affected. Below are a series of kinetics traces at 480 nm for **2** photolysed at 308 nm. Power values were measured at the sample holder:

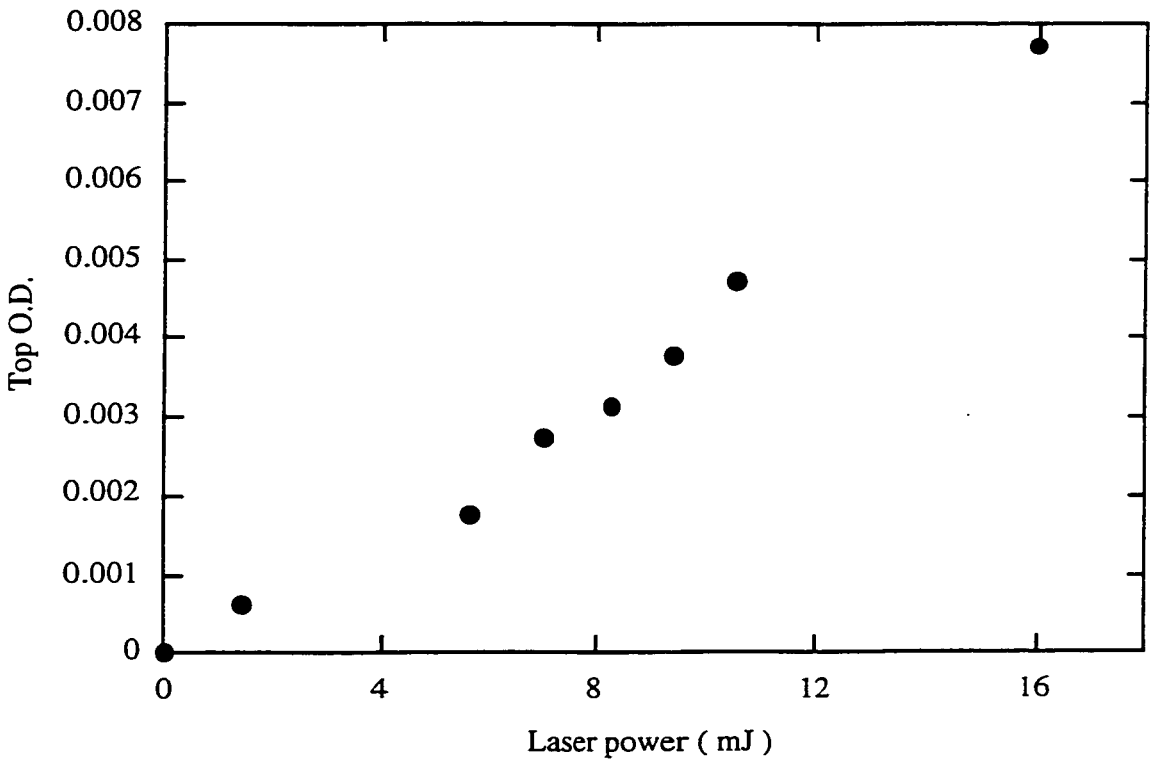

Figure 4.15 Plot of maximum signal amplitude vs. laser dose for growth signal at 480 nm.

This plot does not clearly indicate one way or the other whether the growth of the signal is due to a single-photon (straight line) or a two-photon (curved line) process. A better indication of what is happening can be obtained from studying the kinetics of the growth at various laser powers, as shown in figure 4.16 below:

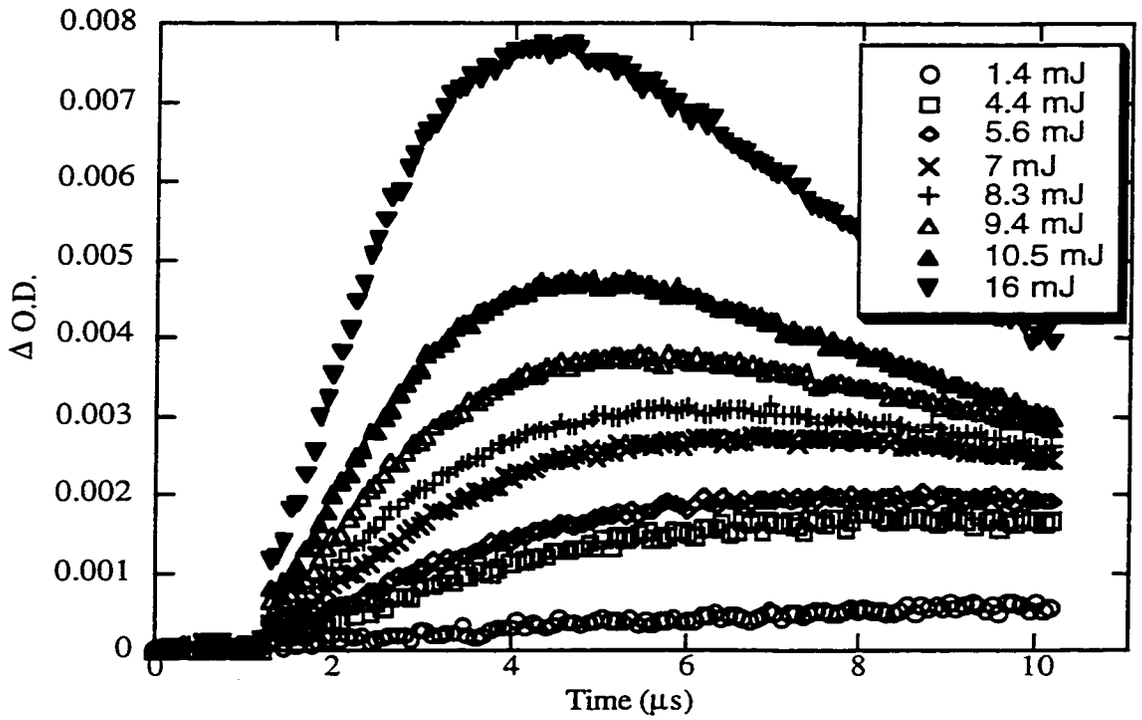

Figure 4.16 Plot of kinetics of growth at 480 nm for various laser power values.

This plot shows that as the laser power is decreased, the half-life of the growth signal increases systematically along with a decrease in signal intensity. This observation is consistent with the involvement of a second-order, bimolecular reaction. The likely bimolecular step is the reaction of two benzoyl peroxyl radicals according to scheme 3.6. The reaction of oxygen with the benzoyl radicals produced in step (1) of this scheme is too fast to account for the kinetics observed, and would not be influenced by the laser dose.

Another study undertaken involved the determination of the effect of oxygen concentration on the growth kinetics of the 480 nm signal. Various percentages of oxygen were bubbled through the sample and the growth kinetics and magnitude of the 480 nm signal were measured. Below is a plot of signal intensity vs. percentage oxygen in the mixture:

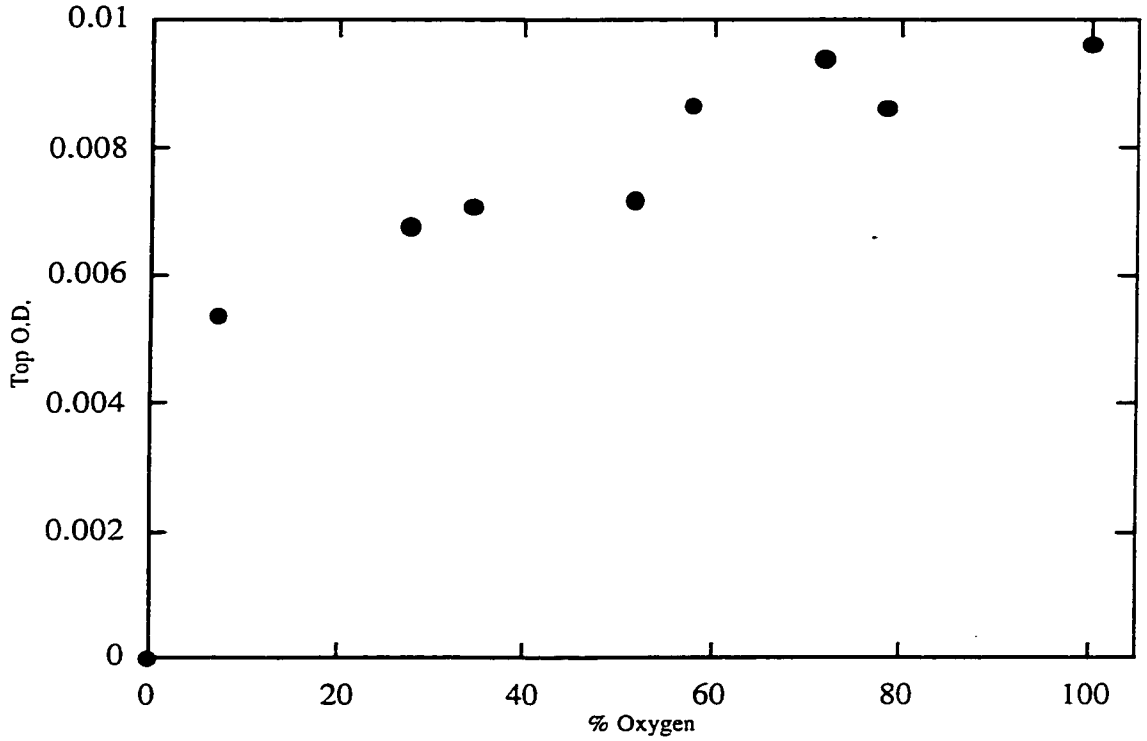

Figure 4.17 Plot of % oxygen in solution vs top O.D. for **2**.

This plot shows that even with only ~7% oxygen present, the top O.D. of the growth is already at 56% of the level it reaches at 100 % oxygen. The kinetics of the growth are not significantly dependent upon the concentration of oxygen. These observations also fit with the proposed mechanism, given that the reaction of benzoyl radicals with oxygen is very fast, so that this step is not the rate-determining one in the process.

These studies lent much support to the provisional mechanism, but further proof was still needed. Product studies were undertaken to determine if the final products conformed to the proposed reaction scheme.

4.2.3 Product studies of laser photolysed photoinitiator

Product studies were performed by HPLC analysis after **2** was photolysed by approximately 500, 308 nm laser shots. A laser had to be used as the source to generate enough radicals to enable coupling reactions to occur. Details of the HPLC instrument and methods will be outlined at the end of this chapter. The instrument is equipped with a diode array detector which allowed the absorption spectra of the various components of the product mixture to be acquired. A product study of photolysed **1** from the literature[22] gave indications of what products to expect from the benzoyl portion of the molecule, but since the irradiation in our laboratory was done with a laser, some different products might be found.

The products were confirmed by HPLC analysis of authentic samples with comparison of retention times and absorption spectra. Below is a table of the products:

Product	**Retention time (authentic sample)**	**Retention time (reaction mixture)**
starting material	6.74 min	6.75 min
benzoic acid	5.77 min	5.71 min
benzoyl peroxide	12.60 min	12.54 min

Table 4.1 Table of products isolated by HPLC and comparison of retention times with authentic samples.

The presence of benzoic acid as the major product makes sense considering that step (4) of the proposed scheme shows the formation of two benzoyloxyl radicals, which could abstract a hydrogen to form benzoic acid. Another method of forming the same product could be the decomposition of the peracid which is formed in step (5) to benzoic acid. The formation of benzoyl peroxide is shown in step (3) of the scheme, and although the yield was quite low as detected by HPLC, part of the reason for this small yield could be the fact that benzoyl peroxide absorbs 308 nm light, which would cause it to decompose in the reaction vessel. The products identified, then, are completely consistent with the proposed mechanism.

4.3 Discussion

Originally the focus of the research outlined above was to determine conclusively whether or not the mysterious growth signal at 480 nm observed upon laser photolysis of the photoinitiator compounds was due to the formation of benzoyl tetroxide. Many of the experiments which were performed were done with this in mind, but as more and more information was gathered, it became clear that whether or not the tetroxide was formed was irrelevant. Only upon photolysis with a high-powered source such as a laser are the radical-radical reactions favored which lead ultimately, in this system, to the formation of phenylperoxyl radicals. This is illustrated in scheme 4.6 in steps (3) and (4). Step (3) leads to benzoyl peroxide which, although benzoyl peroxide is a stable product, it can be decomposed by subsequent laser pulses to ultimately generate phenylperoxyl radicals. Step (4) shows the creation of benzoyloxyl radicals which decarboxylate quickly in step(6) with the resulting phenyl radicals reacting quickly with oxygen to produce phenylperoxyl radicals. Both of these steps, then, contribute to the concentration of phenylperoxyl radicals in the system. The key, self-reaction step of the cascade process which occurs in

both steps (3) and (4); however, cannot occur unless the concentration of radicals is sufficiently high to allow this step to compete with other processes, such as the hydrogen abstraction shown in step (5). Under steady-state irradiation this radical self-reaction does not occur, as the radical concentration is never high enough.

Peroxyl radicals are among the group of species collectively known as Reactive Oxygen Species (ROS). These species, which also include superoxide, are known to be quite damaging to biological tissue. It is important, then to be aware of the possibility of causing tissue damage via a process similar to this one when a laser is utilized for medical purposes. If a chromophore is present which can absorb the laser light and initiate a cascade reation such as this, then collateral damage to tissues other than those undergoing photolysis can occur. Benzoyl peroxide, for example, is often used as a topical medication for acne. These experiments have shown that this compound can enter into the cascade of reactions leading to phenyl peroxyl radicals. It would be possible, then, if a laser of the appropriate wavelength were used on skin to which the benzoyl peroxide had been applied, to create peroxyl radicals in the tissue. This might cause damage to the tissue which, though not due directly to the use of the laser, is certainly related to it.

4.4 Experimental details

Both compounds **1** and **2** were generous gifts from Ciba-Geigy. Compound **1** was recrystallized 2x from ethanol and **2** was used as received. All other compounds used were from Aldrich and were either of special high purity or were purified prior to use. The acetonitrile used as solvent was from BDH, optical grade. The oxygen and nitrogen used for sample purging were high-purity grade purchased from Air Products.

All laser flash experiments were performed on the system which was described previously in Chapter 2 of this thesis. Lasers with outputs of either 308 nm or 355 nm

were utilized in this study. Samples were contained in a 7 x 7 mm suprasil quartz cuvette though which sample was continuously flowed during the laser experiments to prevent product buildup. A reservoir containing the sample connected to a nitrogen or oxygen line and continuously purged. The sample flowed through teflon tubing to the quartz cell and out into a waste vessel. All data was plotted using Kaleidagraph software.

Samples which were laser photolysed in preparation for product studies were contained in 7x7 mm suprasil quartz cuvettes which were purged with oxygen for about 15 minutes prior to irradiation. The sample was placed in a special holder and shaken after every 20 shots.

HPLC analyses were performed with a Varian instrument equipped with a reverse-phase column and a diode array detector. The eluent chosen was 25% water - 75% acetonitrile increasing by 2% acetonitrile per minute after 5 minutes for 12.5 minutes until the eluent was composed entirely of acetonitrile. Both solvents were HPLC grade. Authentic samples of the products were analysed via the same method to allow for direct comparison of elution times.

4.4 References

(1) Fischer, W. G., Partridge Jr., W.P., Dees, C., Wachter, E.A. *Photochem. Photobiol.* **1997**, *66*, 141.

(2) Srinivasan, R. *Science* **1986**, *234*, 559.

(3) Fluhler, E.; Hurley, J. K.; Kochevar, I. E. *Biochim. Biophys. Acta* **1989**, *990*, 269.

(4) Smith, G.; McGimpsey, W. G.; Lynch, M. C.; Kochevar, I. E.; Redmond, R. W. *Photochem. Photobiol.* **1994**, *59*, 135.

(5) Garcia, C.; Smith, G. A.; McGimpsey, W. G.; Kochevar, I. E.; Redmond, R. W. *J. Am. Chem. Soc.* **1995**, *117*, 10871.

(6) Norrish, R. G. W.; Bamford, T. *Nature* **1937**, *140*, 195.

(7) Brown, C. E.; Neville, A. G.; Rayner, D. M.; Ingold, K. U.; Lusztyk, J. *Austr. J. Chem.* **1995**, *48*, 363.

(8) Russell, G. A. *J. Am. Chem. Soc.* **1957**, *79*, 3871.

(9) Bartlett, P. D., Guaraldi, G. *J. Am. Chem. Soc.* **1967**, *89*, 4799.

(10) Thomas, J. R. *J. Am. Chem. Soc.* **1965**, *87*, 3935.

(11) Bartlett, P. D.; Traylor, T. G. *J. Am. Chem. Soc.* **1963**, *85*, 2407.

(12) Wayne, R. P. *Principles and Applications of Photochemistry;* first ed.; Oxford University Press: Oxford, 1988, pp 255.

(13) Howard, J. A.; Ingold, K. U. *J. Am. Chem. Soc.* **1968**, *90*, 1056.

(14) Ingold, K. U. *Acc. Chem. Res.* **1969**, *2*, 1.

(15) Nakano, M., Takayama, K., Shimizu, Y., Tsuji, Y., Inaba, H., Migita, T. *J. Am. Chem. Soc.* **1976**, *98*, 1974.

(16) Niu, Q. J., Mendenhall, G.D. *J. Am. Chem. Soc.* **1992**, *114*, 165.

(17) Rodgers, M. A. J.; Snowden, P. T. *J. Am. Chem. Soc.* **1982**, *104*, 5541.

(18) Hurst, J. R.; Schuster, G. B. *J. Am. Chem. Soc.* **1983**, *105*, 5756.

(19) Parker, J. G.; Stanbro, W. D. *J. Am. Chem. Soc* **1982**, *104*, 2067.

(20) Nau, W.; Scaiano, J. C. *J. Phys. Chem* **1996**, *100*, 11360.

(21) Kanofsky, J. R. *J. Org. Chem.* **1986**, *51*, 3386.

(22) Phan, X. T. *J. Radiat. Curing* **1986**, 11.

(23) Alfassi, Z. B., Khaikin, G.I., Neta, P. *J. Phys. Chem.* **1995**, *99*, 265.

(24) Mertens, R., von Sonntag, C. *Angew. Chem. Int. Ed. Engl.* **1994**, *33*, 1262.

(25) Encina, M. V.; Lissi, E. A.; Lemp, E.; Zanocco, A.; Scaiano, J. C. *J. Am. Chem. Soc.* **1983**, *105*, 1856.

(26) Chatgilialoglu, C.; Lunazzi, D.; Macciantelli, D.; Placucci, G. *J. Am. Chem. Soc.* **1984**, *106*, 5252.

CHAPTER 5: ENZYME PHOTODEGRADATION BY TiO_2, A COMMON SUNSCREEN INGREDIENT

5.1 Introduction

The ozone layer is thinning, the incidence of skin cancers is increasing,we do not want to have skin that looks much older than our real age. This is the basic motivation behind the huge industry of sun-protection. We are advised never to go out into the sun unprotected by physical cover (hat, long-sleeved shirt) and of course we must also douse ourselves in sun creams. These sun creams, or sunscreens, come in various colors, styles, fragrances, and formulations. There are two basic types of compounds which are the active ingredients in sunscreens; chemical sunscreens and physical sunscreens. Chemical sunscreens absorb light strongly in the UV range, but undergo no net chemical change as a result of the absorption; therefore they can undergo "infinite" cycles of absorption and deactivation and provide protection to the skin cells which they are covering. Examples of chemical sunscreens include compounds such as p-aminobenzoic acid (PABA) which has been banned from use in sunscreens due to its carcinogenic potential. Physical sunscreens, on the other hand, are not designed to absorb the UV light. They scatter it, thereby preventing absorption. Examples of compounds which are frequently referred to as physical sunscreens include small particles of zinc oxide and titanium dioxide which are suspended in the sunscreen mixture. Most commercially available sunscreens contain a

combination of chemical sunscreen ingredients and possibly titanium dioxide or zinc oxide as a physical sunscreen component. This type of mixture gives the user protection over a broader range of wavelengths of light, which is an important criteria to the consumer. Some examples of chemical sunscreening agents which are utilized commercially are derivatives of benzophenone and methoxycinnamates, the respective structures of which are shown below:

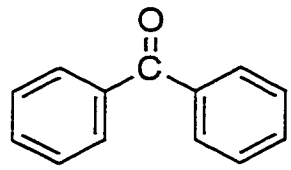

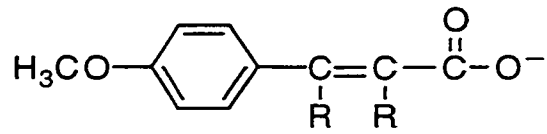

Many chemical sunscreens have been evaluated for their toxicity, thus the withdrawal of PABA from use in sunscreens. Physical sunscreens, because of their scattering mode of action, have been touted as the best type of sunscreen ingredients because of their lack of reactivity. In fact, many physicians recommend formulations which contain TiO_2/ ZnO_2 to their child patients, because as physical sunscreens they have been assumed to be innocous, non toxic, and effective sunscreening agents.

The work described in this chapter will focus only on titanium dioxide, which is likely the most active of the physical sunscreens due to its light-absorption properties.

Titanium dioxide is a well-known semiconducting material. The band-gap between the valence and conduction bands depends upon the crystal structure and has been determined to be 3.23 eV for anatase crystals and 3.06 eV for rutile crystals[1]. These band-gaps correspond to light of wavelengths in the near UV and visible regions of the spectrum. Titanium dioxide, therefore, does not only scatter light, it absorbs very strongly in the region of the spectrum in which it is supposed to be merely acting as a scattering agent. Titanium dioxide has been utilized very heavily as a photocatalyst for various processes including as a bactericide and in the breakdown of environmentally troublesome

compounds found in waste water[2-6]. It would be a somewhat amazing coincidence if a compound which is proven to be a very effective photocatalyst in the breakdown of organics and in killing bacteria or other pathogens could act merely as an innocuous light scatterer when mixed into a sunscreen formulation.

Recent work has focussed on studies of the photocatalytic power of TiO_2 to break down nucleic acids and amino acids[7-13]. This work has indicated that the degradation of these biomolecules is fairly efficient and questions are being raised as to the wisdom of using this catalyst to help protect ourselves from the sun. This choice needs to be reevaluated.

Upon absorption of a photon in the UV by titanium dioxide an electron is promoted from the valence band to the conduction band, creating an electron-hole pair:

$$TiO_2 + hv \longrightarrow e^- + h^+$$

According to studies by Serpone et al.[14] 90% of these pairs recombine within a few picoseconds with no net effect. However, at least some of these pairs do persist for at least a few nanoseconds, allowing for reaction with other species, particularly in aqueous environments. In an aqueous solution when oxygen is present, the species of Scheme 5.1 could be envisioned.

1. $TiO_2 \longrightarrow h^+ + e^-$

2. $h^+ + H_2O \longrightarrow \cdot OH + H^+$

3. $O_2 + e^- \longrightarrow O_2^{-\bullet}$

4. $O_2^{-\bullet} + H^+ \longrightarrow HO_2^{\bullet}$

5. $HO_2^{\bullet} + HO_2^{\bullet} \longrightarrow H_2O_2$

6. $H_2O_2 + O_2^{-\bullet} \longrightarrow {}^{\bullet}OH + OH^- + O_2$

7. $h^+ + OH^- \longrightarrow {}^{\bullet}OH$

8. $H_2O_2 + e^- \longrightarrow {}^{\bullet}OH + OH^-$

Scheme 5.1 Outline of the possible species created in aerated aqueous solution upon UV photolysis of titanium dioxide.

Initial work involved the study of TiO_2 in aqueous suspensions by laser flash photolysis to determine if trapped holes or electrons could be observed and what effect the addition of amino acids would have on their lifetimes. Unfortunately, system limitations did not allow for very meaningful results to be gathered by transmission methods. Attempts to study the same system by way of diffuse reflectance laser flash photolysis were more successful but still no clear conclusion could be drawn from this work. Nevertheless this work did pave the way for the steady state experiments so they will be discussed briefly.

The focus of chapter 5, though, is an attempt to study a more complex biologically relevant sytem by studying the effect of irradiation of TiO_2 in the presence of enzymes and monitoring for a loss of activity, which would be the ultimate manifestation of changes of protein structure. The enzymes chosen for this study were horseradish peroxidase and

bovine α-chymotrypsin. Both of these enzymes are commercially available in very pure formand are stable in aqueous solutions at a mid-range pH. The amino acid sequences, three-dimensional structures, and mechanisms of action of both are also known. Both are also easy to assay for activity via spectrophotometric methods.

5.2 Results

5.2.1 Transmission laser flash photolysis experiments

Suspensions of titanium dioxide were prepared by sonication of the solid in phosphate buffer. The samples were only mildly cloudy and thus were suitable for use in transmission experiments with the laser system. An excitation wavelength of 355 nm was chosen as it corresponds well with the bandgap of the anatase crystal form of TiO_2. Laser excitation should therefore create electron-hole pairs and it was hoped that some of the ~10% of electrons which do not recombine with their partner holes within picoseconds could be studied. Unfortunately, no signal due to solvated electrons could be observed. The extinction coefficient of the solvated electron is modest (1200 L/mol cm)[15] and this fact combined with the fact that only ~10% of the incident electrons created remain after the laser pulse explains why no solvated electrons were observed with our system.

In light of the failure to detect the electrons directly, it was decided to attempt to trap them through the use of the compound methyl viologen (**1**):

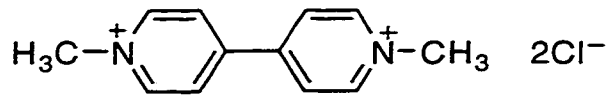

1 $\cdot xH_2O$

According to studies by Moser and Grätzel, methyl viologen reacts with the electrons created by light absorption by TiO_2 at a rate which is governed by the pH of the medium[16]. The pH of the solvent employed in these experiments was 7.4 to mimic physiological conditions, which corresponds to a k value of ~ 10^6 M^{-1} s^{-1}. Once **1** reacts with an electron it is reduced to the monocationic form which has a characteristic absorption spectrum with large extinction coefficients in the UV and visible regions of the spectrum (398 and 603 nm)[16].

Initial experiments were very qualitative in nature and were done in order to determine if, and how detectable, a signal due to the trapped electrons would be. Below is a transient absorption spectrum of TiO_2 in buffer upon the addition of methyl viologen:

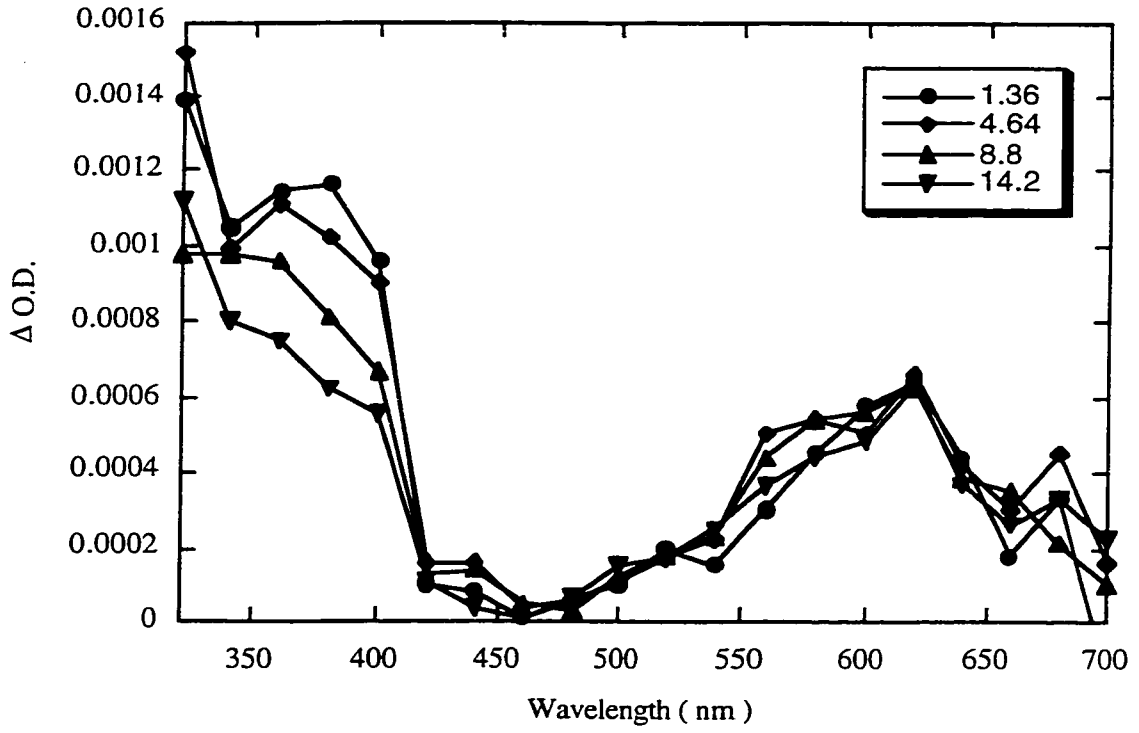

Figure 5.1 Transient absorption spectrum of TiO_2 suspension in phosphate buffer, pH 7.4 with methyl viologen (0.0002 M) added. Excitation wavelength = 355 nm The legend shows the time in microseconds corresponding to the center of the time window analysed.

This spectrum clearly shows the characteristic maxima at the appropriate wavelengths which are due to the absorptions of the methyl viologen monocation. No growth in signal is detectable on this timescale, indicating that the monocation of methyl viologen is formed very quickly. Obviously then, free electrons are being created by the laser pulse which excited the TiO_2 and at least some portion of these are being trapped by the methyl viologen.

Once the best conditions in terms of concentrations were determined, the next step was to add some amino acid and determine if the electrons would react with the amino acid competitively with the methyl viologen. In this manner we could study the rate of reaction

of the amino acid with the electrons produced from the TiO_2. The maximum concentrations of both methyl viologen and amino acid which could be added to the system are constrained by their absorptions at the laser wavelength. Direct excitation of any species other than the TiO_2 is undesirable as transient absorptions due to excited states of these compounds add complications to an already complex system, making any meaningful data hard to collect.

Several transmission experiments were done with various amino acids, but one representative experiment is sufficient to illustrate the results obtained in all cases. In this case tyrosine was the amino acid employed. A set concentration of methyl viologen was added to the TiO_2 suspension (0.0006 M) and tyrosine was added incrementally until it began to absorb at the laser wavelength. At this point the kinetics of the system were studied and compared with the kinetics of another similar sample in the absence of the amino acid. As well, the spectra of samples with and without amino acid were compared to determine if another transient species appeared upon addition of the tyrosine to the system. Below, in Figure 5.2, are the kinetic traces obtained for the appearance of the methyl viologen monocation in the presence and absence of tyrosine:

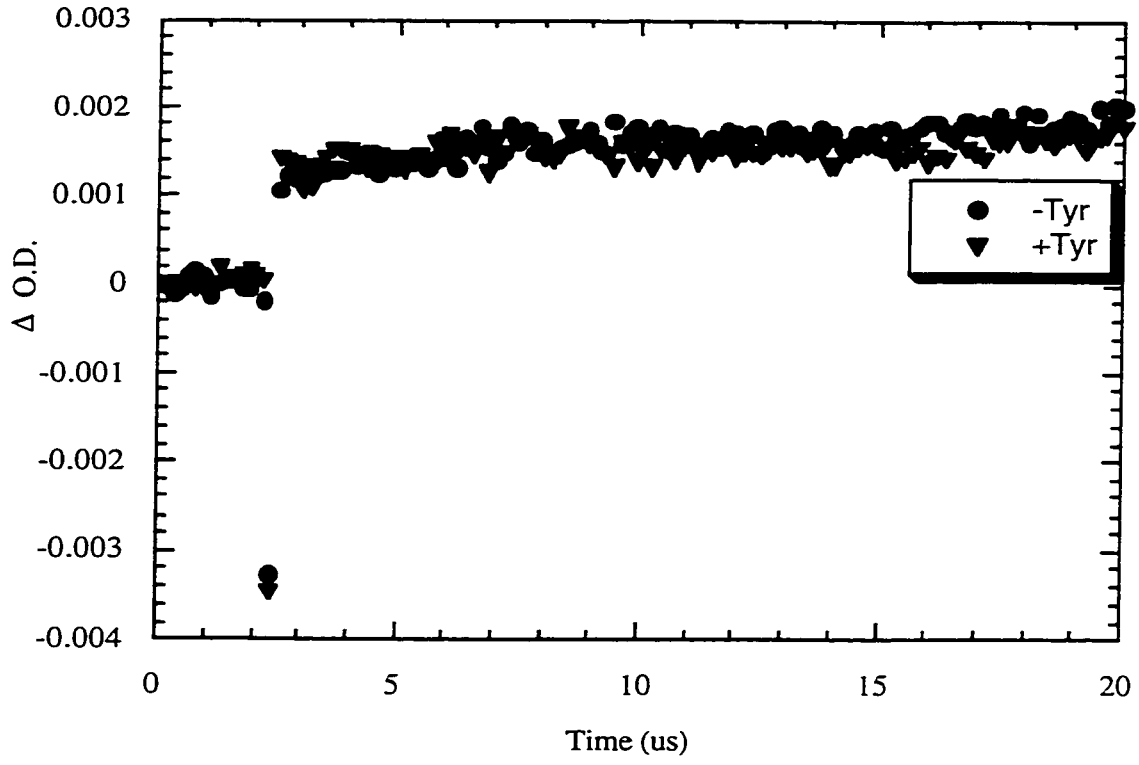

Figure 5.2 Kinetic traces for the growth of signal due to the methyl viologen monocation in the absence and presence of tyrosine. Solvent = PBS, pH 7.4. [methyl viologen] = 0.0006 M; [TiO_2] = 0.00004 M; [tyrosine] = 300 µl, 2 M stock.

It can be easily seen that neither the kinetics of formation of the methyl viologen monocation, nor the yield of monocation are affected in any way by the presence of the amino acid. The transient absorption spectra was in no way affected by the presence of tyrosine either. These results indicate that at the concentrations of amino acid employed in this study, no competition exists between the methyl viologen and the amino acid for trapping of the electrons created upon photolysis of TiO_2.

It should be noted from the above kinetic traces and the transient absorption spectrum that the signals are quite small. We could not optimize the signal quality beyond this level with the transmission setup in our laboratory, so it was decided to attempt time-resolved diffuse reflectance studies using solid samples of TiO_2. In this setup, which is described in chapter #2, much more TiO_2 would be available for light absorption, possibly enhancing signal intensity.

Attempts to observe solvated electrons directly when solid TiO_2 was moistened with distilled water yielded no signal, so once more methyl viologen was employed as a means to trap the electrons and create a visible signal. Below is a transient diffuse reflectance spectrum of solid TiO_2 moistened with PBS and treated with methyl viologen (0.002 M):

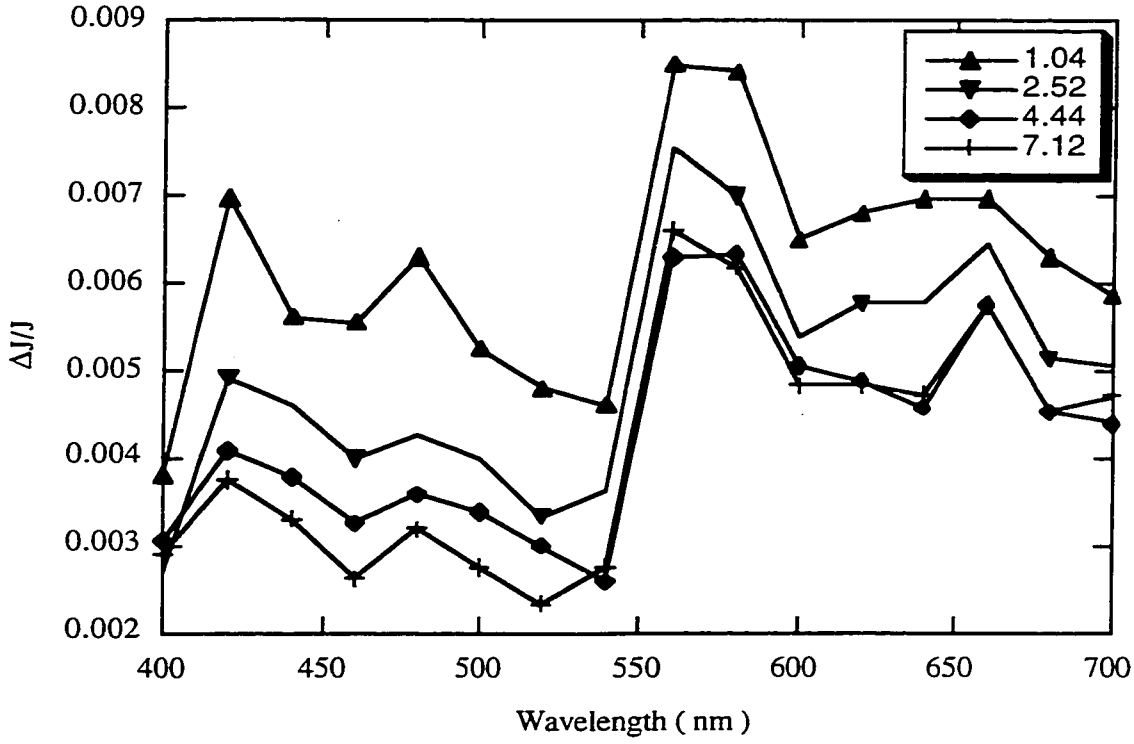

Figure 5.3 Transient diffuse reflectance spectrum of moist TiO_2 treated with methyl viologen ($\lambda exc = 355nm$). Legend refers to center of time windows (μsec).

Once again this spectrum shows the characteristic peaks associated with the presence of the monocation of methyl viologen, but in this case the signal amplitude is enhanced to approximately double the value achieved by transmission methods.

Once again attempts were made to create a competition between the methyl viologen and an amino acid for capture of the electron. It was hoped that since the overall signal intensity was enhanced that small differences in the kinetics would be more noticeable. The amino acid chosen here was glycine. A saturated solution of glycine in PBS was added incrementally to the sample up to the point when it began to absorb at the laser wavelength (355 nm). the kinetics of the methyl viologen monocation were compared, as well as transient absorption spectra acquired before and after the addition of glycine.

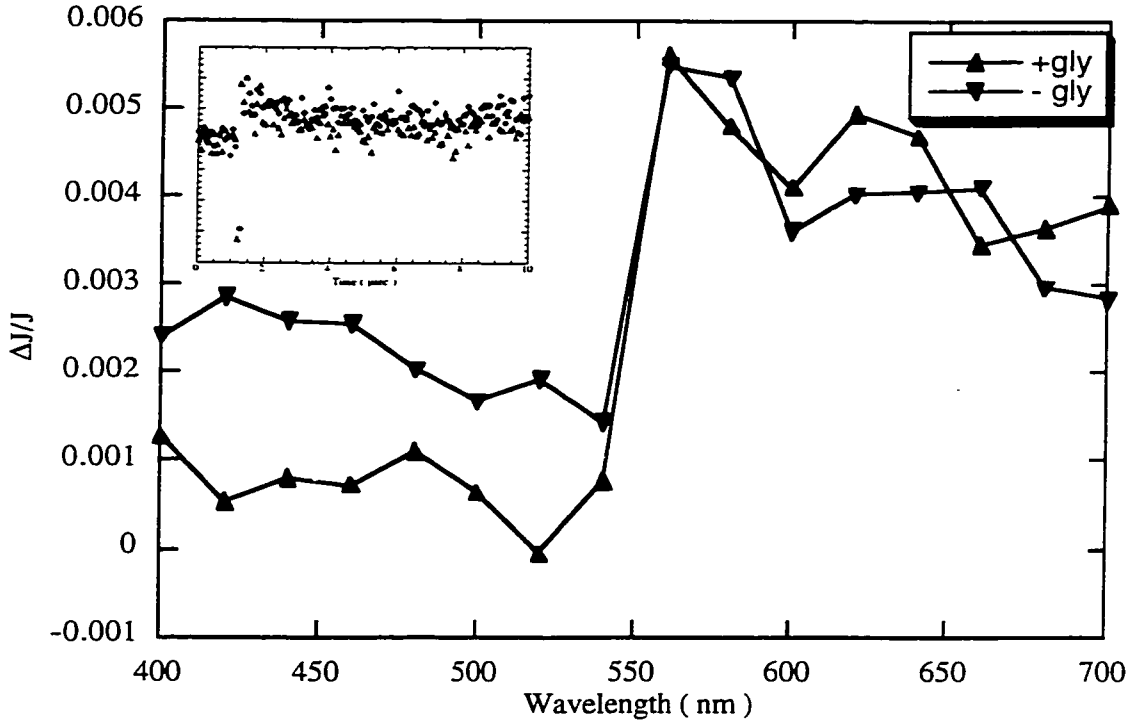

Figure 5.4 Transient diffuse reflectance spectrum of TiO_2 + PBS in the absence and presence (400 µl saturated solution) of glycine (λexc = 355 nm). Only one time window is shown for clarity. **Insert**: Kinetics trace acquired at 560 nm.

The spectra have not been normalized indicating that there is a difference in the magnitude of the absorption in the 400-550 nm region, but nevertheless the two spectra are essentially duplicates of one another, indicating that no competition exists between the methyl viologen and the glycine for the electron. The kinetics traces are also identical in the presence and absence of the glycine. It is possible that there simply was not a high enough concentration of amino acid to compete effectively, but direct absorption of the laser light by the amino acid at higher glycine concentrations prevented increasing the concentrations beyond a certain point. Another contributing factor may be that the methyl viologen is clinging to the surface of the TiO_2 particles, allowing it to trap the electrons immediately.

No further information could be gotten from these time-resolved experiments, so it was decided to suspend the laser experiments and try another approach. Enzyme samples in solution were mixed with TiO_2 suspensions and photolyzed with UVA radiation centered at 350 nm. After photolysis the samples were separated from the TiO_2 and activity assays were performed on the enzymes to determine if their activity had been affected in any way.

5.2.2 Steady state irradiations and activity assays

The first enzyme chosen for these studies was horseradish peroxidase (HRP). As mentioned previously,the enzyme is easily obtainable commercially and the assay procedure described in the experimental section of this chapter was quite easy to perform and required no special equipment.

HRP is an enzyme containing a heme group which has a molecular weight of approximately 40,000. HRP belongs to the group of enzymes known as peroxidases, and catalyses the reduction of hydrogen peroxide to water. It is also active on methyl and ethyl peroxide. *In vivo* HRP is an intracellular protein and there is oxygen present in its

proximity, which is an important condition for allowing a large amount of ROS to be created by UVA photolysis of TiO_2.

In order for the enzymatic process to take place a hydrogen donor must also be present in the system. A large number of hydrogen donors are acceptable in this system, including 2,2'-azino-bis(3-ethylbenzthiazoline-6-sulfonic acid)diammonium salt or ABTS (**2**) . The reaction with hydrogen peroxide and ABTS is as follows:

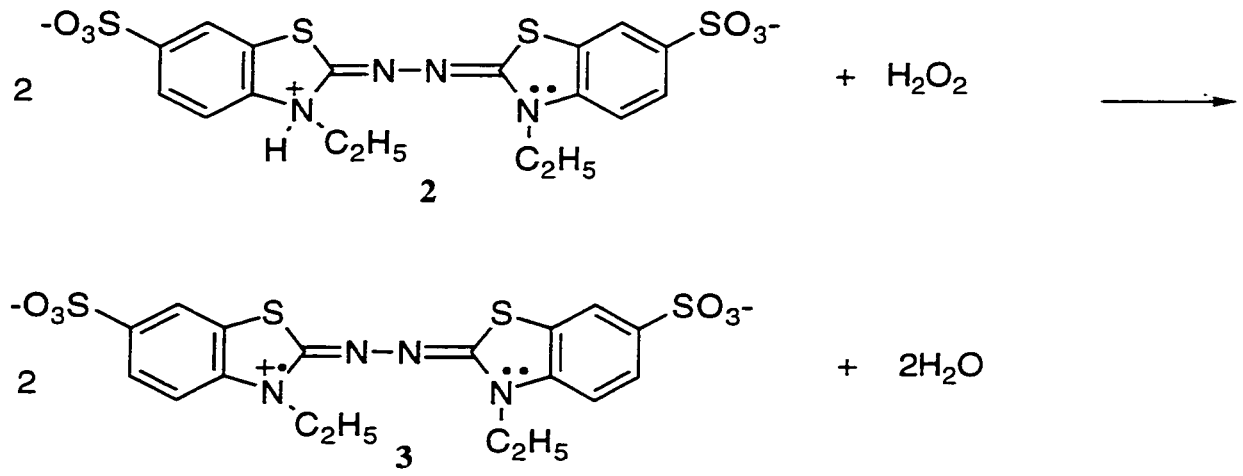

Scheme 5.2 Reaction of peroxidase with hydrogen peroxide in the presence of **2** as hydrogen donor to produce **3**, a radical cation with $\lambda^{max} = 412$ nm.

The radical cation of ABTS has an absorption band in the visible region of the spectrum ($\lambda^{max} = 412$ nm) so the activity of the enzyme was measured via the appearance of this reaction byproduct.

Prior to the photolysis the absorption spectra of the samples were obtained:

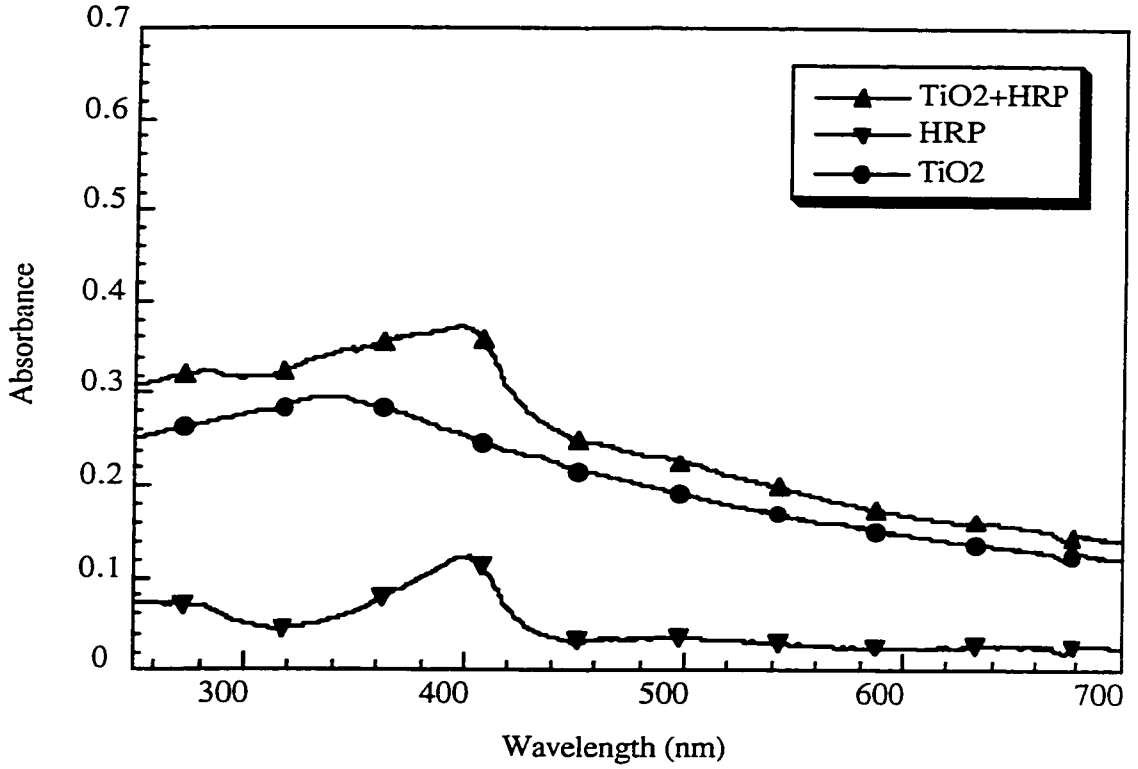

Figure 5.5 Absorption spectra of HRP (0.05 mg/ml), TiO_2 (0.05 mg/ml) and a 50/ 50 mixture of the two.

This shows that although the HRP does absorb some UVA light (with a band in the visible as well due to the heme group) the vast majority of light of all wavelengths is either absorbed or scattered by the TiO_2. It would therefore be expected that if TiO_2 acts merely as a light scatterer, then samples photolyzed in its presence would undergo less UVA-induced deactivation than samples which are photolyzed directly with the UVA in the absence of TiO_2.

Below are representative growth curves acquired at 412 nm for various samples after photolysis had taken place. These curves reflect how active the enzyme samples are:

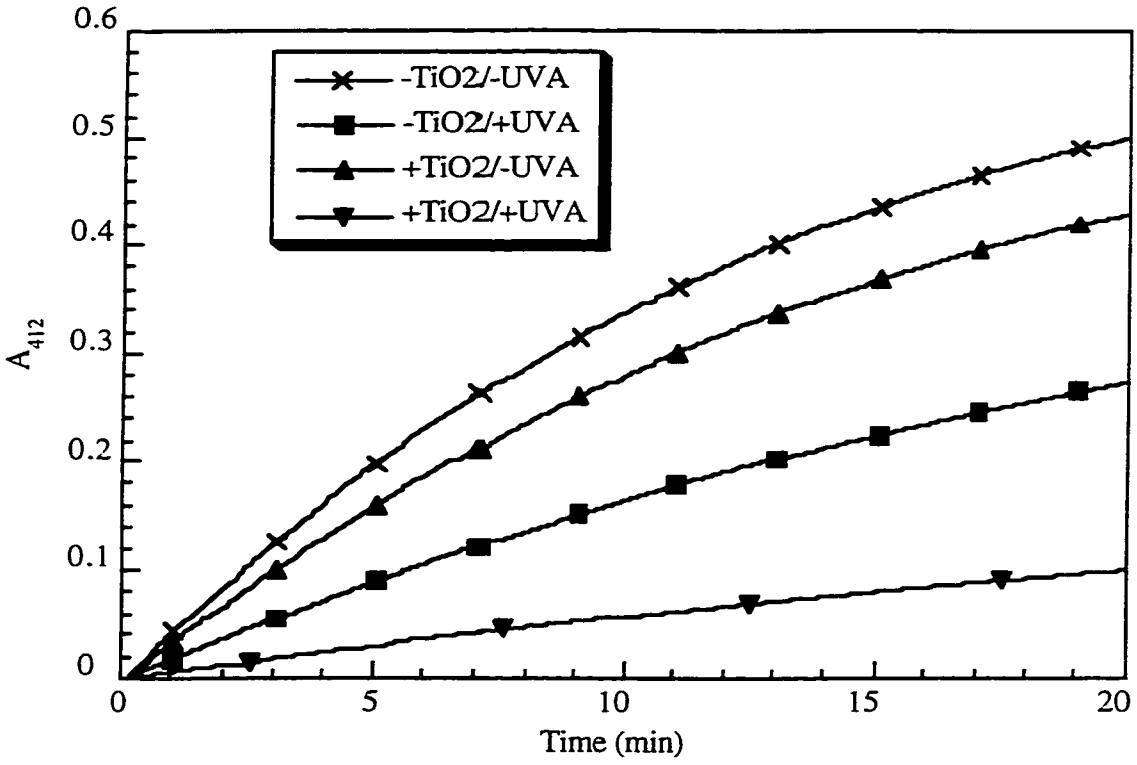

Figure 5.6 Representative plots of the signal growth due to the ABTS radical cation measured at 412 nm as a result of HRP activity for various enzyme samples. Samples were purged with N_2 prior to irradiation.

If all of these curves are analyzed relative to each other then it would seem that the HRP samples which were not treated with UVA or TiO_2 are fully active (some variation in activity between these two seems to be present, but it is likely within experimental error). On the other hand, samples which were exposed to UVA without TiO_2 exhibit some loss of activity. This would be due to direct UVA absorption by the protein and is to be expected. The surprising result is that the samples which contained TiO_2 were deactivated to a very large degree relative to the samples which remained in the dark. This indicates that instead

of protecting the enzyme from UVA the TiO_2 actually contributes very significantly to its degradation.

In order to make these results more easily visualized the curves can be fitted with a second-order polynomial expression:

$$A_{412} = a + bt + ct^2 \quad \textbf{(5.1)}$$

where A = the absorbance and t = time

The coefficients a, b, and c are fitting parameters. Taking the first derivative of this expression with respect to t gives:

$$dA/dt = b + 2ct \quad \textbf{(5.2)}$$

which at t = 0 is equal to b. In other words, b is the initial slope of the curve at t = 0. Initial velocity, or v_0 values, are a commonly used parameter to define enzymatic activity.

Once the curves were fitted with this expression the average initial slope values can calculated for each sample type and be presented in a tabular format to make the results more easily visualized. It is worthwhile to note that the correlation coefficients of the experimental curves with the fitting expression were extremely good ($R > 0.999$). Following are the results of an activity assay performed after enzyme samples were photolysed for 15 hours at a fluence of ~2.4 mW/cm^2 under nitrogen atmosphere:

	-TiO_2,-UVA	-TiO_2,+UVA	+TiO_2 -UVA	+TiO2,+UVA
Ave. activity	0.039	0.024	0.036	0.003
Std. dev.	0.005	0.004	0.003	0.003

Table 5.1 Table of average initial velocity values (activity) for various enzyme samples calculated after fitting of the ABTS radical cation growth curve.

It is much easier to see from this table that the deactivation of the HRP is much more pronounced in the case in which it has been treated with TiO_2 and exposed to UVA light.

Some deactivation takes place in the absence of TiO_2 but as mentioned previously there is some direct absorption of the UVA light by the enzyme so this effect is expected. The presence of TiO_2 alone is not sufficient to cause any degradation of the enzyme, at least not any significant deactivation, but the TiO_2 and UVA combined clearly have a dramatic effect on the enzyme's ability to function. Clearly, the role of the TiO_2 in this system is more complex than a simple light-scattering agent which protects the enzyme from direct UVA absorption.

The above results were obtained under a nitrogen atmosphere. In order to determine the extent of deactivation in an aerobic environment, a similar experiment was performed under air. Samples were irradiated for 3 hours under air at a fluence of 2.4 mW/cm^2. The results which were obtained from the activity analysis were as follows:

	-TiO_2,-UVA	-TiO_2,+UVA	+TiO_2,-UVA	+TiO_2,+UVA
Ave. Activity	0.106	0.093	0.089	0.0003
Std. dev.	0.005	0.006	0.006	0.0003

Table 5.2 Average activities calculated for samples irradiated at 350 nm under air.

This irradiation lasted for only 3 hours as opposed to the 15 hours duration under nitrogen. It can be easily seen, however, that 3 hours is more than sufficient to render the enzyme completely inactive which has undergone photolysis in the presence of TiO_2. Obviously the presence of oxygen in the system accelerates the processes by which the enzyme is deactivated. As outlined in scheme 5.1, several reactive oxygen species (ROS) may be created upon photolysis of TiO_2 in an aqueous environment under aerobic conditions. In the absence of oxygen, many of the damaging species would not be present and the damage to the enzyme would take much longer to occur. This is supported by the experimental data acquired under nitrogen and air outlined above.

In order to determine more accurately how quickly the enzymatic degradation occurs under aerobic conditions, a photolysis experiment was performed in which many samples containing TiO_2 were photolysed at 350 nm. Several samples were removed and assayed for activity at 40 minute intervals. Below are the initial slope values obtained upon fitting of growth curves:

	0 minutes	40 minutes	80 minutes	120 minutes
Ave. Activity	0.070	0.024	0.007	0.003
Std dev.	0.015	0.002	0.001	0.0004

Table 5.3 Average activity values obtained after assay for samples containing HRP and TiO_2 were photolysed at 2.5 mW/cm^2 for various times.

This data indicates that within the first 80 minutes of irradiation at this fluence the majority of the enzyme activity has already been lost. The additional 40 minutes of irradiation after this causes a small decrease, but relative to that which has already occurred this is fairly minor. The fact that the chief loss of activity occurs within the first 80 minutes suggests that the mechanisms by which the deactivation is occurring are relatively efficient.

5.2.3 Photolysis results with bovine α-chymotrypsin

In order to determine whether or not the enzymatic degradation observed for HRP is specific to that enzyme or whether the effect is, in fact, general, another enzyme was utilized in steady-state photolysis/ activity assay experiments. The second enzyme chosen was bovine α-chymotrypsin. Chymotrypsin met the selection criteria explained earlier in terms of availability, known sequence, known three-dimensional structure, etc. As well, chymotrypsin represents a different type of enzyme from HRP in that it is extracellular and it does not contain a heme group.

Chymotrypsin catalyses the hydrolysis of peptide bonds. It is present in the digestive tract of mammals. The assay procedure, therefore, called for the use of a

polypeptide with a group which gives an absorption in the visible once the hydrolysis has occurred. The compound used in this case was succinyl-ala-ala-pro-phe-p-nitroanilide, which the chymotrypsin acts upon and hydrolyses, producing p-nitroaniline which has an absorption centered at 410 nm. The growth of this absorbance, then, is a reflection of the enzymatic activity.

Samples containing chymotrypsin and TiO_2 were photolysed at the same concentrations as those employed for HRP. Samples were prepared in Tris buffer, pH 7.8. Prior to photolysis, absorption spectra of these samples were acquired:

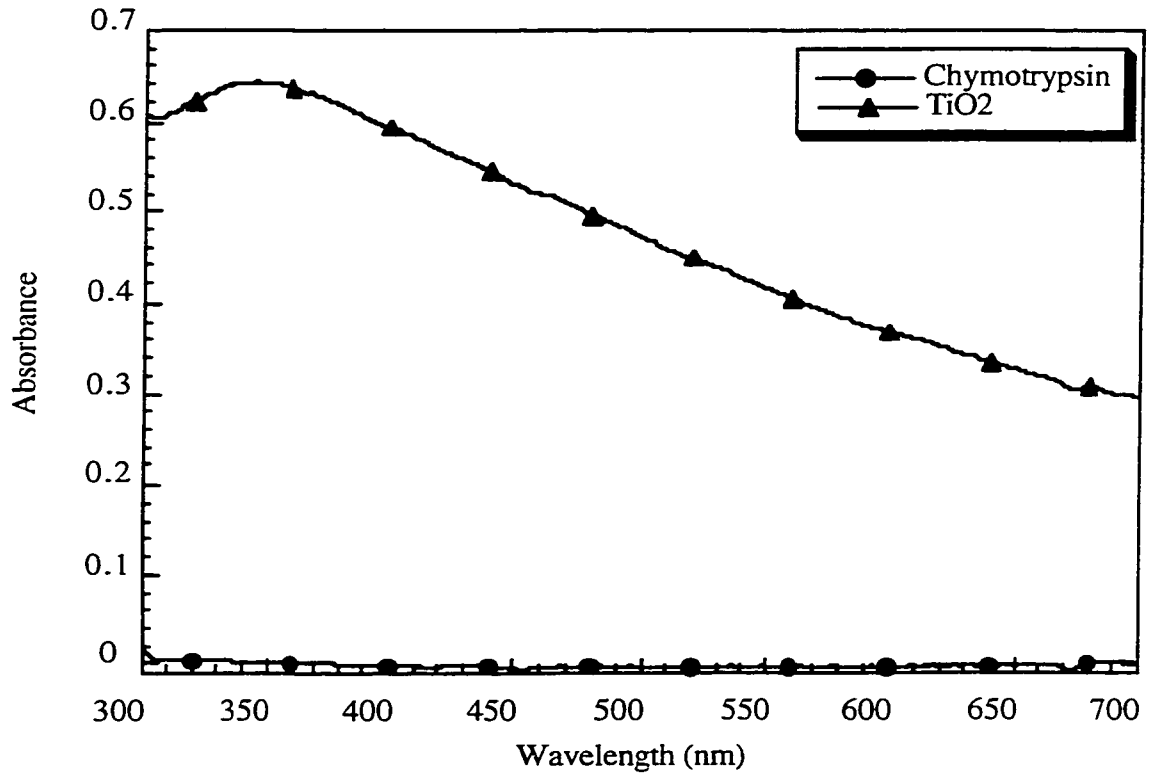

Figure 5.7 Absorption spectra of bovine α-chymotrypsin and TiO_2 suspension (concentrations = 50 mg/ml) as obtained in Tris-HCl, $CaCl_2$ buffer, pH = 7.8.

These spectra indicate that the chymotrypsin has no absorption bands in the near-UV or visible region of the spectrum. It seems likely, then, that there will be no direct UV-induced damage taking place in the absence of the titanium dioxide as there was in the case of HRP.

After photolysis was complete (4 hours at ~1.8 mW/cm^2 under air) the samples containing TiO_2 were centrifuged and the activity assay was performed. The following average activity values were calculated based on the same fitting equation as used for HRP:

	-TiO_2,-UVA	**-TiO_2,+UVA**	**+TiO_2,-UVA**	**+TiO_2,+UVA**
Ave. activity	0.367	0.379	0.366	0.254
Std. dev.	0.009	0.006	0.009	0.028

Table 5.4 Average activity values calculated for samples containing chymotrypsin +/- TiO_2, +/- UVA exposure.

Two main differences are apparent between this data and that collected for HRP. First, there is no decrease in activity over dark controls for samples which contained no TiO_2 but which were exposed to UVA. This result is consistent with the fact that chymotrypsin, which is not a heme protein, has no absorption in the UVA region, but HRP does. The other difference is that whereas the enzymatic activity of HRP was almost completely destroyed by UVA exposure in the presence of TiO_2, the activity loss for chymotrypsin (30%) though significant, is much less dramatic. Activity analysis after a much higher radiation dose (15 hours at ~2.4 mW/cm_2 under air) showed that the chymotrypsin activity decreased by approximately 65 % as compared with controls. It seemed at this point that chymotrypsin is more hardy than HRP when it comes to radical

attack by ROS. It was thought that perhaps the presence of a heme group in the active site somehow renders the enzyme more vulnerable to deactivation by ROS.

A question arose at this time as to whether some chymotrypsin deactivation was occurring as a result of autolysis prompted a change of pH to 6.5 from 7.8, where chymotrypsin exhibits less catalytic activity. Below are the slope values (in mAU/sec) of the linear portion of the p-nitroaniline growth curve for chymotrypsin irradiated for 3 hours in phosphate buffer, pH= 6.5 and at a radiation dose of about 2.4 mW/cm$_2$:

	-TiO_2,-UVA	-TiO_2,+UVA	+TiO_2,-UVA	+TiO_2,+UVA
Ave. activity	30.2	29.4	30.5	-.002
Std. dev.	.685	1.04	.875	.038

Table 5.5 Average activity values calculated for samples containing chymotrypsin +/- TiO_2, +/- UVA exposure in phosphate buffer, pH 6.5.

This table shows results which differ significantly from the previous ones. Whereas before the extent of deactivation was only approximately 30 % upon UVA irradiation of samples containing TiO_2, the above data shows complete deactivation, the same result as that obtained for HRP. This cannot be merely a pH effect, since all samples were prepared at the same pH, and the controls show no such dramatic deactivation. The only variable which could account for this discrepancy in results is the use of phosphate buffer instead of Tris buffer. Further study proved that indeed, Tris prevents a certain amount of deactivation by ROS by acting as a scavenger for these radicals.

Chymotrypsin, then, is deactivated entirely upon exposure to UVA light in the presence of TiO_2, just as HRP is when no radical is present in the system. The heme group does not appear to play role in rendering HRP more sensitive to ROS attack, as was originally thought. The results obtained in phosphate buffer with chymotrypsin reinforce

those obtained with HRP and indicate that the damaging effect of the presence of TiO_2 in the system combined with UVA exposure is very likely general in the case of enzymes.

5.2.4 Photolysis results with TiO_2 extracted from a commercial sunscreen

The results which have ben presented to this point have all been acquired as a result of photolysis of enzyme/TiO_2 mixtures composed of TiO_2 purchased in the pure anatase form (the most active catalytically) from a chemical company. The obvious criticism of this work is that the results do not necessarily reflect what would happen using the TiO_2 which is employed in the manufacture of sunscreens, which may or may not be the anatase form, and may or may not be processed in some way. The most reasonable way to address this criticism, then, is to use TiO_2 from an actual sunscreen along with an enzyme and determine whether or not the same sort of enzymatic deactivation can be observed upon photolysis.

TiO_2 was extracted (see experimental section) from a sunscreen purchased from a local pharmacy (Bébé Block®) and the same procedure and concentrations employed in previous experiments were duplicated with this titanium of unknown composition along with the same enzyme, horseradish peroxidase, utilized previously. Another difference between this and the previous experiments was in the manner in which the activity assay was performed. The concentrations of reagents/substrates were kept the same as before, but instead of analysing one sample at a time with a conventional spectrophotometer, a microplate reader was used which can analyse 96 samples simultaneously. This allows for more trials for each sample to be performed and also ensures that all samples are assayed under exactly the same conditions.

Below are the results obtained for the activity assay performed after sunscreen titanium was mixed with HRP and photolysed. Average activity values are calculated from three separate samples assayed 3x each and are displayed in units of mAU/sec:

	-TiO_2,-UVA	-TiO_2,+UVA	+TiO2,-UVA	+TiO2,+UVA
Ave. Activity	4.710	2.754	5.885	0.270
Std Dev.	1.013	0.629	0.922	0.028

Table 5.6 Specific activity data for HRP samples photolysed (4 h, ~1.5 mW/cm^2) under air in the presence and absence of extracted commercial sunscreen titanium dioxide.

This particular experimental data are somewhat strange in that there seems to be higher activity in the presence of TiO_2 when no exposure to light has taken place. Another experiment performed under exactly the same conditions showed that the activity was the same in the presence and absence of TiO_2, so this slight difference is likely due to sample handling. The most important observation to be made with respect to these data is that just as in the case of the anatase titanium utilized previously, the enzymatic activity is severely curtailed when TiO_2 is present in the system and UVA exposure has taken place. It seems quite apparent, then, that titanium contained in at least some sunscreens is just as capable of degrading proteins as the pure anatase form.

5.3 Discussion

The mechanism by which the degradation of these enzymes is occurring is undoubtedly due to redox reactions involving the various radical species created upon the

photolysis of the TiO_2 particles, but what steps are actually occurring? To our knowledge no studies for the mechanism of TiO_2-photoinduced degradation of proteins have been performed to this date, but several studies have been done on the degradation of amino acids by photocatalysis of TiO_2 suspensions and studies of the initial events in the particle upon the absorption of a photon by the TiO_2 have also been done. Pooling the information obtained through both of these approaches may help to give some idea of the initial events in the decomposition process taking place within the enzyme.

Studies of the primary events in the photocatalysis process within TiO_2 particles were performed by Serpone et al. [14,17]. They used picosecond laser flash photolysis to study the initial events occurring in the particles and came up with the following scheme:

1. Charge carrier generation and separation

$$TiO_2 + h\nu \longrightarrow TiO_2(e^-/h^+) \longrightarrow e^-_{CB} + h^+_{VB}$$

where CB and VB refer to the valence and conduction bands, respectively.

2. Charge carrier migration to the surface

a. $e^-_{CB} \longrightarrow e^-_S$

b. $h^+_{VB} \longrightarrow h^+_S$

c. $e^-_S, h^+_S \longrightarrow$ surface migration

3. Charge carrier trapping into shallow traps (ST)

a. $e^-_{CB} + ST \longrightarrow e^-_{TR}$

b. $h^+_{VB} + ST \longrightarrow h^+_{TR}$

c. $e^-_S + A_S \longrightarrow A^-_S$

d. $h^+_S + D_S \longrightarrow D^+_S$

where ST = shallow trap, TR = trapped, and S = surface.

4. Charge carrier recombination (radiative and nonradiative)

a. $e^-_{CB} + h^+_{VB} \longrightarrow h\nu_1 + TiO_2$

b. $e^-_{TR} + h^+_{VB} \longrightarrow h\nu_2 + TiO_2$

c. $e^-_{CB} + h^+_{TR} \longrightarrow h\nu_3 + TiO_2$

d. $e^-_{TR} + h^+_{TR} \longrightarrow h\nu_4 + TiO_2$

The recombination processes described in (4) account for the fate of $\geq$ 90% of the e-/h+ pairs created upon the absorption of the UV photon. These recombination events occur very quickly (within ~ 500 picoseconds). Ten nanoseconds after the laser pulse, only ~ 10% of the original absorption due to the electron can still be observed. The extinction coefficient of the electron in aqueous solution is only 1200 L/mol cm, so the magnitude of the signals is quite small. These observations also account for our failure to observe the elestron directly during our laser experiments. The rise time of our system would not allow us to observe the electron until after 90% of the e-/h+ pairs had recombined, and the very low extinction coefficient would make resolution of a signal very difficult.

Since only 10% of the e-/h+ pairs survive the recombination process, only these remain available to participate in redox reactions with other materials.

Monig et al. studied the effect of irradiating (x-rays, γ-radiation, pulse radiolysis) aqueous TiO_2 suspensions in the presence of oxygen and various amino acids.[18] They found that the amino acids were degraded quite efficiently upon irradiation and that NH_3 and CO_2 were given off as the amino acids were decomposed.

Some of the initial steps in the complex decomposition process were elucidated. In simple aliphatic amino acids the electron may react with the acid via either one of two processes:

1. deamination of the acid:

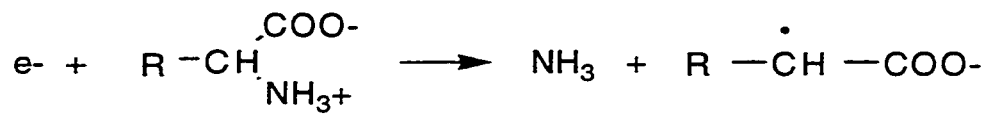

2. hydrogen atom formation:

With respect to hydroxyl radical reactions with the amino acids, it was determined that although the radical can theoretically abstract a hydrogen from any position in the carbon skeleton, the actual site from which the abstraction takes place depends, at least somewhat, upon the protonation state of the amino group. In a neutral or acidic environment, where the amino group is protonated, abstraction of the H atom takes place from positions which are remote from the carbon atom which carries the amino and carboyl substitutents. In basic environment there is another pathway which becomes available in addition to hydrogen atom abstraction. In this case the hydroxyl radical can attack directly at the nitrogen atom which initiates decarboxylation with a simultaneous formation of an α-amino radical. Both of these scenarios are illustrated below:

1. Hydrogen atom abstraction from R group in acidic medium:

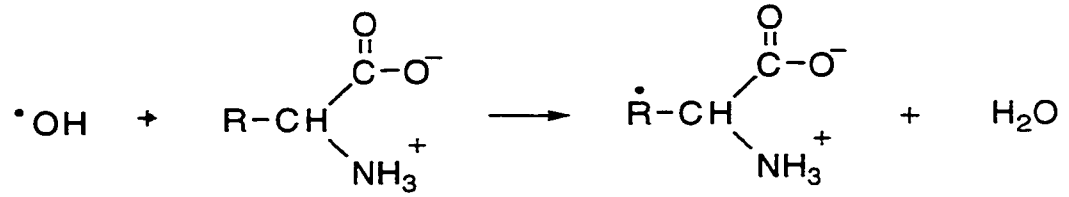

Scheme 5.3 Illustration of H atom abstraction by OH radical from amino acid with protonated amino function.

2. OH radical attack on unprotonated amino group in basic solution:

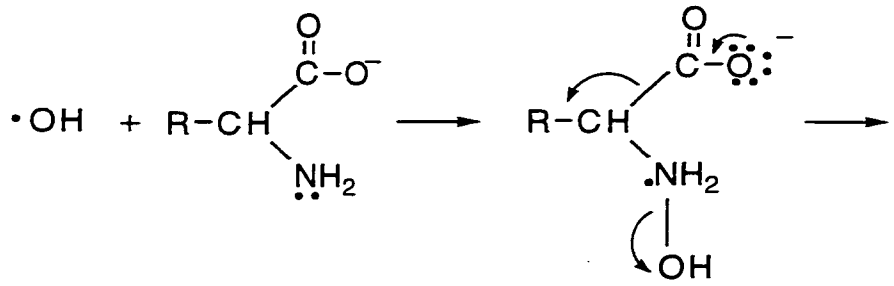

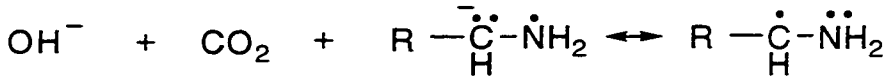

Scheme 5.4 Illustration of OH radical attack on amino function in basic medium.

Another study by Hidaka et al. confirmed the above schemes and provides a more detailed mechanism for the degradation of amino acids outlined. Below is a detailed scheme as given in this paper[12]:

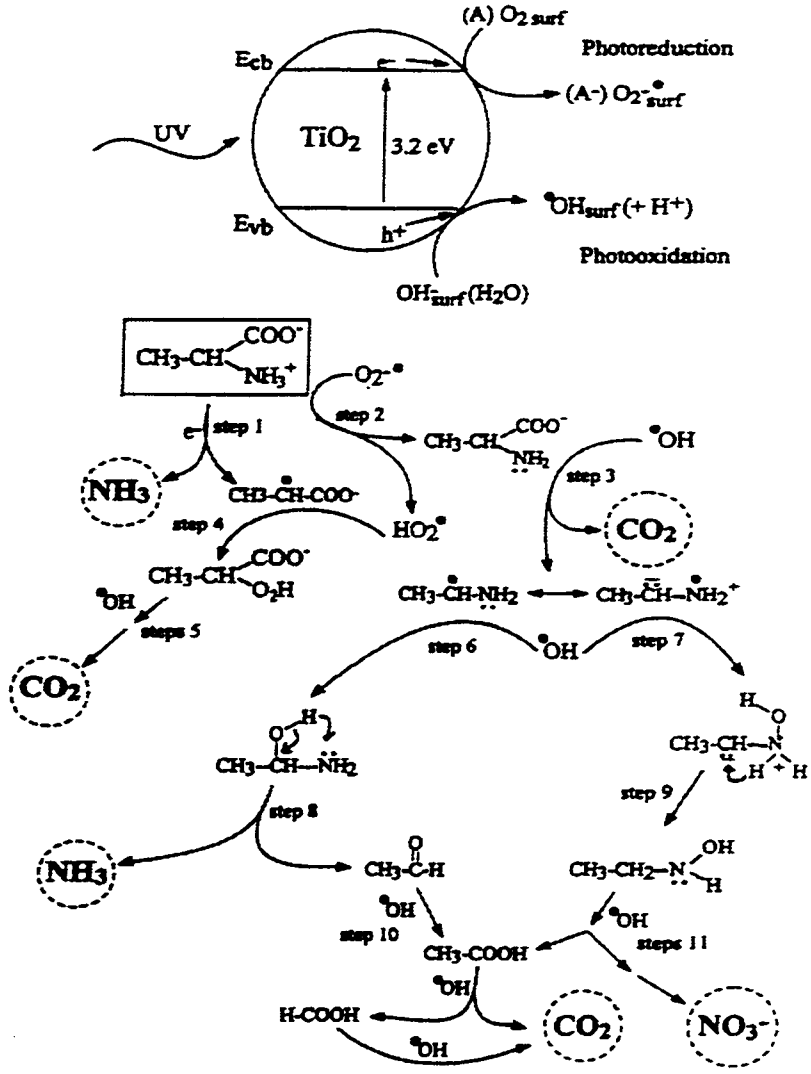

Scheme 5.5 Scheme of degradation of amino acid by reactive oxygen species created upon photolysis of TiO_2.

It can easily be seen that the mechanism is quite complex, and of course there are variations depending upon the medium being acid or basic. These studies were all performed on

amino acids in solution; thus, the level of complexity is quite low compared to a functioning enzyme, which has many many amino acids strung together, a very complicated pattern of folding, and sometimes a transition metal center (like in the case of HRP). Nevertheless some information on how the species created upon photolysis of TiO_2 react with the amino acids composing the enzyme can be gained from this work.

The results outlined above clearly indicate that titanium dioxide, whether the pure anatase form or an extract from a commercial sunscreen, definitely deactivates enzymes when exposed to UVA light in the presence of oxygen. Under anaerobic conditions the enzyme can still be deactivated, but the light dose required is much greater. This result can be rationalized considering that according to the scheme shown previously (Scheme 5.1) several of the active species responsible for the damage will not be formed in the absence of oxygen. As for the actual mechanism by which the deactivation is taking place, the work outlined with respect to amino acids in solution gives insight, but since no work of this type has been done, to our knowledge, with amino acid chains or proteins, not much specific information is available regarding what may be happening in these complex structures. Some studies by others in this laboratory indicate that in the case of HRP the heme group is at least one site within the protein which is affected by the radicals created upon photolyis of TiO_2. Monitoring of the absorption due to the heme group before and after irradiation shows that the heme absorption deteriorates quickly upon exposure to UVA in the presence of TiO_2. Below is a three-dimensional picture of HRP which highlights the location of the heme group as well as some amino acid residues which are possible sites for radical attack within the protein:

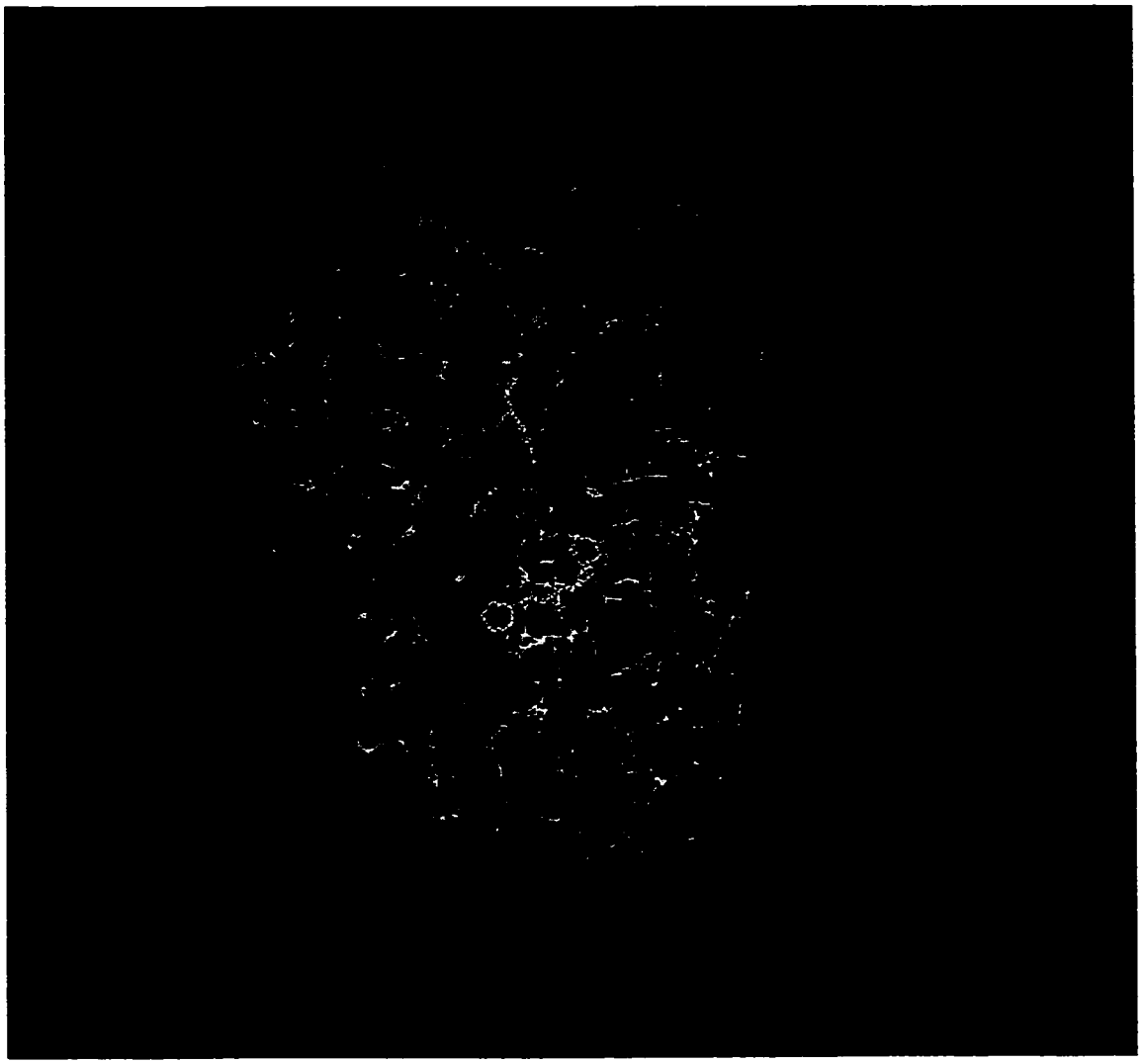

Figure 5.8 Three-dimensional structure of HRP. Heme group is shown in blue. Cysteine, tyrosine, histidine, and tryptophan residues are shown in purple, green, yellow, and red respectively.

Figure 5.8 indicates that the heme group is at least partially on the surface of the protein. This location leaves it vulnerable to attack by hydroxyl radicals and other ROS. That the heme group is somewhat exposed is not surprising given that the function of this enzyme is to catalyse redox processes, but this design renders it particularly susceptible to ROS damage. Other studies including gel electrophoresis and mass spectrometry have shown

that the protein remains whole and does not undergo a mass change upon photolysis. Other sites which are likely candidates for attack by free radicals are cysteine, tyrosine, tryptophen, and histidine amino acid residues, as they contain phenolic groups (tyrosine), thiol groups (cysteine), or amine (tryptophan and histidine) on their side chains which are stabilized after hydrogen abstraction by free radicals. In the case of the experiments involving the irradiation if TiO_2 in the presence of HRP, the pH was 4.4. Since the pKa values of all ofthe above mentioned amino acid residues are approximately 9, at the pH the experiment was carried out, they would all be protonated. This means that these residues would not then be significantly more likely to react with ROS via hydrogen transfer. The fact that at least some of these residues are located on the surface of the protein may enhance their potential to be attacked by ROS, however.

Another three dimensional picture in figure 5.9 shows the structure of α-chymotrypsin with the cysteine, tyrosine, tryptophan, and histidine groups highlighted:

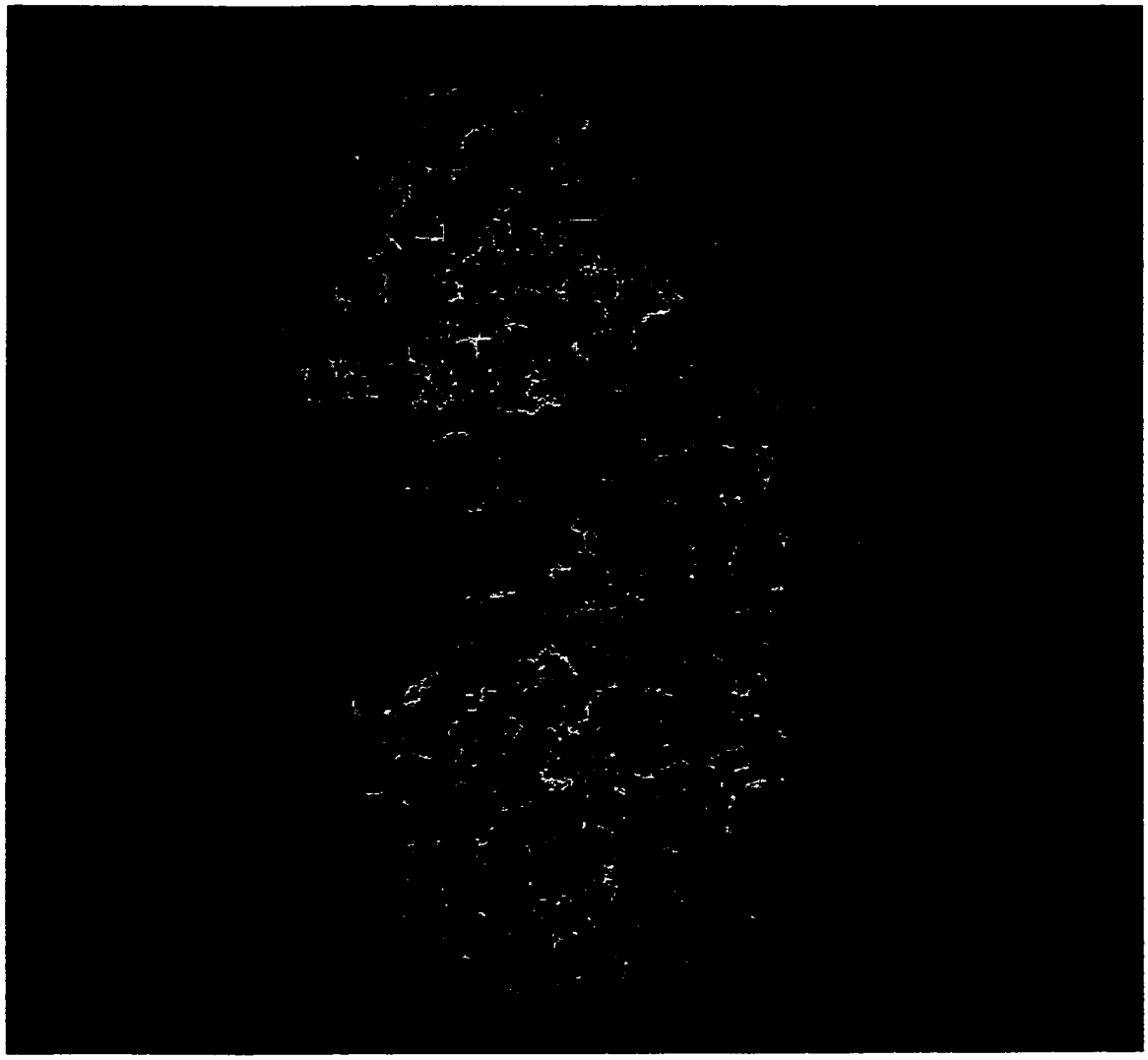

Figure 5.9 Three dimensional structure of α-chymotrypsin. Cysteine, tyrosine, histidine, and tryptophan are shown in purple, green, yellow, and red respectively.

Chymotrypsin does not contain a heme group, but does have several tyrosine, cysteine, histidine, and tryptophan residues in its structure. The pH at which the irradiation experiments were done was either 6.5 or 7.4 for this enzyme, so some of the above-mentioned residues would be deprotonated, and therefore more likely to be ROS targets.

In Chymotrypsin, however, the cysteine residues are not free to react because the S-H groups are involved in disulfide bonding.

Obviously the reactivity of specific residues can be affected by many factors such as pH, location on the protein (surface or embedded), bonded or free (cysteine versus cystine), and general reactivity. It is extremely difficult to make predictions as to where the damage to these proteins is occurring. The bottom line is; however, clear. The enzyme, whether chymotrypsin or HRP, can no longer function to the extent that it could prior to photolysis by UVA in the presence of TiO_2. It has been shown that TiO_2 particles can penetrate through the stratum corneum to the deeper layers of the skin cells[19-21]. The implication of this is that the titanium dioxide can become embedded within the skin where if it is exposed to light, reactive species can result which can cause damage to cellular components. Since smaller and smaller particles are being used in cosmetics and sunscreens because of the greater esthetic appeal of these less visible particles, the likelihood of penetration into the skin is enhanced. This then increases the chances of photodamage occurring to living cellular material.

5.4 Experimental details

Titanium dioxide, pure anatase, with an average particle size of 32 nm was purchased from Alfa Aesar. This particle size is comparable with that commonly employed in commercial sunscreen formulations. Horseradish peroxidase (HRP), type VI-A, bovine α-chymotrypsin, 2,2'-azino-bis(3-ethylbenzthiazoline-6-sulfonic acid) diammonium salt (ABTS), succinyl-ala-ala-pro-phe-p-nitroanilide, and methyl viologen were purchased from Sigma in high purity and used as received. PBS, pH 7.4 (0.01 M) was purchased from Sigma and the acetate (pH 4.4), Tris-HCl (pH 7.2), and phosphate (pH 6.5) buffers

employed for other experiments were prepared using filtered millipore water (Millipore Milli-Q system) and reagent grade chemicals. These in-house prepared buffers were also treated with iminodiacetic acid, a chelating resin (Sigma) to remove any metal ions.

Laser experiments were conducted in solution (transmission detection) and solid (diffuse reflectance detection) using a Nd/Yag laser at 355 nm for excitation. Details of the laser system have been provided in the general experimental chapter of this thesis. Samples used in transmission experiments were contained in 7 x 7 mm quartz cells. Samples used in diffuse reflectance experiments were contained in 3 x 7 mm quartz cells or 10 x 10 mm polymethylmethacrylate (PMMA) disposable cuvettes which are transparent at the laser wavelength. All samples were purged with nitrogen prior to analysis to avoid any scavenging of electrons by oxygen.

Titanium dioxide was extracted from a commercial sunscreen by washing several times with acetonitrile, acetone, ethanol, chloroform, aqueous acid, and water. The solid titanium dioxide was then dried and crushed into a fine powder before being used in experiments.

Enzyme solutions and titanium dioxide suspensions were prepared in buffers at the appropriate pH for optimum enzymatic activity. In the case of HRP the pH was 4.4 ; for α-chymotrypsin the pH was 7.2. Enzyme powder was simply dissolved in the appropriate buffer; TiO_2 was suspended by sonication.

Steady-state photolyses were performed using an irradiation chamber fitted with between four and eight 350 nm Rayonet UVA lamps, depending upon the experiment. Each lamps contributes approximately 0.3 mW/cm^2 at the sample. Samples containing only enzyme HRP or chymotrypsin) at a concentration of 50 μg/ml as well as enzyme + TiO_2, both at concentrations of 50 μg/ml were photolysed in Pyrex test tubes (1 cm or 7 mm i.d., depending on the particular experiment). Samples were placed on a rotating carousel to ensure uniform light exposure. Dark control samples were covered with aluminum foil and

placed in the chamber as well so that all samples were kept under the same conditions. The temperature in the chamber remained constant at approximately 32^{0}C.

After the photolyses were complete and prior to activity assay, all samples which contained TiO_2 were centrifuged to remove the particles from suspension (~ 1700 g). In the case of HRP, samples were diluted by a factor of 100 with buffer to achieve the appropriate enzyme concentration called for in the assay procedure of Porstmann et al [22]. Chymotrypsin samples were assayed at the photolysis concentration according to the procedure of DelMar et al [23]. Growth of absorbance due to enzymatic activity was monitired using a Carey 1E, UV-visible spectrophotometer in kinetics mode, which is controlled by an IBM computer equipped with Varian software. Growth of signal was monitored at 412 nm in the case of HRP and 410 nm in the case of chymotrypsin. Plots of the kinetic data were constructed using Kaleidagraph software and fitted with a second order polynomial to extract initial slopes.

5.5 References

(1) Mitchnick, M. A. *Cosm. And Toil.* **1992**, *107*, 111.

(2) Burrows, H., Ernestova, L., Kemp, T., Skurlatov, Y., Purmal, A., Yermankov, A. *Progress in Reaction Kinetics* **1998**, *23*, 145.

(3) Huang, N.; Xiao, Z.; Huang, D.; Yuan, C. *Supram. Sci.* **1998**, *8*, 559.

(4) El-Ekabi, H.; Serpone, N. *J. Phys. Chem.* **1988**, *92*, 5726.

(5) Lee, S.; Nakamura, M.; Ohgaki, S. *J. Environ. Sci. Health* **1998**, *A33*, 1643.

(6) Lee, S.; Nishida, K.; Otaki, M.; Ohgaki, S. *Wat. Sci. Tech.* **1997**, *35*, 101.

(7) Hidaka, H.; Horikoshi, S.; Ajisaka, K.; Zhao, J.; Serpone, N. *J. Photochem. Photobiol. A: Chem.* **1997**, *108*, 197.

(8) Dunford, R.; Salinaro, A.; Cai, L.; Serpone, N.; Horikoshi, S.; Hidaka, H.; Knowland, J. *FEBS Letters* **1997**, *418*, 87.

(9) Hidaka, H.; Horikoshi, S.; Serpone, N.; Knowland, J. *J. Photochem. Photobiology A: Chem.* **1997**, *111*, 205.

(10) Wamer, W.; Yin, J.; Wei, R. *Free Radical Biol. Med.* **1997**, *23*, 851.

(11) Horikoshi, S.; Serpone, N.; Yoshikawa, S.; Knowland, J.; Hidaka, H. *J. Photochem. Photobiol. A: Chem.* **1999**, *120*, 63.

(12) Reprinted from *J. Photochem. Photobiol. A: Chem.*, *118*, Horikoshi, S.; Serpone, N.; Zhao, J.; Hidaka, H., *118*, "Towards a better understanding of the initial events in the photocatalyzed mineralization of amino acids at the titania/water interface. An experimental and theoretical examination of L-alanine, L-serine, and L-phenylalanine", pp.123-129, Towards a better understanding of the initial events in the photocatalyzed mineralization of amino acids at the titania/water interface. An experimental and theoretical examination of L-alanine, L-serine, and L-phenylalanine." Copyright (1998) with permission from Elsevier Science.

(13) Dhananjeyan, M. R.; Annapoorani, R.; Renganathan, R. *J. Photochem. Photobiol.* **1997**, *A, 109*, 147.

(14) Serpone, N.; Lawless, D.; Khairutdinov, R. *J. Phys. Chem.* **1995**, *99*, 16655.

(15) Moser, J.; Gratzel, M. *J. Am. Chem. Soc.* **1983**, *105*, 6547.

(16) Serpone, N.; Lawless, D.; Khairutdinov, R. *J. Phys. Chem.* **1995**, *99*, 16646.

(17) Monig, J.; Chapman, R.; Asmus, K.-D. *J. Phys. Chem.* **1985**, *89*, 3139.

(18) Lademann, J.; Weigmann, H.-J.; Rickmayer, C.; Barthelmes, H.; Schaefer, H.; Mueller, G.; Sterry, W. *Skin Pharmacol. Appl. Skin Physiol.* **1999**, *12*, 247.

(19) Dupre, A.; Touron, P.; Daste, J. *Arch. Dermatol.* **1985**, *121*, 656.

(20) Tan, M.-H.; Commens, C.; Burnett, L.; Snitch, P. *Australasian J. Dermatol.* **1996**, *37*, 185.

(21) Porstmann, B., Porstmann, T., and Nugel, M. *J. Clin. Chem. Biochem.* **1981**, *19*, 435.

(22) DelMar, E. G.; Largman, C.; Brodrick, J. W.; Geokas, M. C. *Analytical Biochemistry* **1979**, *99*, 316.

CHAPTER 6: CLAIMS TO ORIGINAL RESEARCH

The overall aim of the work described in this thesis was to gain insight into chemical processes as they may occur within biological systems. The biological systems were modeled through the use of various molecules such as DNA and enzymes in the hope that the knowledge acquired could be relevant to how such reactions might proceed within living organisms. The contributions in this thesis to research in this field are:

1. It has been shown that an applied magnetic field causes a clear, consistent, and measurable difference in the kinetics of the radicals when the field is applied for the two systems investigated.

2. LFP experiments utilizing DNA as one half of the radical pair and also as the "cage" allowed the determination of estimates for the exit lifetimes (length of time the radical will remain associated with the DNA before it enters into the aqueous environment and becomes available for other reactions) for the two molecules studied.

3. A mechanism has been evaluated and proposed whereby laser irradiation of certain compounds in the presence of oxygen leads to the generation of peroxy radicals.

4. It has been determined that photolysis of suspended TiO_2 in the presence of enzymes causes significant activity loss in two different enzymes.

Publications arising from the work presented in this thesis:

1. Mohtat, N.; Cozens, F.L.; Hancock-Chen, T.; McLean, J.;, Kim, J.; Scaiano, J.C. *Photochem. Photobiol.* **1998**, 67, 111.

2. Hancock-Chen, T.; Scaiano, J.C. *Photochem. Photobiol.* **1998**, 67, 174.

3. Hancock-Chen, T.; Scaiano, J.C. *J. Photochem. Photobiol. B: Biol.* **2000**, *submitted.*